UNIVERSITY OF CALIFORNIA, SAN DIEGO

Optical Studies On Cell Division (Mitosis)

A dissertation submitted in partial satisfaction of the
requirements for the degree
Doctor of Philosophy

in

Electrical Engineering (Photonics)

by

Norman Miyamoto Baker

Committee in charge:

Professor Michael W. Berns, Co-Chair
Professor Sadik Esener, Co-Chair
Professor Michael Heller
Professor Zhaowei Liu
Professor Yu-Hwa Lo

2010

The dissertation of Norman Miyamoto Baker is approved, and it is acceptable in quality and form for publication on microfilm and electronically:

_____

_____

_____

_____
Co-Chair

_____
Co-Chair

University of California, San Diego

2010

DEDICATION

For my awesome wife, Jinny, my parents, Everett and Yuriko, my brothers, Everett Jr., David and John.

TABLE OF CONTENTS

LIST OF ABBREVIATIONS

53BP1 ..... Tumor Suppressor p53-binding protein 1
α ..... alpha
ATM ..... ataxia telangiectasia, mutated
Aurora B ..... Chromosome passenger protein Aurora B
ADP ..... telomeric poly-ribosylase known as tankyrase
β ..... beta
bp ..... base pair
BP ..... blocked path
BS ..... beam splitter
°C ..... degrees Celsius
c ..... speed of light in free space
CAN ..... controller area network
CCD ..... charge-coupled device
CENP-A ..... Centromere protein A
Chk2 ..... Checkpoint homolog Chk2
cm ..... centimeter
cm^{-1} ..... 1 divided by centimeter
cm^2 ..... centimeter squared (area)
cm^3 ..... centimeter cubed (volume)
COM ..... serial port cable
DM ..... dichroic mirror
DMEM ..... Dulbecco's Modified Eagle Media
DNA ..... deoxyribonucleic acid
DPBS ..... Dulbecco's phosphate-buffered saline
eCFP ..... enhanced cyan fluorescent protein
eYFP ..... enhanced yellow fluorescent protein
E ..... Energy, usually a vector
ECFP ..... enhanced cyan fluorescent protein
ECM ..... extracellular matrix
Eg5 ..... plus end directed motor protein

f . . . . . focus position
FRT . . . . . Flippase Recognition Target
FSM . . . . . fast steering mirror
GFP . . . . . green fluorescent protein
GDP . . . . . guanosine diphosophate
GTP . . . . . guanosine triphosphate
h . . . . . planck's constant
H2AX . . . . . gene coding for histone H2A
HeLa . . . . . Immortal cell line taken from cancer patient Henrietta Lacks, Cervical
Hr . . . . . hour
I(r) . . . . . Intensity profile of Gaussian Beam
I-Scel . . . . . homing endonuclease
j . . . . . joules
k . . . . . wave vector
κ . . . . . characteristic interaction of the medium
λ . . . . . wavelength
PXI . . . . . Peripheral Interface
L' . . . . . L' is the length between pole and kinetochore where laser ablates.
L" . . . . . L" is the length between pole and kinetochore where laser does not ablate.
LASER . . . . . Light amplification stimulated emission of radiation
MAPs . . . . . microtubule assisted or associated proteins
MHz . . . . . megahertz
mCherry . . . . . Red colored fluorescent protein
mL . . . . . milliliter
mm . . . . . millimeter
mp . . . . . multiphoton
mRNA . . . . . messenger ribonucleic acid
ms . . . . . milliseconds
MSI . . . . . microscope stage incubator
MT . . . . . microtubule
mW . . . . . milliwatt

n ..... refractive index of the medium
NA ..... numerical aperture
Nbs1 ..... Nibrin
nm ..... nanometer
ω ..... angular oscillation frequency of light
PC ..... personal computer
PCI ..... peripheral component interconnect
pN ..... piconewton
ps ..... picosecond
PtK2 ..... Potorous Tridactylis epithelial cells.
Rad51 ..... human gene rad51
ROI ..... Region of Interest
Robolase ..... Robotic controlled Laser Microscope
RNAi ..... ribonucleic acid interference
SAC ..... Spindle Assembly Checkpoint
s ..... seconds
S polarized ..... S polarized light. P polarized light form entire basis.
SHG ..... second harmonic generator
sp ..... single photon
T_d ..... Thermal diffusion time
T_m ..... Stress wave propagation time
TEM00 ..... Transverse Electric Magnetic Gaussian mode of propagation
TEM ..... Transmission Electron Microscope
TIFs ..... Telomere Dysfunction-Induced Focus
UCSD ..... University of California, San Diego
U2OS ..... Cells used in CENP-A.
um ..... micron
um^2 ..... micrometer squared
uM ..... micromolar
UV ..... Ultraviolet (below 400 nm) wavelength
W ..... Watts

w . . . . . beam waist

WT . . . . . wildtype

LIST OF FIGURES

ACKNOWLEDGEMENTS

I would like to thank my advisor Dr. Michael Berns for everything he has done for me. Very supporting, always willing to talk, and allowing an Electrical Engineer to be in a Bioengineering lab and have fun too. I'd also like to thank Dr. Sadik Esener, my co-chair and advisor from Electrical Engineering who was very supportive of biophotonics-oriented research in satisfaction of Ph.D. and for help in my early years at University of California, San Diego. Dr. Yu-wha Lo, Zhaowei Liu and Michael Heller for additional perspectives and suggestions.

I'd also like to thank Dr. Sam Zeitlin and Dr. Jagesh Shah for contribution to experimental design, reagants and valuable advice on many different levels. Thank Dr. Chung-Ho Sun for making and proving me with cells throughout the years and Thank the Berns Lab (San Diego and Irvine) for all of their contribution, help, advice, and making my lab experience quite fun.

Most of all, I'd like to thank my wife, Jinny Baker, for her laughter and encouragement to finish my Ph.D.. My parents, Everett and Yuriko Baker, for encouraging me and giving me the drive to pursue a Ph.D.; My brothers, Everett Jr., David and John Baker, who were always there for me while growing up and pursuing my Ph.D.; My friends who prayed for me and kept me sane in my career.

The Material presented in Chapter 4, in full, is a reprint of the material as it appears in Baker Norman M, Zeitlin Samantha, Shi Linda, Shah Jagesh, Berns Michael, "Chromosome tips damaged in anaphase inhibit cytokinesis", Plos1, in press, August 2010. The dissertation author was the main author of this paper.

The material presented in Chapter 5, in full, is a reprint of the material to be published Baker Norman, Tsay Angela, Shi Linda, Shah Jagesh, Berns Michael, "Mitotic spindle regulation following selective laser ablation," in preparation. The dissertation author was the main author of this paper.

The material presented in Chapter 6 was done with the help of Angela Tsay and Linda Shi.

The material presented in Chapter 7 was done with the help of Samantha Zeitlin.

The material presented in Chapter 8 is, in part, a reprint of the material as it appears in Zeitlin, G. Samantha, Baker M. Norman, Chapados R. Brian, Soutoglou Evi,

Wang Y.J. Jean, Berns W. Michael, Cleveland W. Don., ”Double-stand DNA breaks recruit the centromeric histone CENP-A”, Proceedings of the National Academy of Sciences of the United States of America, 106(37):15762-7, 2009. The dissertation author was a co-author of the paper.

VITA

2004	B.S. in Electrical and Computer Engineering University of California, San Diego, La Jolla, CA
2008	M.S. in Electrical Engineering (Photonics) University of California, San Diego, La Jolla, CA
2010	Ph.D., in Electrical Engineering (Photonics) University of California, San Diego, La Jolla, CA

PUBLICATIONS

Zeitlin Samantha G, Baker Norman M, Chapados Brian R, Soutoglou Evi, Wang Jean Y J, Berns Michael W, Cleveland Don W. "Double-stand DNA breaks recruit the centromeric histone CENP-A"', *Proceedings of the National Academy of Sciences of the United States of America*, 106(37):15762-7, 2009.

Baker Norman M, Zeitlin Samantha G, Shi Linda, Shah Jagesh, Berns Michael, "Chromosome tips damaged in anaphase inhibit cytokinesis", *Plos1, in print*, August 2010.

Baker Norman M, Botvinick Elliot, Wu George, Shi Linda, Berns Michael, "Mitotic Spindle Dynamics Studied using Laser scissors", *SPIE, #6326-87*.

Baker Norman M, Zeitlin Samantha, Shi Linda, Shah Jagesh, Berns Michael, "Laser ablation of Telomeres in anaphase causes delay in cytokinesis", *ASCB, 2704 B415*.

ABSTRACT OF THE DISSERTATION

Optical Studies On Cell Division (Mitosis)

by

Norman Miyamoto Baker

Doctor of Philosophy in Electrical Engineering (Photonics)

University of California, San Diego, 2010

Professor Michael W. Berns, Co-Chair
Professor Sadik Esener, Co-Chair

Mitosis is the process by which cells, after having duplicated their DNA content, segregate chromosomes equally into two identical daughter cells. Mitosis is a very short part of a normal cell cycle (usually 24+hours) and ranges from 30 minutes to an hour depending on cell type and environmental conditions. During this incredibly short amount of time, the cell undergoes several complex re-arrangements, biomechanically and biochemically. Microtubules, 20 nm width dimer polymers, play an essential role as the building blocks that provides the cytoskeleton and mitotic spindle for the cell, provide the force that segregates chromosomes (anaphase), to satisfaction of tension and attachment based checkpoints (metaphase-anaphase transition). To elucidate the key role microtubules have in mitosis, drugs such as taxol and nocodazole have been used to impart catastrophic global damage to the mitotic spindle and study the effects on cellular division. However, catastrophic global damage can not answer specific questions regarding highly spatially localized damage and temporally transient damage. In elucidating the role of microtubules, chromosomes and other key biological structures, there is the need for a transient perturbation on the mitotic process. To study the effects

of transient perturbation on mitosis, a Laser microscope system (Robolase) was developed to deliver spatially localized (0.4 um) and temporally-specific disruption inside living cells (nanosurgery). Specifically, the affect of ablating chromosome tips, mitotic spindles, and chromatid are examined, and the relationship between damaged sites and pathways controlling the progression of the cell cycle and DNA damage pathways are examined. In conclusion, an optically based method for studying mitosis with transient perturbation has been developed and used to determine that chromosome tip disruption affects cytokinetic progression, prolonged disruption of mitotic spindle reveals force sensing in the metaphase spindle, and double-strand breaks of DNA recruit CENP-A in addition to known DNA damage proteins.

1 Microscopy in biology

1.1 Introduction

Dynamic light-microscopy of living cells and organisms alone does not reveal the high level of complexity of cellular and subcellular organization. All observable processes rely on the activity of biochemical and biophysical processes. Experimentally it is not trivial to apply a perturbation to a specific process without inadvertently perturbing the cell overall. Drugs and RNAi in particular have a global and catastrophic effect on cell physiology and function. Traditional biochemical techniques affect the entire cell and, in many cases, are permanent, lethal, or non-transient in nature and limit the amount of information that can be gained by biochemical experiments alone.

Scientists traditionally rely on a ”reductionist” view in which a specific process is perturbed from its' physiological equilibrium and then the physical, biochemical, and biological parameters are measured and characterized with respect to their role and influence on normal operating parameters. For the study of microtubules, drugs that destabilize microtubules, such as nocodazole, or stabilize microtubules, such as taxol, have contributed significantly to understanding the relationship between subcellular components (microtubules) and their roles in signaling pathways. However, the global and catastrophic nature, for example of nocodazole, restricts scientists ability to ask certain questions such as ”How does the cell respond to a complete loss of tubulin?”

Pulsed laser technology allows a highly spatially and temporally specific ablation event to occur at any point inside subcellular regions of a cell. Lasers provide an ideal method for highly localized transient perturbations on a cell and the study of the overall cell system (”Mitosis” in this thesis) without catastrophic, global, or intrinsically permanent damage to the cell.

1.2 Mitosis

Mitosis is the process by which sister chromatids carrying identical copies of their replicated genome are segregated into two distinct daughter cells. Underlying this precisely coordinated series of events is a complex microtubule-based spindle, motor proteins which slide along microtubules and a complex series of molecular processes and biomechanical changes. [1, 2, 3, 4, 5, 6]. The early stage of mitosis (prophase - metaphase) is dominated by microtubule dynamics, motor proteins, capture of chromosome via kinetochore attachment and satisfaction of the spindle assembly checkpoint (SAC) of a bipolar spindle [1, 5, 7, 8, 9, 10, 11]. After satisfaction of the SAC, the cell initiates anaphase and sister chromatids unglue and segregate to opposite poles (Anaphase A) while the pole to pole microtubules elongate and push the poles apart (Anaphase B). [1, 7]

1.2.1 Microtubules

The most important subcellular structures for the successful completion of mitosis are the microtubules that form the bipolar mitotic spindle. Microtubules are essential cytoskeletal polymers that are made up of repeating α/β - tubulin heterodimers. An individual microtubule (MT) is a hollow cylinder of 25 nm diameter built from 13 protofilaments [12].

Microtubules interact with a large number of microtubule-associated proteins (MAPs), and provide structural stability to the cell. The motor proteins slide along them, and provide force for chromosome separation. [1, 9, 13, 14, 15]

Perhaps the most interesting feature of microtubules is that they are highly dynamic and undergo dynamic instability [16, 17]. This is characterized by alternating cycles of growth and catastrophe that results in a force-balance on the mitotic spindle. This non-equilibrium behavior is based on the binding and hydrolysis of GTP by tubulin subunits. Each tubulin monomer binds one molecule of GTP but β-tubulin can hydrolyze the nucleotide resulting in GDP-tubulin subunits which are unstable. [18, 19, 20] If this ”GTP cap” is stochastically lost, or induced via laser ablation [21], then the microtubule rapidly depolymerizes. The stability of the microtubules and its' rate equa-

tion change dramatically throughout the phases of mitosis and kinetochore attachment to the mitotic spindle. Further discussion regarding laser ablation of microtubules and the role of microtubules in the structure and dynamics of the metaphase bipolar spindle are in Chapter 3 and 5 respectively.

1.2.2 Why use lasers to study mitosis?

Mitosis is relatively short with most organisms having a 30 minute mitotic phase (depending on environmental conditions) out of a full 24+ hour cell cycle. Mitosis is further split into several phases and each phase involves a complex reorganization of the mitotic spindle including changes in protein and enzymatic reactions, and in the checkpoint(s) that are necessary to ensure that mitosis proceeds normally [1-11, 22]. This immense complexity presents several problems for traditional biochemical techniques which are mostly global and non-specific. For example, traditional anti-MT drugs [23, 24, 25] that have been used to study mitosis, such as nocodazole, taxol and colchine (colcemid) affect all of the main target substrates, the microtubules, present inside the cell. These drugs cause sufficient disruption to the cell that the mitotic spindle assembly checkpoint (SAC) will prevent the cell from proceeding further until the drug, and the effect, and washed out. Thus any attempt to study the mitotic pathways requires precise timing for the injection of the drug and even with perfect timing, the duration of metaphase and anaphase are so short that accurate measurement within that timeframe is difficult. Knockout (RNAi) or depletion of key proteins may be too catastrophic and the cell can't enter into mitosis due to the lack of vital proteins. In addition to the above disadvantages, most biochemical techniques are permanent such that the drug either can't be washed out, or injection of the protein (due to knockout) can't easily be accomplished because of the short duration of the key phases of mitosis. (prophase, metaphase, anaphase, and telophase).

Laser microscopy (microbeam irradiation) permits specific spatial-temporal disruption. Consequently, studies that require the alteration of a small subset of substrates can be performed. In this thesis dissertation, specific disruption of chromosomes, chromosome tips (presumptive telomeres), kinetochores and spindle microtubules is achieved, and subsequent cell responses are analyzed. These experiments could not be

performed using inhibitory drugs or other biochemical/molecular approaches that affect a much broader array of cell organelles and biochemical pathways.

1.3 Lasers in Biology Research: Mitosis

Laser surgery of biological cells and tissue has been studied and applied for over 40 years and has contributed to elucidating several key elements in mitotic systems. [26-34]. These experiments all took advantage of the high spatial-temporal specificity of the laser in order to study phenomena that could not be easily studied via biochemical techniques using drugs, RNAI knockouts, etc. In each case, experiments could not be easily performed using standard biochemical techniques to answer the specific question about the cellular effect of the loss of a specific subcellular compartment.

1.4 Scope of Thesis

Chapter 2 introduces the theory behind optical ablation and the type of damage done. Chapter 3 describes the optical setup used in a laser microscope and additional material and methods involved in this thesis. In chapter 4, Laser ablation of chromosome tips (presumptive telomere region) is performed, and the perturbation on cytokinesis is described. In chapter 5, laser ablation of the mitotic spindle in metaphase is performed, and the dynamic re-shaping of the spindle is described. In chapter 6, studies on the ablation of individual kinetochores and the subsequent movement of chromosomes are studied. In chapter 7, I present preliminary data on the perturbation of mitotic spindles in anaphase and the mislocalization of Aurora B due to the disruption. In Chapter 8, a collaborative study done with Samantha G. Zeitlin (SGZ) is described where laser ablation of chromatid was performed and recruitment of DNA repair and recognition proteins, in particular CENP-A, are analyzed. Finally, in chapter 9, I will discuss some of the future projects possible with the Robolase (laser microscope) system and present the conclusions of this thesis.

1.5 Summary

This chapter described the usage of lasers in biology, and focused particularly on the usage of lasers in mitosis. Mitosis is described since chapters 4, 5, 6 and 7 are performed specifically when the cells are in mitosis.

1.6 Bibliography

[1] Mitchison T.J., Salmon E.D. *Mitosis: a history of division* Nature Cell Biology 2001

[2] Mitchison T.J., Maddox P., Gaetz J., Groen A., Shirasu M., Desai A., Salmon E.D., Kapoor T.M. *Roles of polymerization dynamics, opposed motors and a tensile element in governing the length of Xenopus extract meiotic spindles* Mol. Biol. Cell 2005

[3] Walzak C.E., Heald R. *Mechanisms of mitotic spindle assembly and function* Int. Rev. Cytol. 2008

[4] Mogliner A., Wollman R., Civelekoglu-Scholey G., Scholey J. *Modeling mitosis* Trends Cell Biology 2006

[5] Gatlin J.C., Matov A., Danuser G., Mitchison T.J., Salmon E.D. *Directly probing the mechanical properties of the spindle and its matrix* Journal of Cell Biology 2010

[6] Sharp D.J., Rogers G.C., Scholey J.M. *Roles of motor proteins in building microtubule-based structures: a basic principle of cellular design.* Biochim. Biophys. 2000b

[7] Uchida K.S.K., Takagaki K., Kumada K., Hirayama Y., Noda T., Hirota T. *Kinetochore stretching inactivates the spindle assembly checkpoint* J. Cell Biology report 2009

[8] Maresca T.J., Salmon E.D. *Intrakinetochore stretch is associated with changes in kinetochore phosphorylation and spindle assembly checkpoint activity* Journal Cell Biology 2009

[9] Loncarek J., Kisurina-Evgenieva O., Vinogradova T., Hergert P., La Terra S., Kapoor T.M., Khodjakov A. *The centromere geometry essential for keeping mitosis error free is controlled by spindle forces* Nature 2007

[10] McIntosh J.R., Grishchuk E.L., Morphew M.K., Efremov A.K., Zhudenkov K., Volkov V.A., Cheeseman I.M., Desai A., Mastronarde D.N., Ataullakhanov F.I. *Fibrils connect microtubule tips with kinetochores: A mechanism to couple tubulin dynamics to chromosome motion* Cell 2008

[11] Huang H., Hittle J., Zappacosta F., Annan R.S., Hershko A., Yen T.J. *Phosphorylation sites in BubR1 that regulate kinetochore attachment, tension and mitotic exit* Journal of Cell Biology 2008

[12] Nogales E. *Structural insights into microtubule function.* Annual Review Biochemistry 2000

[13] Welte M.A. *Bidirectional transport along microtubules* Current Biology. 2004

[14] Cai S., Weaver L.N., Ems-McClung S.C., Walczak C.E. *Kinesin-14 family proteins HSET/XCTK2 control spindle length by cross-linking and sliding microtubules* MBoC 2009

[15] Kapitein L.C., Peterman E.J.G., Kwok B.H., Kim J.H., Kapoor T.M., Schmidt C.F. *The bipolar mitotic kinesin Eg5 moves on both microtubules that it crosslinks* Nature 2005

[16] Mitchison T., Kirschner M *Dynamic instability of microtubule growth* Nature 1984

[17] Desai A., Mitchison T.J. *Microtubule polymerization dynamics* Biophysics Journal 2004

[18] Janosi, I.M., Chretien D., Flyvbjerg H. *Structural microtubule cap: Stability, catastrophe, rescue, and third state* Biophysics Journal 2002

[19] Hinow P. *Continuous model for microtubule dynamics with catastrophe, rescue and nucleation processes.* Physical Review E 2009

[20] Joglekar A.P., Hunt A.J. *A simple, mechanistic model for directional instability during Mitotic chromosome movements* Biophysics Journal 2002

[21] Wakida N.M., Lee C.S., Botvinick E.L., Shi L.Z., Dvornikov A., Berns Michael *Laser nanosurgery of single microtubules reveals location-dependent depolymerization rates.* J Biomed Opt. 2007

[22] Ferenz N.P., Paul R., Fagerstrom C., Mogilner A., Wadsworth P. *Dynein antagonizes Eg5 by crosslinking and sliding antiparallel microtubules* Current Biology 2009

[23] Sept D., Limbach H.J., Bolterauer H., Tuszynski J.A. *A chemical kinetics model for microtubule oscillations* Journal theoretical biology 1999

[24] Goshima G., Wollman R., Stuurman N., Scholey J.M., Vale R.D. *Length control of the metaphase spindle* Current Biology 2005b

[25] Severin F., Habermann B., Huffaker T., Hyman T. *Stu2 promotes mitotic spindle elongation in anaphase* J. Cell Biology 2001

[26] Ilagan A.B., Forer A., Spurck T. *Backward chromosome movement in anaphase, after irradiation of kinetochores or kinetochore fibres* Protoplasma 1997

[27] Forer A., Spurck T., Pickett-Heaps J.D. *Ultraviolet microbeam irradiations of spindle fibres in crane-fly spermatocytes and newt epithelial cells: resolution of previously conflicting observations* Protoplasma 1996

[28] McNeill P., Berns M.W. *Chromosome behavior after laser microirradiation of a single kinetochore in mitotic PtK2 cells* Journal of Cell biology 1981

[29] Aist J.R., Bayles C.J., Tao W., Berns M.W. *Direct experimental evidence for the existence, structural basis and function of astral forces in anaphase B in vivo* J. Cell Science 1991

[30] Aist J.R., Berns M.W. *Mechanics of chromosome separation during mitosis in Fusarium (fungi imperfecti): New evidence from ultrastructural and laser microbeam experiments* J. Cell Biology 1981

[31] Aist J.R., Liang H., Berns M.W. *Astral and spindle forces in PtK2 cells during anaphase B: A laser microbeam study.* J. Cell Science 1983

[32] Botvinick E.L., Venugopalan V., Shah J.V., Liaw L.H., Berns Michael *Controlled ablation of microtubules using a picosecond laser* Biophysics Journal 2004

[33] Khodjakov A., La Terra S., Chang F. *Laser microsurgery in fission yeast: Role of the mitotic spindle midzone in anaphase B* Current Biology 2004

[34] Spurck T.P., Stonington O.G., Snyder J.A., Pickettheaps J.D., Bajer A., Molebajer J. *UV Microbeam irradiations of the mitotic spindle. 2. Spindle Fiber dynamics and force production* J. Cell Biology 1990

2 Optical ablation

2.1 The Laser

'Laser' is an acronym for Light Amplification by Stimulated Emission of Radiation. In a laser, an active laser medium, referred to as a 'gain medium' is placed within a resonant optical cavity [Reviewed 1, 2]. An external energy source, such as a light-emitting diode array or flash lamp, pumps the electrons of the gain medium into an excited energy state. If the electrons relax back to the ground state (nanosecond time scale) then spontaneous emission occurs resulting in emitted photons of narrow spectral bandwidth, random orientation, direction, polarization and phase. This spontaneous emission can be transient or a stable mode depending on the resonant cavity mirrored walls and the boundary conditions supplied by them. A spontaneous emission will eventually occur that is in a stable propagating mode within the boundary conditions of the laser cavity and along the optical axis. This spontaneously emitted photon serves as the seed catalyst whereby the dipole to dipole interactions between the photon and the gain medium causes any further electrons that emit photons to be identical in phase, frequency, polarization, and direction. This stimulated emission ensures that all further photons made from the gain medium have a narrow range of phase, frequency and polarization. Photons traveling back and forth due to reflection of the mirrored ends of the resonant cavity will stimulate the emission of more photons with identical characteristics resulting in a 'avalanche' effect where the single seed photon produces millions of identical photons. The resonant cavity's mirrors are designed so that a percentage of light passes through one of the mirrors (typically 95% reflectance range) and is totally reflected by the other. The 'power lost' from the resonant cavity is the actual 'useful' light and the laser beam is typically collimated, coherent, monochromatic, po-

larized and of a constant power. Conventional illumination sources (halogen, mercury arc lamp, etc.) are incoherent, have wide spectral content, are randomly polarized, and have random intensity fluctuations.

2.2 Light

The functional principles of the laser can only be described by both wave and particle characterization. The wave nature of light is helpful when considering the propagation and focusing of light, while the particle description is necessary for describing and understanding light-matter interactions.

In the wave description of light, light propagates as a transversely propagating oscillation of an electric field. $E = \mathbf{Eo}*\mathbf{Re}[\mathbf{Exp}(-\mathbf{ikx}-\mathbf{i}\omega\mathbf{t})]$. In this expression, Eo is a vector whose magnitude and direction corresponds to the amplitude and polarization of the oscillation. $\mathbf{k} = (\mathbf{2}\pi/\lambda) * \mathbf{z}$ is the wave vector and defines the direction of propagation which is typically taken to be the z-axis (optical axis) as indicated by the unit vector. $\omega = 2\pi c/\lambda$ is the angular oscillation frequency of the wave. λ is the wavelength and $c = 3.0 * 10^8$ m/s is the speed of light in a vacuum. In the particle description, light is quantized such that a single photon (energy quanta) has energy of $E = hc/\lambda$ where $h = 6.626 * 10^{-34}$ J/s as Planck's constant.

Dependent on the resonant cavity described previously, specific boundary conditions constrain the stable modes that can propagate and continue inside the cavity. With respect to this thesis and producing a diffraction limited Gaussian spot, we will be using TEM_{00} mode. Assuming zero order mode reduces the Gaussian distribution function to $TEM_{00} = exp[-(x^2 + y^2)/(w^2)]$ [3] and is accurate for the minimum achievable beam spot size with our system..

2.3 Gaussian Beam

TEM_{00} (Gaussian beam) has several important properties that are relevant for microbeam applications. In particular, these are the minimum focal volume that the laser can be focused to and the stable propagation of this mode from the resonant cavity

to the microscope as well as the energy delivered to the micron size region.

The Gaussian beam intensity profile is given by $I(r) = Ioexp(-2(r^2)/w^2)$ where Io is the peak irradiance, r is the transverse radius $r = (x^2 + y^2)^{1/2}$. At $r = w$, the irradiance has fallen to $1/e^2$ of its' peak value and 86.5% of the Gaussian beam's total power is contained within radial locations smaller than w. The beam radius w is not constant but varies as the Gaussian beam propagates and is given by $w(z) = w_o[1 + ((\lambda z)/(\pi w_o^2))^2]^{1/2}$. At $z = 0$, the beam radius attains a minimum value of w_o which is known as the beam waist and $2w_o$ is often referred to as the beam spot size. The placement of optical elements and beam expander (Chapter 3 of this thesis) ensures that a Gaussian beam enters into the back aperture of the microscope objective. The microscope objective acts as a thin positive lens and it is useful to define a numerical aperture (NA) for the objective which is the radius of the objective divided by the focal length of the objective, $NA = d/2f$. Since the Gaussian beam enters the microscope such that the propagating beam width $2w_o$ fills the aperture of the objective, the objective is placed at the beam's waist and thus focuses the beam to a new w_o'. This w_o' can be calculated as $2w_o' = 1.22\lambda/NA$. This is used in Chapter 3 in calculating the minimum beam spot size for a given NA and wavelength.

2.4 Types of damage

In the previous section, we discussed how a diffraction limited micron sized beam could be focused into a microscope and deliver a specific amount of energy density to a tight focal volume. The studies reported here only use a 532 nm, 12 picosecond laser and the discussion about damage mechanisms will be confined to that system [see 1 and 4 for more comprehensive review].

The mechanisms of damage are typically the following: linear absorption, photothermal, photomechanical and photochemical processes. Linear absorption damage involves the optical absorption of photons by biological chromophores. In this process the light has a high energy density such that the absorbing material (like water, DNA, protein, etc.) is vaporized. This is discussed in detail elsewhere [1, 4]. The absorption coefficient of the material of interest is typically 2-20 cm^{-1} and for an NA of 1.3,

pulse power of 1.3 microjoules, it is not possible to microsurgically vaporize the desired biological material.

When photons are absorbed, they excite molecules from a lower energy state to a higher energy state. This energy can relax back to ground state via emitting of an identical photon or it can lose energy due to vibrational modes (in particular chemical bonds) of molecules. The energy going into vibrational modes is known as a "electron-phonon" interaction and typically occurs in picosecond timescale (as opposed to re-emission of photon in nanosecond time scale). This vibrational energy increases the temperature of the material. Of interest for this thesis is the thermal diffusion time $T_d = (0.124(\lambda)^2/\kappa(NA)^2$. Typical values for NA (0.8 to 1.3) and range of wavelength (337-1064 nm) reveals characteristic thermal diffusion times in the range of 60 ns to 1.5 microseconds [4]. This means that laser sources with pulse durations shorter than 60 ns (in this thesis, we use 532 nm 12 ps) have "thermal confinement" due to the time scale that energy is deposited into the focal volume.

Temperature increase in a material also results in thermal expansion and if the energy is delivered on a time scale faster than the sample can expand, then significant transient stresses can develop: I.e. If the energy deposited is on a time scale longer than the time it takes for an acoustic wave to propagate out of the heated volume, then there is reduced thermoelastic stress. The characteristic time for stress wave propagation can be calculated by $t_m = 0.61\lambda/(c_a(NA))$ where c_a is the speed of sound in the material. Typical wavelengths ranging from 337-1064 nm have characteristic stress propagation times in the range of 100-550 ps [4]. In this thesis, the 12 picosecond laser pulse duration is significantly below this range such that thermoelastic stress confinement is achieved in the focal volume. In an earlier study thermoelastic damage on microtubules is examined and, due to small cylindrical size of microtubules (20nm) is not likely the method of damage that occurs in the studies reported here [5].

High photonic energy can exceed the dissociation energy of many molecular bonds [4, 6, 7] and result in chemical changes in the targeted material. This requires a higher energy dose (UV) and is typically on a macrosize scale (tissues) and not observed as a dominant mechanism in subcellular nanosurgery applications.

2.4.1 Multiphoton, microplasma damage

Since 532 nm has a low absorption coefficient by most common cellular constituents it can achieve a deeper penetration depth in most living cells. This 'low' absorption and high cellular transparency implies that at low intensities photons don't interact with the cellular material. When light passes through it transiently interacts with the electrons of the molecules via dipole-dipole interactions and can be considered to temporally excite electrons into forbidden energy levels. The lifetime of this interaction is in the short femtosecond (10^{-15}) range and the photon typically passes straight through without permanently altering the material. In the case of high energy density, high photon density in a confined material, then there is the probability of multiphoton absorption within this femtosecond time scale such that multiple photons are spatially localized and k photons interact simultaneously with a molecule to promote it from a ground state to an excited state. A multiphoton event could be considered a "single-photon" absorption where $\lambda_{sp} = \lambda_{mp}/k$. In the case of 532 nm and a 2 photon absorption, this corresponds to 266 nm which is in the UV range and is highly absorbed by most material. Multiphoton absorption is used in this thesis to precisely deliver a specific energy dosage inside a biological material (depth penetration) without interacting with material not in the focal plane. Multiphoton absorption could be responsible for nonlinear absorption and vaporization of material but for microtubules and DNA (the target substrates for this thesis) a large enough energy and interaction is probably not provided.

Nonlinear absorption refers to changes in the intrinsic absorption coefficient of a material at high irradiances. This typically occurs at irradiances of $10^{10} - 10^{13}$ W/cm^2 even in normally transparent media such as water and cytoplasm [4]. The high electric field strengths lead to ionization of the medium and generation of a quasi-free electron. In terms of this thesis and using picosecond multiphoton absorption, a 'seed' electron is generated via a multiphoton absorption. This 'seed' electron can absorb more photons and this imparts kinetic energy to the electron which can then move and hit other electrons, imparting kinetic energy to them and making them quasi-free electrons. This leads to a avalanche effect where a quasi-free electron density of 10^{21} cm^{-3} can be created. This is referred to as 'plasma formation' and when induced by a laser beam produces an

”optical breakdown” of the material. Multiphoton ionization, in which a high density of photons all interact to generate individual quasi-free electrons, can also occur and in the time scale of this thesis it is likely that both processes can contribute, but multiphoton ionization is the dominant mechanism.

The elevated free electron density (plasma) formed results in extremely localized elevation of temperature and pressure (called a plasma gas). The evolution of complex thermomechanical processes that result in terms of thermal diffusion, thermoelastic, and phase transition is described in the literature [1, 6, 7]. For picosecond pulse durations used in the research reported here, the microplasma formed results in direct vaporization of the cellular material due to the high temperature and pressure generated in the focal volume. For microtubules, a sub-plasma ’microplasma-mediated’ ablation has been described in which only vaporization occurs but the damage is confined [5, 8]. At higher powers and in most plasma formation cases, the plasma expands and compresses the surrounding material and a radiating shock-wave ensues. The expansion also cools the plasma leading to electron-ion recombination and the formation of a cavitation bubble that expands and then collapses resulting in catastrophic mechanical damage to the immediate surrounding material.

The values used in this thesis and described in [5] can be less than the irradiances listed here since thermal absorption coefficients can play a role in lowering the threshold density for microplasma ablation. For DNA damage via multiphoton and microplasma damage see [9] in which DNA is disrupted either due to a microplasma-mediated event or due to multiphoton breakage of bonds.

2.5 Summary

This chapter described the physics behind lasers, propagation of lasers into the microscope, optical ablation and the mechanism of damage in ablating microtubules and DNA which, in terms of this thesis, is predominately multiphoton and microplasma based.

2.6 Bibliography

[1] Vogel A., Noack J., Huttman G., Paltouf G. *Mechanisms of femtosecond laser nanosurgery of cells and tissues* Applied Physics. B 2005

[2] Svelto O. *Principles of Lasers* Plenum Press 1998

[3] Silfvast, W.T. *Laser fundamentals* Cambridge, New York, NY 1996

[4] Berns Michael, Greulich K.O., et al. *Laser manipulation of cells and tissues.* Methods Cell Biology; Vol 82 2007

[5] Botvinick E.L., Venugopalan V., Shah J.V., Liaw L.H., Berns Michael *Controlled ablation of microtubules using a picosecond laser* Biophysics Journal 2004

[6] Venugopalan V., Guerra A., Nahen K., Vogel A. *Role of laser-induced plasma formation in pulsed cellular microsurgery and micromanipulation* Physical Rev. Letter. 2002

[7] Vogel A., and Venugopalan V. *Mechanisms of pulsed laser ablation of biological tissues.* Chemistry Review 2003

[8] Vogel A., Capon M.R.C., Asiyo-Vogel, M.N., and Birngruber, R. *Intraocular photo disruption with picosecond and nanosecond laser pulses:Tissue effects in cornea, lens, and retina.* Investig. Ophthalmol. Vis. Sci. 1994

[9] Kong X., Mohanty S., Stephens J., Heale J., Gomez-Godinez V., Shi L.Z., Kim J., Yokomori K., Berns M.W. *Comparative analysis of different lasers systems to study cellular responses to DNA damage in mammalian cells* Nucleic Acids Research 2009

3 Hardware, software and optical design

3.1 Introduction

For this dissertation, we developed a laser microscope system (hereafter referred to as Robolase) to apply a specific laser energy dosage to specific regions of cells in mitosis or interphase. By developing a customized system, all the laser and optical parameters can be precisely controlled. This chapter will describe the microscope, hardware and software of the robolase system that is used in all experiments.

3.2 RobolaseII Microscope, hardware and software

All laser ablation experiments in this dissertation used a Axiovert 200M (Zeiss, Thornwood, NY) with motorized objective turret, reflector turret, condensor turret, and a 63x plan-apochromat phase III, NA 1.4 oil immersion objective. The microscope has a built-in computer, which uses a controller area network (CAN) to communicate with motors and encoders within the microscope stand. The CAN can receive commands through a serial interface attached to a computer running an image acquisition/microscope control program. Custom-made Robolase Labview software controls the microscope through CAN.

The motorized reflector turret is shift-free, which allows repeated switching between filter cube positions with no detectable pixel shifts. This allows fluorescence images to be taken on one filter cube position then switched to an empty filter cube

position (the laser firing port) and the laser ablation event will occur at the pre-selected pixel location. The reflector turret contains several filter cubes for CFP, YFP and 49002 ET GFP C104267. (all filters are manufactured by Chroma Corp., Bellows Falls, VT) Motorized objective focus control is achieved through the CAN by the Zeiss Harmonic Drive DC motor, providing 25 nm steps with 10 mm travel for precise focus control.

Specimens were mounted in an X-Y stepper stage (Ludl Electronic Products, Hawthrone, NY) controlled with a PXI-7344 stepper motor controller (National Instruments, Austin, TX) and an MID-7604 power drive (National Instruments). The motion board was mounted in a PXI chassis (National Instruments), connected to the host computer through two MXI4 boards (one in the PXI chassis, the other in the host computer) through the MXI-3 fiber-optic cable (National Instruments).

Robolase implements a Hamamatsu Orca-AG deep-cooled 1,344 by 1,024 pixel 12-bit digital CCD camera (Hamamatsu Photonics, K.K., Hamamatsu, Japan) with digital (fire wire) output. The ORCA can read out sub regions of the chip for increased frame rates, bin pixels for increased signal-to-noise characteristics, and adjust gain and exposure time to trade off between signal-to-noise characteristics and arc lamp exposure times. Robolase uses Hamamatsu's video capture Library for Labview plug-in to communicate with the ORCA camera controller through its DCAMAPI driver.

3.3 Laser and Optical Path

Optics outside the microscope stand were used to guide the laser into the microscope and supply RLII system with automated laser power control, laser exposure time, and laser target acquisition. The laser was a 1064 nm diode-pumped Spectra-Physics Vanguard system with a second harmonic generator (SHG). This provided a TEM_{00} mode 532 nm linearly polarized laser beam with 100:1 purity, 76 Mhz repetition rate, 12 ps pulse duration, and a 2 W average output power. Laser power was controlled by rotating a glan linear-polarizer (CLPA-12.0-425-675, CVI laser, LLC, Albuquerque, NM) mounted in a motorized rotational mount, driven by a 2-phase stepper motor with a 0.05 degree accuracy (PR50PP, Newport Corp). The stepper motor was used to rotate a 2nd polarizer and to specify the angle difference and thus the amount of power

passing into the microscope. A mechanical shutter (Uniblitz, S6ZM2, Vincent Associates Rochester, NY) with a 30-ms duty cycle controlled by a shutter drive (Uniblitz VMM-D3, Vincent Associates) was used to gate the main laser beam to provide controlled bursts of the 76 Mhz beam of 12 ps pulses to the microscope. The laser was then expanded using an adjustable-beam expander (2-8x, 633/780/803 nm correction, Rodenstock, Germany) to completely fill the back aperture of the objective. Telecentric beam steering was achieved using a single dual-axis fast scanning mirror (FSM-300, Newport Corp, Newport, CA) at an image plane conjugate to the back focal plane of the microscope objectives. This image plane is formed by a 250 mm biconvex lens positioned with its front focal plane at the image plane of the microscope *Berns-Keller* port (below the microscope stand) and with its' back focal plane at the fast scanning mirror surface. To access the sub-microscope *Berns-Keller* port, the microscope is raised 70 mm above the table via custom-machined metal alloy posts to leave room for a 458 mirror which vertically redirects incident laser light running parallel to the table through the *Berns-Keller* port. Once inside the microscope stand, the laser light passes through the tube lens and an empty filter cube position of the reflector turret before entering the back of the objective lens. All external mirrors in the ablation laser light path are virtually loss-less dielectric mirrors optimized for 45 degree reflections of 532 nm S-polarized light (Y2-1025-45-S, CVI Laser LLC, Albuquerque, NM).

3.4 Labview

The PXI-7344 computer chassis runs LabVIEW Realtime operating system, which is a graphics-free computing environment designed to maximize performance of control hardware. The RoboLase host computer communicates with the PXI chassis through a local area network (100 Mbps) running TCP/IP protocols. Software for computer control of all hardware and image acquisition was custom coded in the Labview 8.2 (National Instruments) programming language [1]. On the captured computer screen image of the target, shapes were first selected (line or rectangle) and then projected on one or more regions of interest (ROI) on the image. The Robolase software then calculates the number of pixels inside the designed ROI, and using the user-defined ablation

spot size, calculates the number of 30 ms laser exposures necessary to fill in the target ROI. Each 30 ms exposure received 2,280,000 of 12 ps pulses with the fast scanning mirror (FSM) directing each laser exposure to the ROI until the entire ROI is irradiated.

The exact operation and manual for usage of the Robolase microscope using Labview is described in the Appendix.

3.5 Okolab

The basic water jacket microscope stage incubator (MSI) from okolab can be mounted on the Axiovert 200M Zeiss microscope for a temperature and CO_2 controlled environment. The temperature control is set to 37 degrees Celsius via a water jacket and the CO_2 is kept at 5% by injecting a calibrated mixture of CO_2 and air (http://www.oko-lab.com/182.page).

3.6 Constructs and Cell Lines

Cells and methods of cell culture used in these studies were from established sub-lines of rat kangaroo (*Potorous Tridactylis*) kidney epithelium, PtK2. [2, 3].

3.6.1 Measuring laser power

Energy measurements were made by calibrating the photodiode output to laser power measured in the specimen plane. To estimate laser power in the specimen plane, laser output was collected onto a precalibrated laser light meter (Newport Optical Meter, 1918 C). The objective is removed from the objective turret and the shutter is kept continuously open to measure the laser power 'before objective' but after passing through the *Berns-Keller* port and reflector turret. The transmission of the objective was measured using the established dual-objective method [4]. This method corrects for total internal reflection losses at the objective oil-glass-water interfaces. The transmission of the Zeiss 63x/ 1.4 NA objective was determined to be 0.68. The laser pulse energy at the object focal plane was determined by measuring the input energy at the back aperture of the objective ('before objective') multiplied by the transmission factor (0.68) of the

objective. In measuring the power, the shutter is kept continuously open, but for each ablation event, a 30ms exposure time is used which corresponds to 2.28 x 10^6 pulses (12 ps each) per focused spot of 0.17 μm^2. Individual 12 ps pulse energy in the focal spot was 0.098 nJ/pulse. Using a diffraction limited spot diameter of 464 nm and r = 0.61 λ/NAobj) (oil-objective 1.3 NA, 532 nm) gives a peak irradiance of 4.9 x 10^{10} W/cm^2 in the focused spot for ablating chromosomes (discussed in detail in Chapter 6).

For spindle microtubule ablation, the power was measured at the back aperture of the objective and it was determined that the individual 12 ps pulse energy in the focal spot was 0.019 nJ/ pulse. Since the 63X (1.4 NA) microscope objective focuses the beam to a diffraction limited spot diameter of 464 nm, we have a peak focal spot irradiance of 0.885 x 10^9 W/cm^2. For one line scan of 5 micrometer (with $\approx$ 10 spots/line), 0.43 μJ of total energy (energy/pulse x no. of pulses per spot x no. of spots in the line) was delivered to each irradiation site.

3.6.2 Calibrating laser power

A series of control experiments was performed to determine the minimum laser power needed to consistently create mitotic spindle disruption (DNA damage and markers will be discussed in Chapter 8 on CENP-A recruitment). Spindle microtubules were fluorescently tagged (CFP) and upon laser ablation, selected regions would have a loss of fluorescence followed by spindle collapse and partial spindle repolymerization. While this result strongly suggests that the microtubules were disrupted, transmission electron microscopy (TEM) was performed in order to demonstrate that the microtubules in the laser-exposed region of the spindle were ablated and the microtubules outside the laser exposure region were unaffected. (Figure 3) The power used was approximately the same as reported elsewhere. [3]

3.7 Summary

For this dissertation, a custom made optical system for laser ablation studies was designed and built. This chapter described the Robolase microscope and the materials and methods used in performing the experiments in Chapters 4, 5, 6, 7 and 8. The

microscope setup and material also applies to chapter 8, but chapter 8 has additional material and methods.

3.8 Figures

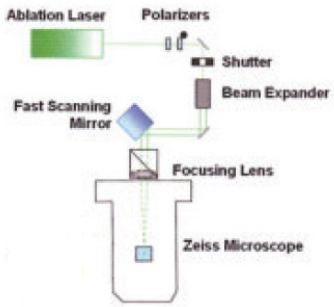

Figure 3.1: A top-down view of RobolaseII Microscope and Laser Path.

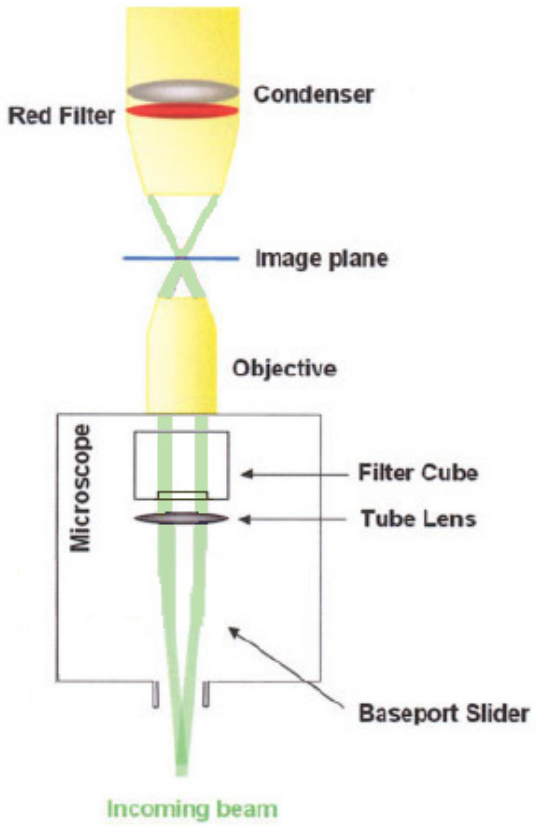

Figure 3.2: A side-view of RobolaseII Microscope.

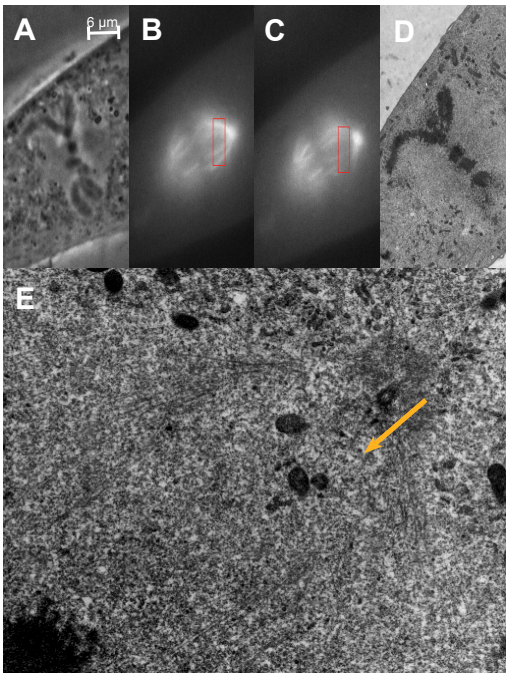

Figure 3.3: Transmission Electron Microscope of severed microtubules. A is normal phase image, B is pre-cut of CFP tubulin, C is post box cut of CFP tubulin, D is TEM image in plane of chromosomes. E is TEM image in plane of cut and the arrow points to a clear area with no microtubules present while microtubules are present on each side.

3.9 Bibliography

[1] Botvinick E.L., Berns Michael *Internet-based robotic laser scissors and tweezers microscopy.* Microscope Res. Tech. 2005

[2] Berns Michael, Aist J., Edwards J., Strahs K., Girton J., McNeill P., Rattner J.B., Kitzes M., Hammer-Wilson M., Liaw L.H., Siemens A., Koonce M. *Laser microsurgery in cell and developmental biology* Science 213 1981

[3] Botvinick E.L., Venugopalan V., Shah J.V., Liaw L.H., Berns Michael *Controlled ablation of microtubules using a picosecond laser* Biophysics Journal 2004

[4] Hiroaki Misawa, Masanori Koshioka, Keiji Sasaki, Noboru Kitamura, Hiroshi Masuhara *Three-dimensional optical trapping and laser ablation of a single polymer latex particle in water* Journal of Applied Physics 1991

4 Optical Manipulation of Chromosomes in Anaphase

4.1 Introduction

Genome maintenance occurs at a variety of levels to ensure high fidelity inheritance by progeny cells. Base-pair lesions, breaks and unattached chromosomes are detected and resolved by surveillance systems that act in part through inhibiting cell cycle machinery. When the underlying genomic instability cannot be repaired, or the surveillance mechanism is dysfunctional, there is evidence for progression to malignancy [1, 2]. Lesions in DNA can occur throughout the cell cycle, and are sensed by specific checkpoint pathways in interphase [3]. DNA damage response mechanisms during mitosis, however, remain relatively unexamined.

Reports of responses to DNA damage in mitosis are varied, and thus far have only addressed the period of mitosis before anaphase onset. A number of studies using laser-mediated ablation or chemical damage of chromosomes have reported no apparent effect on anaphase onset [4, 5, 6]. In other studies, damage during mitosis was observed to delay anaphase onset. Notably, high levels of damage induced by laser pulses resulted in a spindle assembly checkpoint-mediated delay of anaphase onset [7]. In addition, bleomycin-treated nocodazole-arrested U2OS cells were delayed in mitotic exit after both the damaging agent and nocodazole was removed [8]. Thus, while coupling DNA damage and repair to the spindle assembly checkpoint has been observed [7, 8], it is not clear whether these mechanisms are related to the sensing of DNA damage during anaphase.

Cells of the long-nosed potoroo (*Potorous tridactylis*, PtK2) have been widely

used to image, at high resolution, chromosome and kinetochore movements during mitosis. Because of the large size and small number of chromosomes, these cells have been used in a significant number of studies employing laser-mediated damage. An apparent lack of response to laser exposure, even when the damage is significant, such as severing chromosome arms from kinetochores, has been demonstrated [9]. However, upon significant damage to kinetochores, mitosis is perturbed in a spindle assembly checkpoint-dependent manner [7, 10]. Thus, while the threshold for damage may be specific, cells have been observed to mount a checkpoint response to chromosomal damage at an early stage of mitosis, which resulted in arrest prior to anaphase onset.

Here, we investigate the effect of chromosome damage imposed after anaphase has begun, as defined by the morphological criterion that the chromosomes are visibly beginning to separate. Using laser-mediated damage, we demonstrate that focal damage to chromosomes at regions other than the chromosome tips does not cause cells to arrest, with almost all cells proceeding through cytokinesis. However, targeting the chromosome tips, the presumptive telomeres, on chromosomes at either the cell periphery or closer to the spindle interior, causes delay and failure of cytokinesis. Together, these observations implicate a role for a putative telomere-based signaling pathway that couples post-segregation damage to completion of cell division.

4.2 Cell division is disrupted after damage to chromosome tips (presumptive telomeres)

To investigate the response to DNA damage in mitosis after anaphase onset, laser-mediated DNA ablation was directed at cells in which the chromosomes were visibly beginning to separate. Laser energy was applied to the chromosome arms, chromosome tips, or cytoplasm (Figure 1A, B, C respectively) to evaluate the effects of disrupting these structures on mitotic progression. Laser ablation of the cytoplasmic region distal from the midzone resulted in no discernable morphological changes by phase-contrast microscopy (Figure 1C and 2A). This observation was made despite earlier studies that detected the formation of phase-dense granules when longer pulse duration systems (e.g ns pulses) were used on interphase cells [16]. Targeting of chromosome

arms resulted in either a severing of the arm and production of a chromatin fragment free from the motion of the chromosome body [Figure 1A and 2B], or an optical phase-contrast lightening (i.e. change in refractive index) in the irradiated region of the chromosome without distinct severing of the chromosome arm (data not shown, but similar to the phase-lightening seen in Figure 1B following tip irradiation). Finally, targeting of chromosome tips can be observed by loss of chromosome tip structure, also indicated by a distinct phase-lightening at the irradiation site (Figure 1B). These morphological changes helped verify that the laser targeting was accurate and of the expected dose.

Different effects were observed on the progression of anaphase and cytokinesis, depending on the location of the laser damage. In cells targeted with selective focal laser damage to the cytoplasm during anaphase, distal from the midzone, normal timing of cell division was observed, as defined by comparison with non-ablated cells (20 +/- 6 minutes from anaphase ablation, mean +/- stdev, N = 45 cells, Figure 2A, and see Figure 7 for the timing of all conditions) consistent with previous reports [17, 18]. In cells targeted with selective focal laser damage to non-telomere regions of chromosome arms during anaphase, normal timing of cell division, including completion of cytokinesis was again observed (Figure 2B, 16 +/- 4 minutes, N = 95 cells) and was also consistent with previous reports [17, 18].

In contrast, targeting of chromosome tips during anaphase resulted in a significant proportion of cells with perturbed mitotic progression (61%, N = 94/132 cells). Approximately one-third of the tip-targeted cells underwent cytokinesis with timing similar to control non-ablated cells (29%, 27 +/- 10 minutes, N = 38 cells), whereas the remainder of tip-targeted cells could be divided into three categories: (1) cells that did not initiate a furrow over a period of time greater than two hours (Figure 3A, 18%, N = 24 cells) (2) cells that were delayed in furrow formation (Figure 3B, 39%, 65 +/- 17 minutes, N = 52 cells) or (3) cells that exhibited furrow regression after initiating cytokinesis (Figure 3C, 14%, N = 18 cells).

Chromosome tip ablation was observed to exert a dramatic effect on duration of cell division (Figure 4A). While almost all control cells (greater than 90%), including non-ablated and those subjected to cytoplasmic ablation distal from the midzone or chromosome arm ablation, completed cytokinesis within 30 minutes, 68% of cells in which

chromosome tips were ablated did not complete cytokinesis within this time frame. Of the cells that delayed, approximately half exhibited an extended delay, particularly in the earliest stages of cytokinetic furrow ingression (Figure 4B, Blue). Cytokinesis was completed with normal timing in those cells where furrow initiation was successful. The remainder of delayed cells did not complete cytokinesis during the observation time, such that 43% initiated a furrow, but eventually showed furrow regression after an extended delay (Figure 4B, Green). The remaining cells (57%) did not initiate an observable furrow (Figure 4B, Red). These observations indicate that, unlike damage to a chromosome arm or even catastrophic loss of an arm fragment (Figures 1A and 2B), damage to a chromosome tip is sensed by a mechanism that impacts progression through cytokinesis by blocking furrow formation, delaying furrow formation, or inducing furrow regression.

The targeting of damage to anaphase chromosome tips likely includes telomeric regions, and suggests a specific cellular response when these regions are damaged during anaphase versus damage to other regions of the chromosome. Another possible cause of these apparent cellular responses could be exposure of other cellular structures near the chromosome tips, such as the spindle midzone, and the associated microtubule-based structures. Catastrophic damage to the spindle midzone at this early stage of anaphase has been shown to induce complete and irreversible arrest of cytokinesis [19]. To control for this, we performed control cytoplasmic targeting on cellular structures other than chromosomes, including near the plasma membrane, and near the spindle midzone were performed. In a separate control cohort consisting of 33 cells in which the laser was focused adjacent to the tips of the longer chromosomes and near the spindle midzone similar to tip ablation, all cells completed cytokinesis without exhibiting the no furrow or furrow regression responses. The targeting of mitotic midzone structure did result in some cytoplasmic blebbing and a moderate delay in completion of cytokinesis (Figure 2C, Figure 4B, Figure 7) but not the prolonged delay seen with chromosome tip ablation. In addition, when the tips of the smaller chromosomes located in the center of the anaphase chromosome mass, considerably removed from both the midzone and cell membrane, were irradiated, 12 of 20 cases (60%) exhibited either no furrow initiation, or furrow regression. Therefore, we conclude that the chromosome tip, rather than any

cytoplasmic or microtuble-based structure, is the source of a signal that results in altered cytokinesis.

There are three distinct responses to chromosome tip damage: 1) lack of furrow initiation, 2) an extended delay in furrow initiation, but eventual cytokinesis, or 3) furrow initiation followed by furrow regression. While we expect that the chromosomal sites (the tips) being targeted are likely similar in all cases, the difference in outcome could be the result of activating distinct pathways based on the timing within anaphase. It is also possible that variations in the accuracy of targeting, and/or the amount of laser-induced damage, are responsible for the different categories of the observed responses. Nevertheless, our observations demonstrate that after furrow initiation, furrow regression is a frequent result when anaphase chromosome tips are damaged.

4.3 Cytokinetic defects increase with number of telomere ablations.

To determine if there is a relationship between the number of chromosome tips damaged and the effect on cytokinesis, multiple (i.e. two to three) chromosome tips were irradiated in the same cell, each with the same energy dose. Almost half of the cells subjected to multiple tip ablation (Figure 7 1, Figure 3D, 47%, N = 41/87) did not form a furrow, a 2.6 fold increase when compared to single tip ablation. The remaining cells had similar outcomes when compared to the single ablations, however the distribution of outcomes was biased towards furrow regression. With multiple ablations, 24% of cells exhibited furrow regression, as compared to 14% in the single ablation experiments. The percentage of unperturbed cells dropped from 29% to 17% as a result of increasing the number of damaged tips, suggesting an additive effect. The remaining 11% showed a delay similar to single tip ablations (Figure 3E, 65+/-18 minutes, N = 10/87). These results demonstrate that multiple tip ablations changed the proportion of cells with a specific outcome, without changing the timing of the cells that were affected (Figure 7, Figure 3D, E, F). The frequency of defects in cytokinesis increased with the number of irradiated tips, but the timing of the perturbations did not significantly change between single and multiple ablations. This increase in frequency of cytokinesis defects

could be due to a possible inaccuracy in the laser targeting, such that multiple laser exposures simply increases the probability of successfully hitting the target. Given that the chromosome structure may not change appreciably (other than a slight change in refractive index), our ability to positively state that the intended target is always ablated, is arguably statistical. Alternatively, multiple ablations may damage each tip equally, resulting in a cumulative effect, which is reflected downstream by an increase in the frequency of defects in cytokinesis. Distinguishing between these mechanisms to explain the increase in multiple versus single tip targeting will require further study into the pathway that transduces the damage at presumptive telomeric loci into perturbations of mitotic progression.

4.3.1 Conclusion

Telomeres have also been implicated in induction of DNA damage leading to cell cycle arrest, either through senescence [20] or direct uncapping or TIFs (Telomere Dysfunction-Induced Focus) [21-24]. Delays in cytokinesis may proceed via signaling by these or analogous pathways. For example, a recent study suggested a link between the telomeric poly-ADP ribosylase known as tankyrase, and mitotic progression [25]. In that study, the observed effects were proposed to be due to poorly resolved telomeric cohesion or catenation, indicating a mechanical defect in anaphase progression. In our study, we observed that cells respond specifically to damage of chromosome tips (the putative telomeres), but not chromosome arms, when the damage occurs during anaphase. Cytokinesis failure was evident, either by the absence of furrow ingression, delayed furrow ingression, or regression of the furrow.

Our observations are distinct from other studies wherein damage to chromosomes prior to anaphase resulted in mitotic arrest during metaphase [7] or delayed mitotic exit [6]. There are two main distinctions between our work and these previous reports [6, 21, 24, 26]. First, we employed a narrow window of timing for the damage induction after the visible initiation of chromosome segregation, i.e. mid-anaphase, as compared to other studies where the damage was induced prior to mitosis [6, 26] or with unknown timing [26]. Second, damage was targeted only to the chromosome tips, as compared to non-specific chromosome-wide topological damage by chemical

induction [6] or by a possible unknown mechanical mechanism [26].

Studies using genetic perturbations have demonstrated mitotic delay as a result of DNA damage and telomere dysfunction [27]. In these cases, the temporal control of the perturbation limits the interpretation to pre-anaphase timing. The use of laser-mediated ablation allows the study of the effect of DNA damage after anaphase in a time window after the spindle assembly checkpoint has been satisfied. We were able to elicit the defects in cytokinesis from chromosome tip ablation near the spindle midzone or on tips of short arms distal from the spindle midzone near the separating chromosome masses, making it more likely to be a result of DNA damage rather than perturbation of midzone cytoskeletal organization long known to cause cytokinetic defects [18].

Recent studies using laser microsurgery have proposed that Aurora B inhibits completion of cytokinesis when there is chromatin trapped in the cleavage furrow. Laser ablation of telomeres may also act through this pathway, given the common endpoint of cleavage furrow regression [28]. However, there is at present no detailed identification of chromosomal domains, which, when localized to the furrow and subjected to damage, would specifically evoke the failure to complete cytokinesis.

The results reported here suggest a telomere-based signaling pathway that couples post-segregation chromosome damage to completion of cell division. This pathway is likely linked to DNA repair; however, the possibility of other telomeric-specific protein damage/repair pathways cannot be excluded.

4.4 Figures

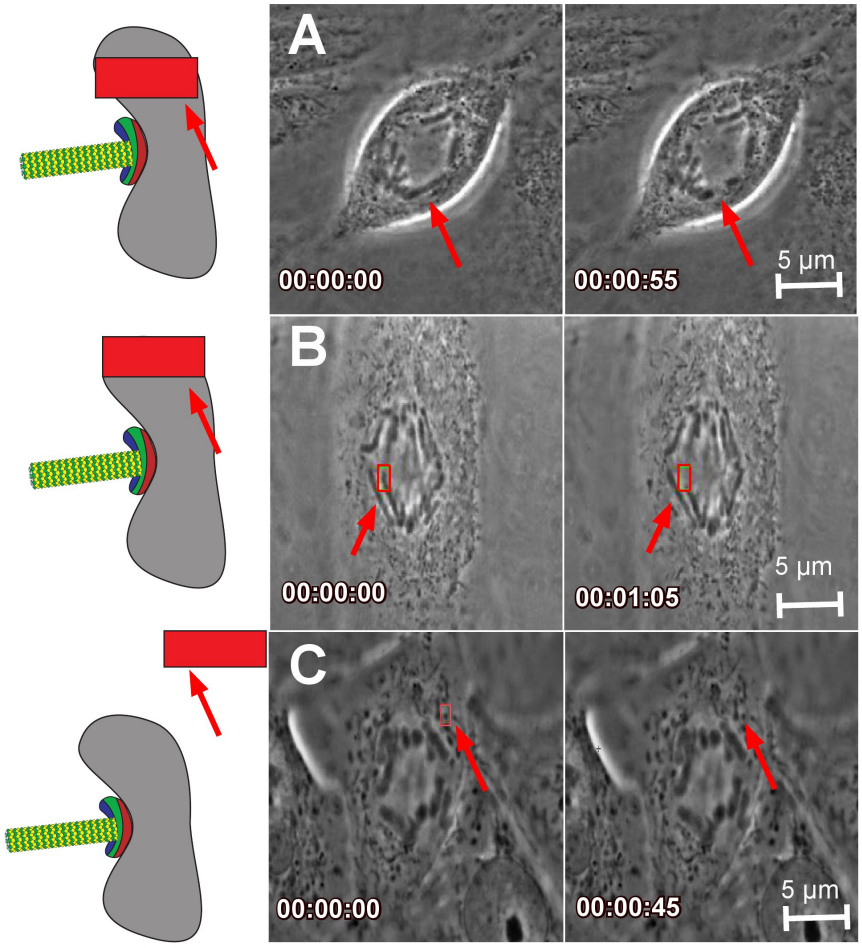

Figure 4.1: A. Arm chromosome ablation in the mid-region between chromosome tip and centromere preserving the distal remnant of the chromosome. B. Chromosome tip ablation eliminates the distal region of the chromosome with no observable chromosome fragment remaining. C. Cytoplasmic ablation avoids chromosomes but may be targeted within or outside the mitotic spindle.

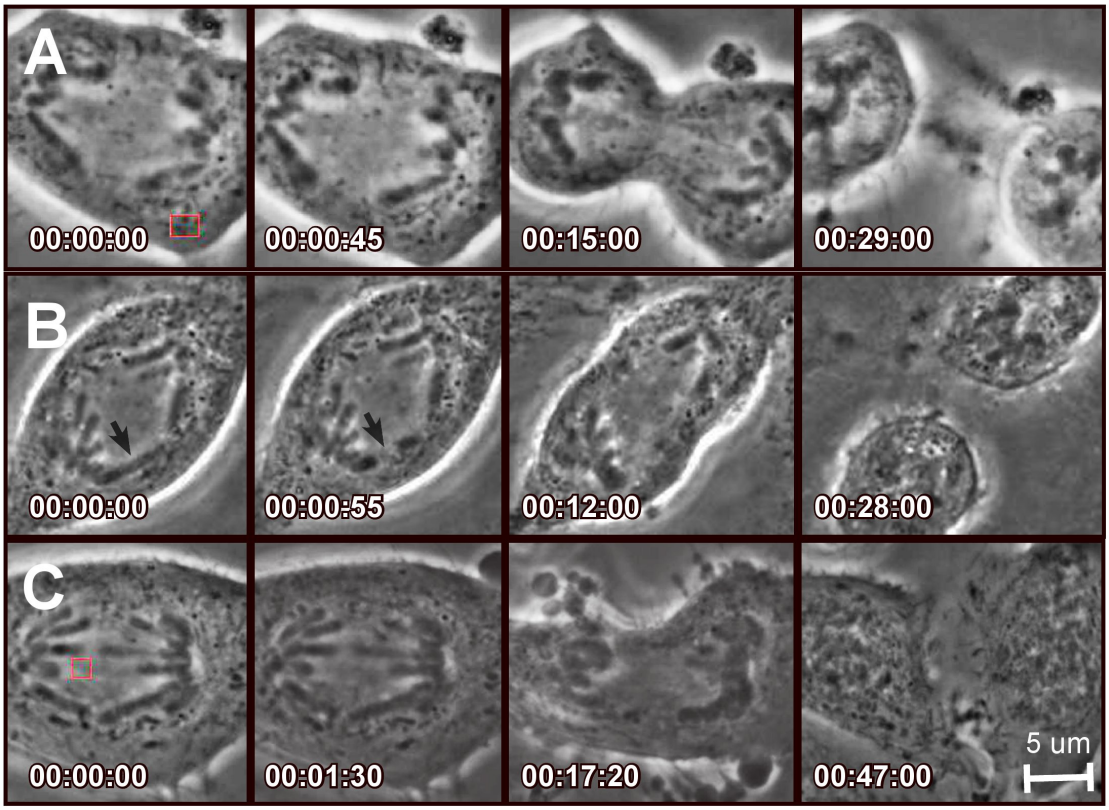

Figure 4.2: A. Cytoplasmic targeting distal from the midzone (box). B. Chromosome arm ablation (arrow). C. Cytoplasmic midzone targeting (box). Time stamps indicated in each figure take 00:00:00 as immediately pre ablation and are formatted as hh:mm:ss. Scale bar represents 5 micrometers.

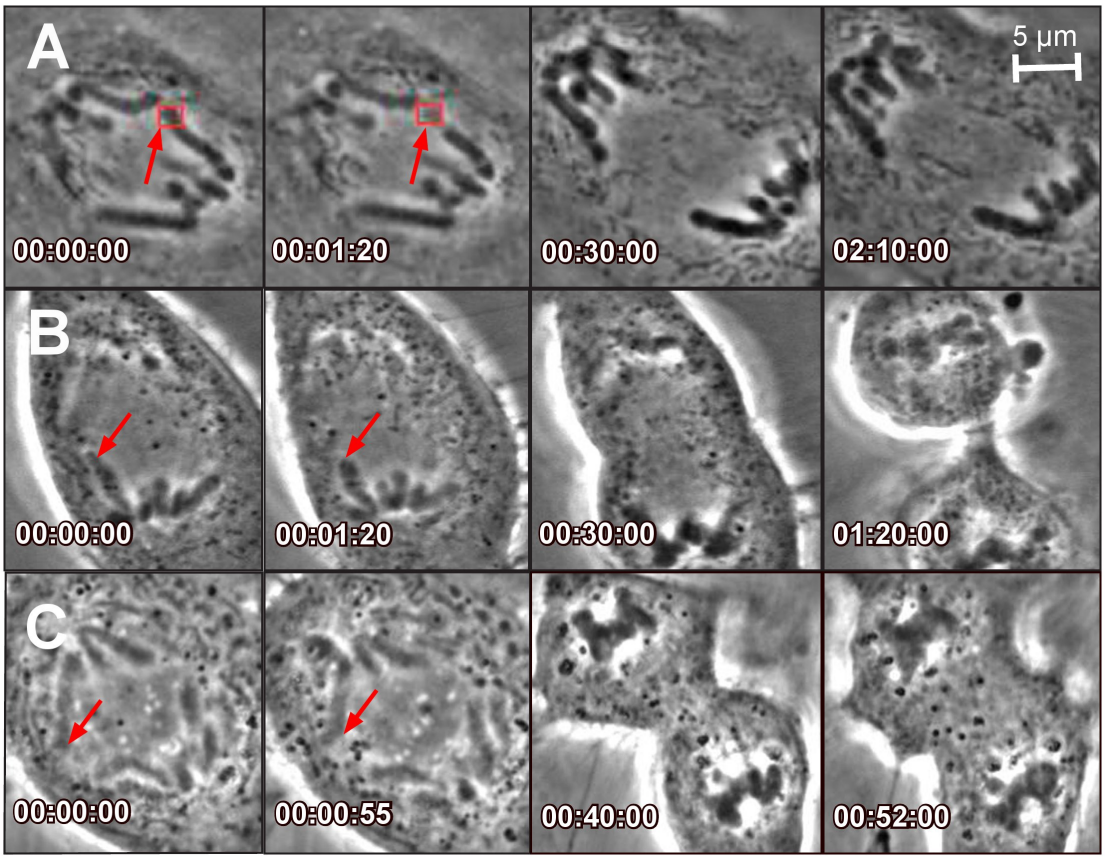

Figure 4.3: A-C. Single tip ablation results in A. no furrow, B. delay in furrow formation and C. regression of established furrow.Time stamps indicated in each figure take 00:00:00 as immediately pre ablation and are formatted as hh:mm:ss. Scale bar represents 5 micrometers.

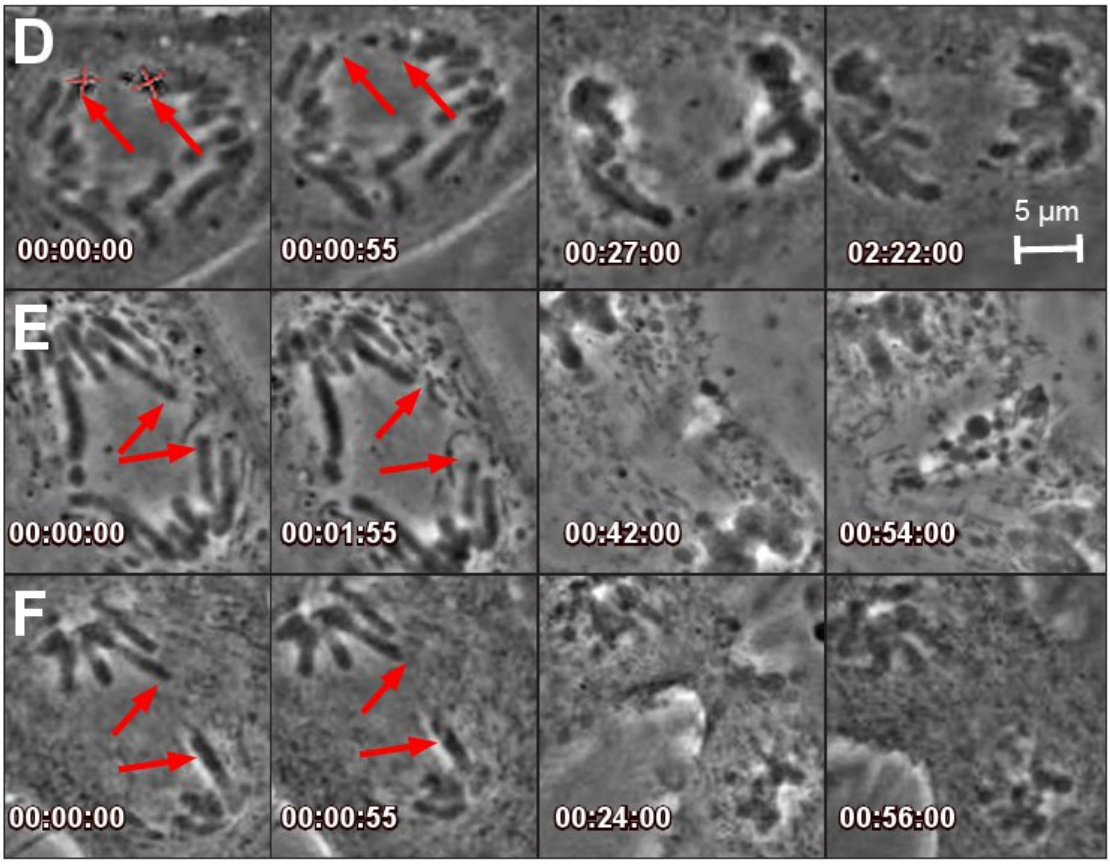

Figure 4.4: D-F Multiple tip ablations show(s) similar outcomes D. no furrow, E. furrow delay and F. furrow regression. Time stamps indicated in each figure take 00:00:00 as immediately pre ablation and are formatted as hh:mm:ss. Scale bar represents 5 micrometers.

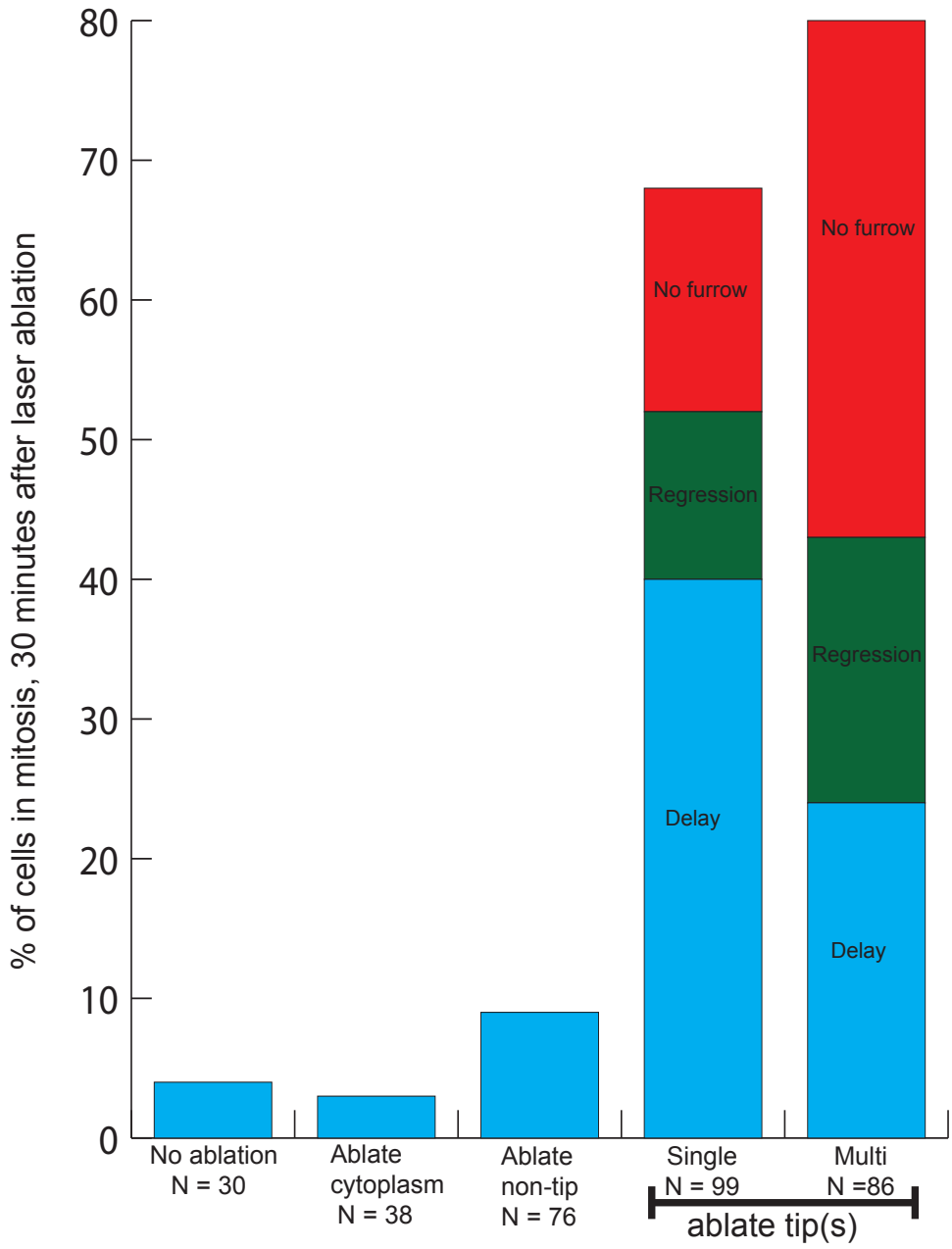

Figure 4.5: Control mitotic cells or cytoplasm and arm laser ablation treated cells predominantly exit mitosis within 30 minutes of anaphase ablation. However, single or multiple chromosome tip ablations result in a dramatic increase in delayed mitotic exit (Red: no furrow formed, Green: furrow regression and Blue: normal cytokinesis exit).

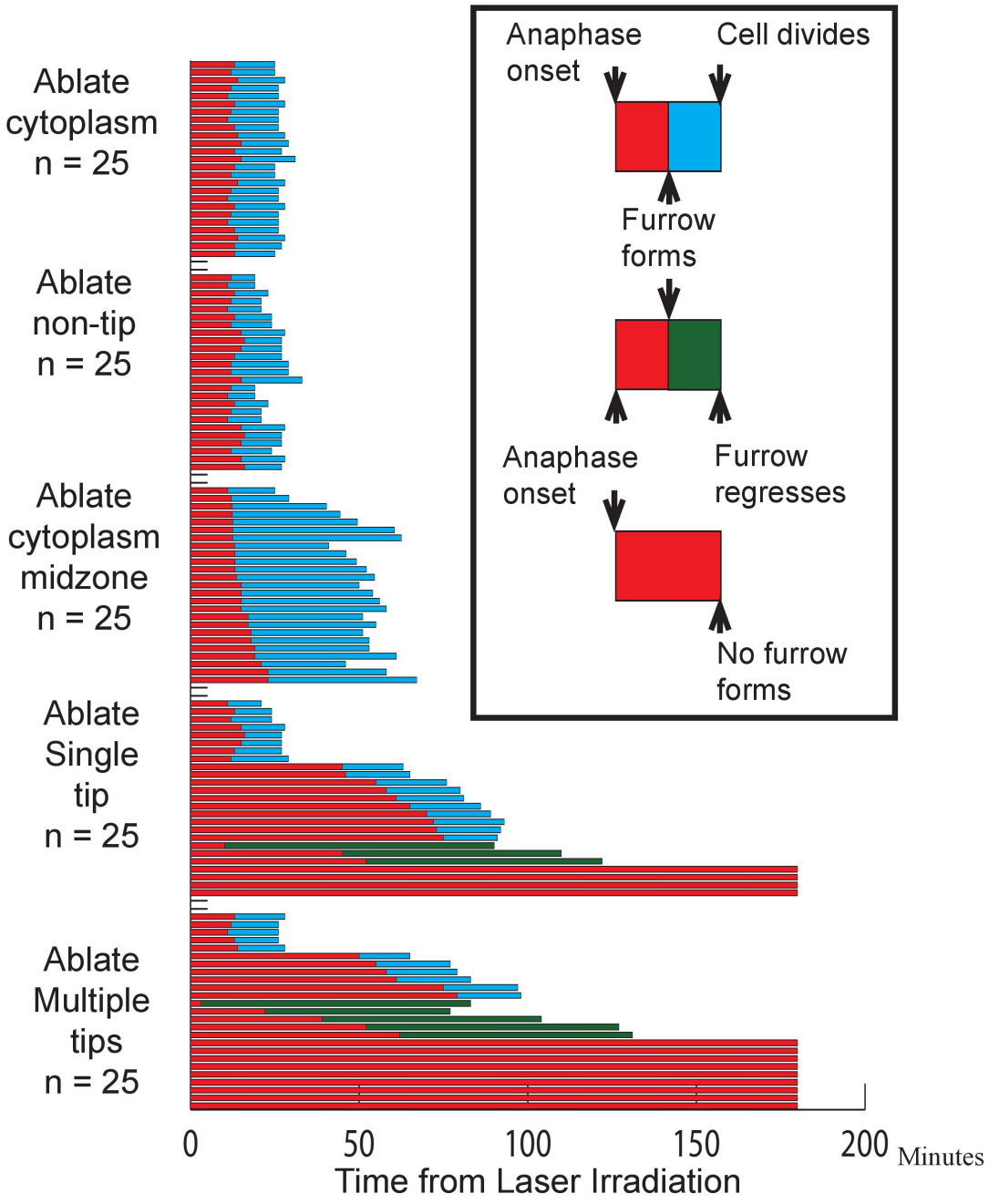

Figure 4.6: Time histograms of 25 representative cells each for cytoplasmic ablation distal from the midzone, chromosome arm ablation, cytoplasmic midzone ablation, and single and multiple chromosome tip ablation. The inset-rectangle on the right side of the figure defines the transitions as well as the beginning and end-points of the cell data in the figure. Transitions are based on morphological criteria of anaphase onset, furrow formation, furrow regression and successful cell division.

Region of Ablation	Outcome	n	% total	Mean time (min)	STDEV
Cytoplasm distal to midzone	Cell divides	38	100	24	4
Cytoplasm midzone	Cell divides	33	100	49	11
Chromosome (non-tip)	Cell divides	76	100	26	7
Chromosome tip (single)	No furrow	16	16		
	Furrow regression	12	12	88	25
	Delay in division	39	40	70	15
	Cell divides	32	32	27	5
	Total cells	**99**			
Chromosome tip (multiple)	No furrow	32	37		
	Furrow regression	16	19	101	32
	Delay in division	21	24	79	14
	Cell divides	17	20	30	4
	Total cells	**86**			

Figure 4.7: Timing of mitotic exit for anaphase laser ablation to cytoplasm, chromosome arm and chromosome tips. T = 0 at laser ablation (anaphase onset).

4.5 Acknowledgements

Chapter 4, in full, is a reprint of the material as it appears in Baker Norman M, Zeitlin Samantha, Shi Linda, Shah Jagesh, Berns Michael, ”Chromosome tips damaged in anaphase inhibit cytokinesis”, Plos1, in press, August 2010. The dissertation author was the main author of this paper.

4.6 Bibliography

[1] Holland, A.J., and Cleveland, D.W. *Boveri revisited: chromosomal instability, aneuploidy and tumorigenesis.* Nat Rev Mol Cell Biol 10, 478-487 2009

[2] Jackson, S.P., and Bartek, J. *The DNA-damage response in human biology and disease.* Nature 461, 1071-1078. 2009

[3] Shrivastav, N., Li, D., and Essigmann, J.M. *Chemical biology of mutagenesis and DNA repair: cellular responses to DNA alkylation.* Carcinogenesis 31, 59-70. 2010

[4] O'connell, C.B., Loncarek, J., Hergert, P., Kourtidis, A., Conklin, D.S., et al. *The spindle assembly checkpoint is satisfied in the absence of interkinetochore tension during mitosis with unreplicated genomes.* J Cell Biol 183, 29-36. 2008

[5] Skibbens, R.V., Rieder, C.L., and Salmon, E.D. *Kinetochore motility after severing between sister centromeres using laser microsurgery: evidence that kinetochore directional instability and position is regulated by tension.* J Cell Sci 108 (Pt 7), 2537-2548. 1995

[6] Skoufias, D., Lacroix, F., Andreassen, P., Wilson L., Margolis, R. *Inhibition of DNA Decatenation, but Not DNA damage, Arrests Cells at Metaphase*. Molecular Cell, Vol 15, 977-990 2004.

[7] Mikhailov, A., Cole, R.W., and Rieder, C.L. *DNA damage during mitosis in human cells delays the metaphase/anaphase transition via the spindle-assembly checkpoint.* Curr Biol 12, 1797-1806. 2002

[8] Anantha, R., Sokolova, E., and Borowiec, J. *RPA phosphorylation facilitates mitotic exit in response to mitotic DNA damage.* Proc Natl Acad Sci USA. 2008

[9] Khodjakov, A., Cole, R.W., McEwen, B.F., Buttle, K.F., and Rieder, C.L. *Chromosome fragments possessing only one kinetochore can congress to the spindle equator.* Journal of Cell Biology 136, 229-240. 1997

[10] Rieder, C.L., Cole, R.W., Khodjakov, A., and Sluder, G. *The checkpoint delaying anaphase in response to chromosome monoorientation is mediated by an inhibitory signal produced by unattached kinetochores.* J Cell Biol 130, 941-948. 1995

[11] Botvinick, E.L., and Berns, M.W. *Internet-based robotic laser scissors and tweezers microscopy.* Microsc Res Tech 68, 65-74. 2005

[12] Sasaki, K., Koshioka, M., Misawa, H., Kitamura, N., and Masuhara, H. *Pattern formation and flow control of fine particles by laser-scanning micromanipulation.* Opt Lett 16, 1463-1465. 1991

[13] Gomez-Godinez, V., Wakida, N.M., Dvornikov, A.S., Yokomori, K., and Berns, M.W. *Recruitment of DNA damage recognition and repair pathway proteins following near-IR femtosecond laser irradiation of cells.* Journal of biomedical optics 12, 020505. 2007

[14] Berns, M.W. *A history of laser scissors (microbeams).* Methods Cell Biol 82, 1-58. 2007

[15] Botvinick, E.L., Venugopalan, V., Shah, J.V., Liaw, L.H., and Berns, M.W. *Controlled ablation of microtubules using a picosecond laser.* Biophys J 87, 4203-4212. 2004

[16] Kong, X., Mohanty, S.K., Stephens, J., Heale, J.T., Gomez-Godinez, V., et al. *Comparative analysis of different laser systems to study cellular responses to DNA damage in mammalian cells.* Nucleic Acids Research 37, e68-e68. 2009

[17] Rieder, C.L., Schultz, A., Cole, R., and Sluder, G. *Anaphase onset in vertebrate somatic cells is controlled by a checkpoint that monitors sister kinetochore attachment to the spindle.* J Cell Biol 127, 1301-1310. 1994

[18] Spurck, T.P., Stonington, O.G., Snyder, J.A., Pickett-Heaps, J.D., Bajer, A., et al. *UV microbeam irradiations of the mitotic spindle. II. Spindle fiber dynamics and force production.* J Cell Biol 111, 1505-1518. 1990

[19] Wheatley, S.P., and Wang, Y. *Midzone microtubule bundles are continuously required for cytokinesis in cultured epithelial cells.* The Journal of Cell Biology 135, 981-989. 1996

[20] Fagagna, F.D.a.D., Reaper, P.M., Clay-Farrace, L., Fiegler, H., Carr, P., et al. *A DNA damage checkpoint response in telomere-initiated senescence.* Nature 426, 194-198. 2003

[21] Davoli, T., Denchi, E.L., and de Lange, T. *Persistent telomere damage induces bypass of mitosis and tetraploidy.* Cell 141, 81-93. 2010

[22] Musaro, M., Ciapponi, L., Fasulo, B., Gatti, M., and Cenci, G. *Unprotected Drosophila melanogaster telomeres activate the spindle assembly checkpoint.* Nat Genet 40, 362-366. 2008

[23] Takai, H., Smogorzewska, A., and de Lange, T. *DNA damage foci at dysfunctional telomeres.* Curr Biol 13, 1549-1556. 2003

[24] Thanasoula, M., Escandell, J.M., Martinez, P., Badie, S., Muoz, P., et al. *p53 Prevents Entry into Mitosis with Uncapped Telomeres.* Curr Biol. 2010

[25] Jasmin N. Dynek, et al. *Resolution of Sister Telomere Association Is Required for Progression Through Mitosis*. Science 304, 97 2004

[26] Pobiega S., Marcand, S. *Dicentric Breakage at telomere fusions.* Genes Dev. 24:720-733 2010

[27] Ciapponi, L. Cenci, G. *Telomere capping and cellular checkpoints: clues from fruit flies.* Cytogenetic Genome Res 122:365-373. 2008

[28] Steigemann, P., Wurzenberger, C., Schmitz, M.H.A., Held, M., Guizetti, J., et al. *Aurora B-Mediated Abscission Checkpoint Protects against Tetraploidization.* Cell 136, 473-484. 2009

5 Optical Ablation of Spindle Microtubules in Metaphase

5.1 Introduction

During mitosis, cells form a microtubule-based bipolar spindle that exerts forces characterized by dynamic instability, chromosomes congressing to the metaphase plate and segregation of chromosomes to opposite poles in anaphase. Although spindles can wildly vary and are highly dynamic in nature due to rapid microtubule turnover, overall spindle morphology and length remain steady [1, 2, 3]. How cells organize and maintain dynamic consistent spindle machinery is not fully understood but it is clear that force, whether from microtubule dynamics, motor proteins, or spindle-associated proteins [2, 4] play a critical role in determination of steady-state spindle length [3]. Studies examining plus-end directed kinesin motor proteins (Eg5+) [1, 5, 6, 7, 8] and minus-end directed dyneins-dynactin complexes [1, 9, 10] and cross-linking and sliding of microtubules [11, 12, 13, 14], molecular perturbation of microtubule dynamics [1, 11, 15, 16] all indicate a force-balance mechanism that influences steady-state spindle length, presumably through microtubule rate equations [17, 18, 19, 20].

Perturbation of microtubules in metaphase to study spindle forces and spindle length has been performed with UV [21, 22, 23]. An observation of these studies was that a transient perturbation of one half-spindle resulted in the 'shrinking' of the mitotic spindle and in particular the uncut side shortened in response to maintain 'equal length' between each half-spindle. This implies that the steady state spindle length (pre-ablation) is altered via disruption of microtubules into a new steady state length and that the cell is able to sense this difference, presumably through adjustment of rate equations,

and arrive at a new 'equilibrium' steady-state length.

Recent studies [24, 25] have shown the ability to precisely ablate and disrupt microtubules without adversely affecting the cell. In this study, we repeat the earlier UV work with a 532 nm, picosecond laser and verify the UV experiments and in addition (1) we apply perturbations to the mitotic spindle at an angle to the pole-to-pole axis (parallel to metaphase plate), and (2) we apply multiple prolonged perturbation to the mitotic spindle to prevent re-polymerization of the mitotic spindle. The results demonstrate that the force balancing mechanism present in mitotic spindles is able to sense magnitude and direction and that it requires bipolar spindle attachment in order to sense the tension and rebalance its' rate equations into a new final steady-state length.

5.2 Results

Laser ablation of the Mitotic Spindle

Ablation of defined regions of the mitotic spindle results in a 3 step process: (1) shrinking of the cut half-spindle pole towards the cut, (2) recovery of the connection between pole and cut microtubule stub in approximately 45-60 seconds that is defined as the re-attachment of the bipolar spindle connection, (3) the uncut half-spindle collapses to equal the length of the ablated side. This process can be repeated once or several times in the same cell, and the cell is still able to successfully complete mitosis. In all further discussion of laser ablations, L' refers to the ablated side and L" is the unablated side with the length being measured from pole to kinetochore/midzone. Unless otherwise specified laser ablation was done perpendicular to the pole-to-pole axis.

5.2.1 Single Line Cut

To investigate the response of the metaphase mitotic spindle to a specific localized perturbation of microtubules, laser-mediated disruption of microtubules was performed. A single line cut, oriented perpendicular to the pole-to-pole axis, was applied to the mitotic spindle (Figure 1) to evaluate the perturbation on spindle dynamics similar to previous UV studies [21, 22, 23]. Similar phenomena are observed in which the spindle experiences (1) disruption of microtubules resulting in microtubule stubs separated

by a 'gap' as observed by loss of fluorescence, (2) re-polymerization of microtubules across this gap and re-establishment of bipolar spindle attachment as the pole moves inwards towards the cut, (3) after bipolar spindle re-attachment, the spindle is uneven in length (L" > L') due to shrinking and pole movement, and the unablated side (L") begins to shrink until a new equilibrium steady-state length is achieved (L" = L').

A time course of the disruption (Figure 2) is obtained by measuring the pole-to-kinetochore distance (L", L') of the uncut and cut side with respect to the laser ablation event. Approximately 1 micrometer on L' (cut side) is loss immediately after laser ablation and re-establishment of bipolar spindle connection occurs within 45 seconds. (Figure 1, 2). After the bipolar spindle re-connection occurs, L" (uncut side) begins to shorten (Figure 1, 2, 10) approximately 41 seconds after recovery. (N = 36, +/- 10 seconds) with the spindle reaching a new equilibrium length 6 (+/- 20 seconds) minutes after the initial laser ablation event. Despite only an initial disruption of only 1 micrometer (L'), the new equilibrium spindle will have shrunk by 5.5 micrometers (L' + L") in order to maintain L' = L" steady-state.

5.2.2 Repeated Line Cut

Laser ablation of a mitotic half spindle is performed but now repeated laser ablation events are performed to ablate the microtubules (single line cut every 20 seconds) to prevent them from repolymerizing in the 'gap' (Figure 3). This stops the half spindles from re-establishing a link to each other and 'recovering' the bipolar spindle attachment during the ablation events. The repeated cuts are continued for an average of 2-3 minutes and then the cell is allowed to recover (Figure 3, T = 2 minute 52 seconds). The ablated side will shorten due to the ablation but the uncut side will not react or shrink at all until approximately 45 seconds after the ablated region has recovered (Figure 3, 10) and then the two sides will begin to move towards a new final equilibrium length. (L" = L', Figure 3, 10). The progression of spindle length is graphed (Figure 4). It is evident that by preventing the re-establishment of bipolar spindle attachment a clear 'prolonged' delay in response is observed for the uncut side.

5.2.3 Single Box Cut

Laser ablation of the mitotic spindle is performed but instead of a single 'thin' line a significantly larger volume (box) is ablated (Figure 5). Despite a significantly larger population of microtubules being disrupted in the xy plane, the timing and kinetics of the cell remain similar to single line cut ablation. The cut (Figure 5) shows a loss of fluorescence, shrinkage, recovery of bipolar spindle attachment, and subsequent equilibrium, similar to the single line cut case (Figure 5, 6, 10).

5.2.4 Diagonal Line Cut

Laser ablation of the mitotic spindle is performed but instead of ablating a region always perpendicular to the pole-to-pole axis, the laser ablation event is at an angle between 20-45 degrees off-axis. Cells (Figure 7) are rotated by image processing such that they initially start off with the pole-to-pole axis aligned horizontally. In addition to loss of fluorescence, shrinkage, and equalization of spindle lengths (Figure 7, 8, 10) there is a distinct rotational shift in the overall spindle orientation (ranging from 10-25 degrees) with the pole always moving in towards the cut. The angled laser ablation event also results in a larger variation of 'spindle re-attachment' in the xy plane and three distinct equilibrium points are observed: initial, transient, and final steady-state length. (Figure 8)

5.2.5 Partial Off-axis Cut

Laser ablation of the mitotic spindle is performed but instead of ablating a specific xy plane or orientation, laser ablation of partial regions (small line cuts) and 'tilted' box cuts are examined. Laser ablation results in the same loss of fluorescence, shrinkage, reconnection of bipolar spindle attachment and equilibrium (Figure 9) but several equilibrium points are observed as L' and L" shrink, reach a steady-state and then shrink again. (Figure 9, 10).

5.3 Discussion

Different effects on spindle dynamics were observed depending on the location of the laser damage and timing of the laser damage. Single line cut ablations reveal similar physiological results as earlier UV studies [21, 22, 23]. If the spindle was ablated with repeated laser ablations (Figure 3) in the same area (L') then cells were still observed to have the same visual phenomena of (1) disruption, (2) recovery, and (3) equilibrium. Repeated mitotic cuts prolonged the duration of disruption (Figure 3, 4, 10). Repeated ablations (N = 18) resulted in a prolonged disruption time that lasts for the entire duration of laser ablation (approximately 150 seconds). During this time, L' is shrinking but L" does not shrink at all (Figure 4). After the last cut, the spindle recovers bipolar attachment (20 seconds). At 34 seconds after recovery (Figure 4, 10) L" begins to shrink to a new equilibrium point. This demonstrates that recovery of bipolar spindle attachment is necessary and that the 3 step process of disruption, recovery, and equilibrium is not governed by simple rate equations or by a loss of tension.

Box ablations (significant xy plane size, 60-100 shots across spindle) were performed to determine whether a larger disruption zone would increase the length of time required for recovery of bipolar spindle attachment and subsequent microtubule dynamics activity. Despite 2-3 micrometers being disrupted in L' (Figure 5), the cut microtubule stubs were still able to polymerize and subsequently re-establish a bipolar spindle attachment in 45-60 seconds (Figure 5, 6, 10). The larger zone of disruption (2-3 micrometers) results in the pole on the cut side moving in 2-3 micrometers towards the cut as compared to a single micrometer for single line cut (N = 12, Figure 10). Presumably, this is the reason why the bipolar attachment is achieved with similar timing to smaller xy plane ablations with similar polymerization rates as the pole re-connection distance is shorter. Once the spindle recovers, L" shortens with similar timing to the single cut ablations (Figure 6, 10). This demonstrates that the 'size' of the disruption does not affect spindle recovery or steady state spindle length.

Diagonal ablations were performed across the spindle at approximately 25-45 degrees off the pole-to-pole axis (Figure 7). L' pole shortens towards the direction of the cut, with the entire mitotic spindle rotating in response (Figure 7, 8). In addition to the 10-15 degree shift (N = 9, Figure 10), the spindle experiences multiple steady-states

(Figure 8). This is most likely due to the variation in xy microtubule disruption, rotating reference frame, and tension variations across the spindle as it re-connects bipolar attachment. The tension that the spindle undergoes varies during the shortening leading to two separate transient 'steady-state' points as L' = L" early on but, presumably due to rotation, new microtubule connections and motor proteins cross-linking, the tension is still not properly balanced and the spindle shrinks again to another steady-state length. Ablations that were not perpendicular to the pole-to-pole axis (partial or box off-axis cuts) resulted in multiple equilibrium points despite equivalent disruption and recovery (Figure 9, Figure 10). This shows that the mitotic spindle senses the magnitude and direction of the tension on the spindle and it is the tension difference (force-balancing) that governs the final steady state pole-to-kinetochore distance.

5.4 Conclusion

Here we verify the 3 step process first observed by earlier UV studies: (1) disruption, (2) recovery, (3) force balancing. These results imply that there is a force-balancing mechanism for the overall spindle and that it influences the individual steady-state length of each half-spindle. It could be argued that this is simply a reaction to a loss of tension that affects the rate equations and that, after a given relaxation time the spindle will achieve a new steady-state spindle length. However, repeated ablation prolongs perturbed spindle duration as it prevents the re-establishment of a bipolar attachment and tension across the spindle. The resulting time delay in shrinking to a new steady-state length implies that the force-balancing mechanism requires a bipolar attachment and that it must sense tension before attempting to re-balance itself. Box cuts reveal that the force balancing mechanism relies more on bipolar spindle tension than on the amount of spindle damage (ablation). Diagonal cuts and off-axis cuts reveal that the force-balancing mechanism senses direction in addition to magnitude. In particular the results demonstrate that the force-balancing mechanism can arrive at multiple steady-state lengths due to variations in the tension sensed, rotation, and the ability of the cell to accurately adjust its' spindle length.

5.5 Acknowledgements

Chapter 5, in full, is a reprint of the material to be published Baker Norman, Tsay Angela, Shi Linda, Shah Jagesh, Berns Michael, Mitotic spindle regulation following selective laser ablation, in preparation. The dissertation author was the main author of this paper.

5.6 Figures

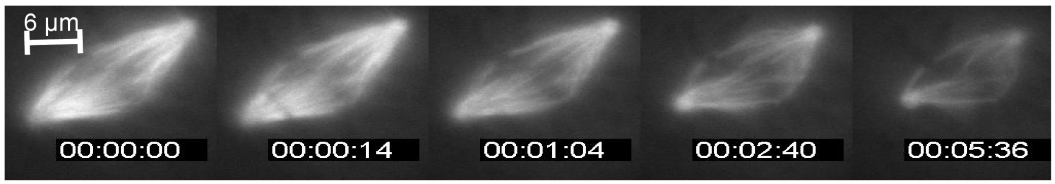

Figure 5.1: Laser ablation of ECFP metaphase mitotic spindle of PTK2 cells. Montage begins with pre-ablation image of Metaphase mitotic spindle at T = 0. Single laser ablation of bottom half spindle occurs at T = 14 seconds. Cut half-spindle recovers, on average 45-60 seconds (T = 1 minute), and the shrinkage of the mitotic spindle with the uncut-side collapsing is observed (T = 2 minute, 40 seconds) and the cell finishes shrinking to a 'new equilibrium' state and the cell goes on to successfully divide.Time stamps indicated in each figure take 00:00:00 as immediately pre ablation and are formatted as hh:mm:ss. Scale bar represents 6 micrometers.

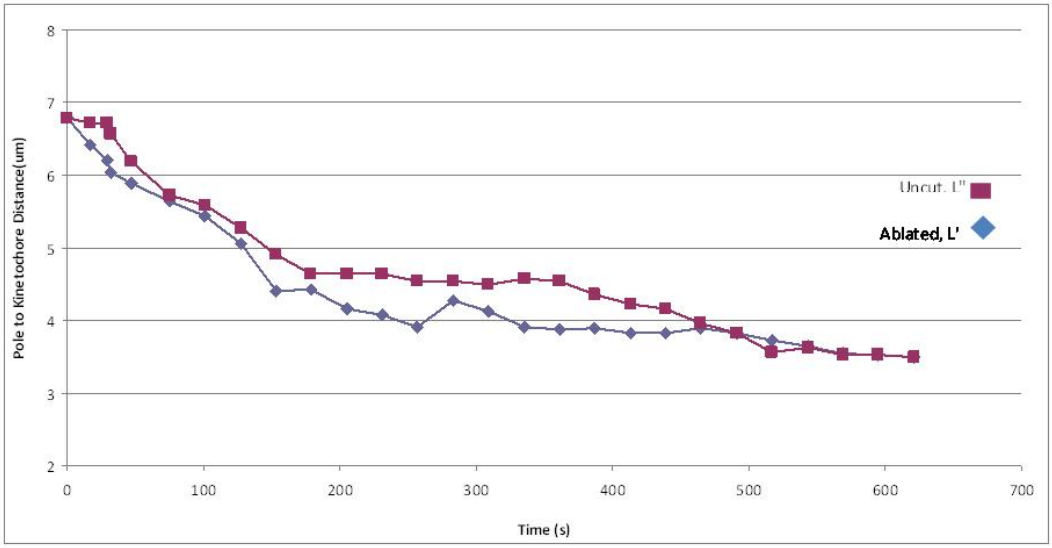

Figure 5.2: Pole to Kinetochore distance for Single Laser ablation of one half spindle. L' is ablated side, L" is unablated side. On Average, cut half-spindle recovers within 45-60 seconds and unablated half spindle begins to shrink and the two continue to shrink until reaching a final new equilibrium.

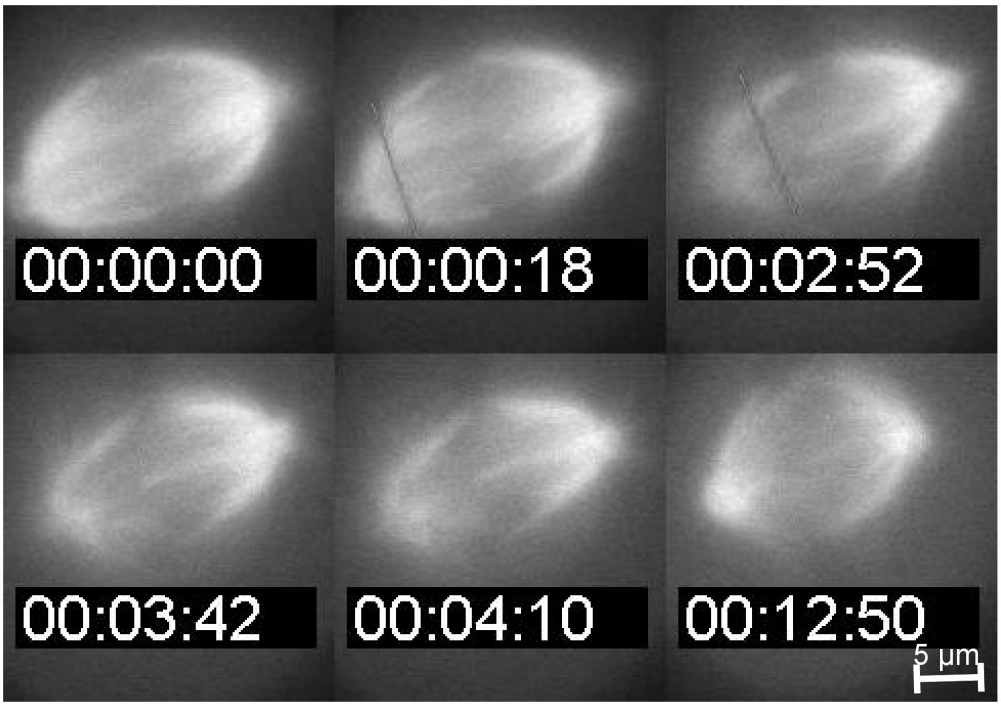

Figure 5.3: Repeated laser ablation of ECFP metaphase mitotic spindle of PTK2 cells. Montage begins with Pre-ablation image at T=0 and first ablation at T = 18 seconds. Repeated ablation in that region is continued for approximately 2 minutes, 30 seconds. 45-60 seconds after final post cut, cell begins to shrink to new final equilibrium. Time stamps indicated in each figure take 00:00:00 as immediately pre ablation and are formatted as hh:mm:ss. Scale bar represents 5 micrometers.

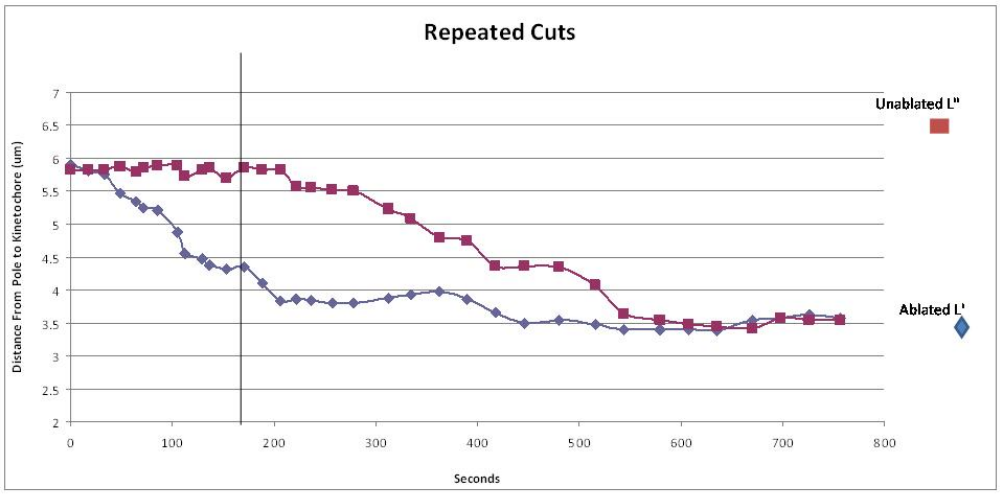

Figure 5.4: Distance from Pole to Kinetechore for 'repeat' single line ablation on one half spindle. L' is ablated side, L" is unablated side. Repeated ablations prevents spindle from recovering and by delaying recovery, the uncut-half spindle's response (shrinking) is also delayed.

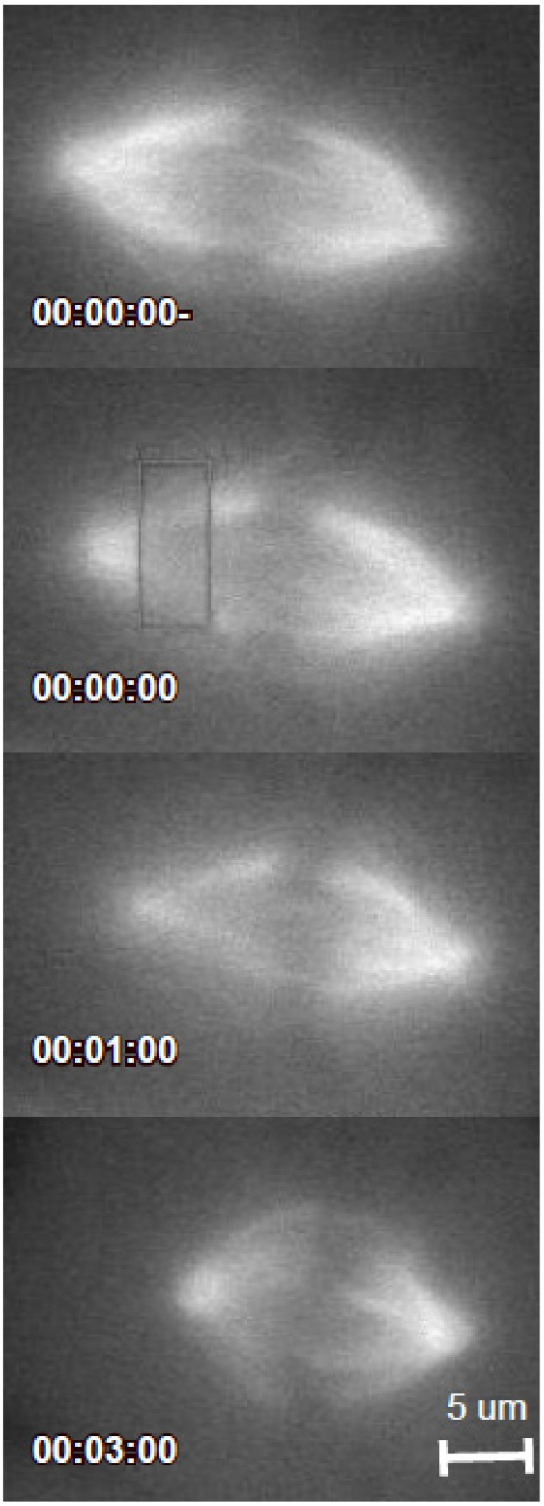

Figure 5.5: Distance from Pole to Kinetochore for single box ablation on one half spindle. L' is ablated side, L" is unablated side. Box cut disrupts a larger population of microtubules but does not significantly delay reconnection of bipolar mitotic spindle.

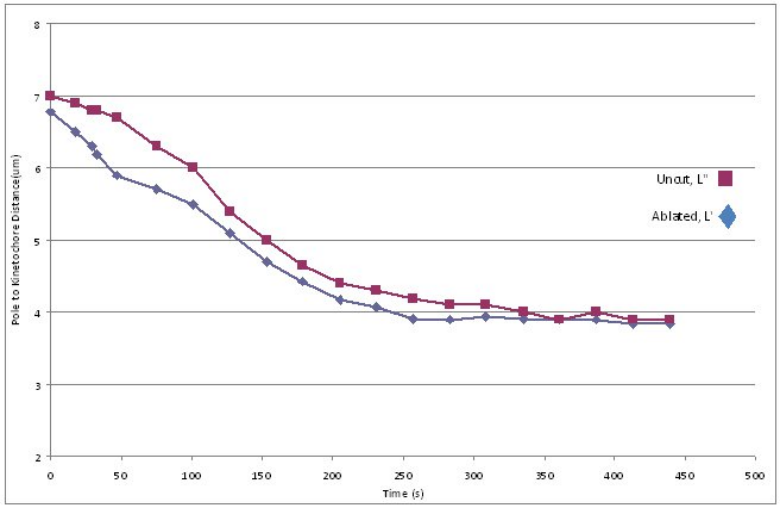

Figure 5.6: Distance from Pole to Kinetochore for single box ablation on one half spindle. L' is ablated side, L" is unablated side. Box cut disrupts a larger population of microtubules but does not significantly affect timing and progression of reconnection of bipolar mitotic spindle if done perpendicular to spindle axis.

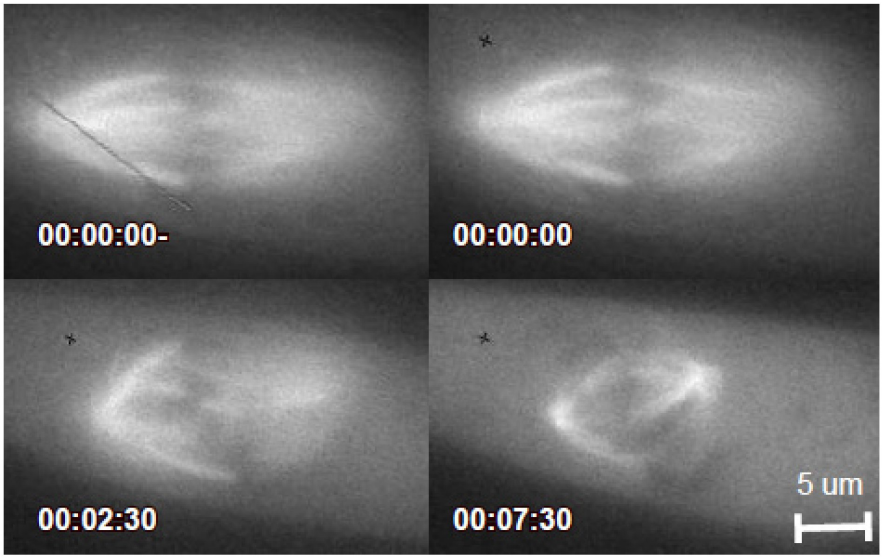

Figure 5.7: Montage of single diagonal ablation on one half spindle. L' is ablated side, L" is unablated side. Cell is rotated to be along horizontal axis initially and rotation from this axis, in direction of the cut is measured (10-15 degrees). Scale bars are 5 micrometers

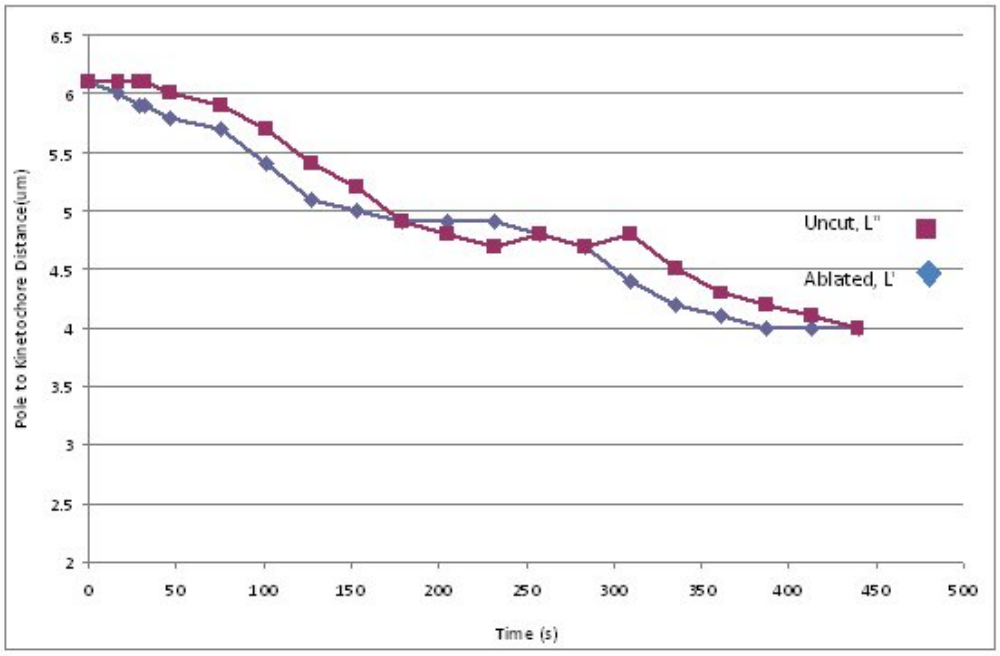

Figure 5.8: Distance from Pole to Kinetochore for single diagonal line cut on one half spindle. L' is ablated side, L" is unablated side. Cell is rotated to be along horizontal axis initially and rotation from this axis, in direction of the cut is measured (10-15 degrees). Multiple equilibrium points due to rotational recovery and longitudinal recovery.

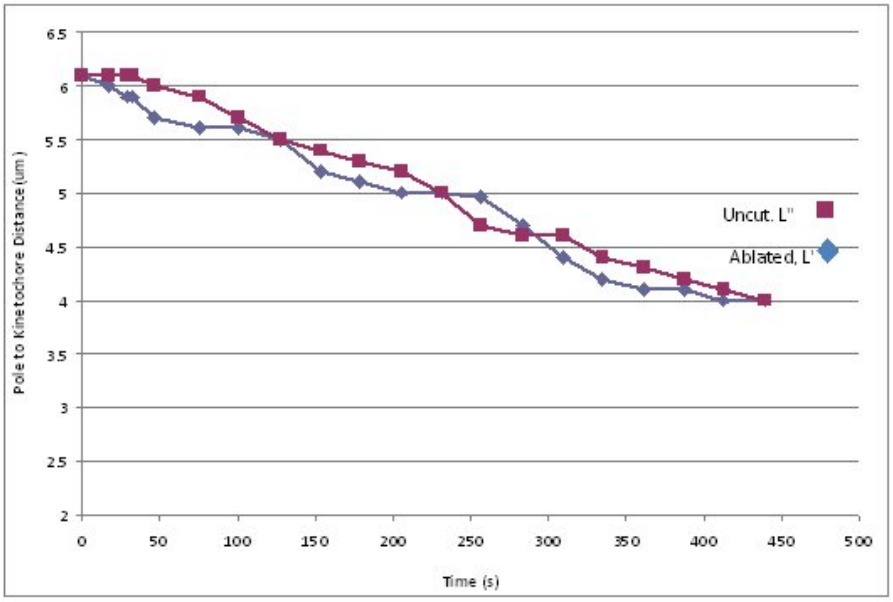

Figure 5.9: Distance from Pole to Kinetochore for sample off-bipolar axis cuts. L' is ablated side, L'' is unablated side. Angled partial cut, line cut or box cut results in multiple equilibrium points due to variations in timing and tension of re-establishment of bipolar spindle and shrinking that occurs at each equilibrium point.

	N	Average L' + L'' shrinkage	Uncut side collapse(sec)	Time to equilibrium (sec)
Single Cut	36	5.5	41	350
Repeated Cut	18	6.4	34 (after cut)	590
Box Cut	12	6	48	370
Diagonal Cut	9	4	45	530
Partial (off-axis) Cut	14	5	39	550

Figure 5.10: Number of trials for types of laser ablation performed and average initial recovery time of the spindle. Line cuts, Repeated Cuts and Box cuts are done such that they are perpendicular to the axis plane that connects pole-to-pole and observe a single equilibrium point. Diagonal and partial off-axis cuts are angled 10-45 degrees off-axis and result in rotation and multiple equilibrium points.

5.7 Bibliography

[1] Mitchison T.J., Maddox P., Gaetz J., Groen A., Shirasu M., Desai A., Salmon E.D., Kapoor T.M. *Roles of polymerization dynamics, opposed motors and a tensile element in governing the length of Xenopus extract meiotic spindles* Mol. Biol. Cell 2005

[2] Walzak C.E., Heald R. *Mechanisms of mitotic spindle assembly and function* Int. Rev. Cytol. 2008

[3] Mogliner A., Wollman R., Civelekoglu-Scholey G., Scholey J. *Modeling mitosis* Trends Cell Biology 2006

[4] Gatlin J.C., Matov A., Danuser G., Mitchison T.J., Salmon E.D. *Directly probing the mechanical properties of the spindle and its matrix* Journal of Cell Biology 2010

[5] Sawin K.E., Mitchison T.J. *Poleward microtubule flux mitotic spindles assembled in vitro* Journal of Cell Biology 1991

[6] Miyamoto D.T., Perlman Z.E., Burbank K.S., Groen A.C., Mitchison T.J. *The kinesin Eg5 drives poleward microtubule flux in Xenopus laevis egg extract spindles* Journal of Cell Biology 2004

[7] Sharp D.J., Yu K.R., Sisson J.C., Sullivan W., Scholey J.M. *Antagonistic microtubule-sliding motors position mitotic centrosomes in Drosophila early embryos* Nature Cell Biology 1999

[8] Kapitein L.C., Peterman E.J.G., Kwok B.H., Kim J.H., Kapoor T.M., Schmidt C.F. *The bipolar mitotic kinesin Eg5 moves on both microtubules that it crosslinks* Nature 2005

[9] Ferenz N.P., Paul R., Fagerstrom C., Mogilner A., Wadsworth P. *Dynein antagonizes Eg5 by crosslinking and sliding antiparallel microtubules* Current Biology 2009

[10] Tanenbaum M.E., Macurek I., Galjiart N., Medema R.H. *Dynein, lis1 and CLIP-170 counteract Eg5-dependent centrosome separation during bipolar spindle assembly* EMBO J. 2008

[11] Goshima G., Wollman R., Stuurman N., Scholey J.M., Vale R.D. *Length control of the metaphase spindle* Current Biology 2005b

[12] Troxell C.L., Sweezy M.A., West R.R., Reed K.D., Carson B.D., Pidoux A.L., Cande W.Z., McIntosh J.R. *plk1(+) and klp2(+): Two kinesins of the Kar3 subfamily in fission yeast perform different functions in both mitosis and meiosis* Molecular Biology Cell 2001

[13] Hoyt M.A., He L., Totis L., Saunders W.S. *Loss of function of Saccharomyces cerevisiae kinesin-related CIN8 and KIP1 is suppressed by kar3 motor domain mutations* Genetics 1993

[14] Burbank K.S., Mitchison, T.J., Fisher D.S. *Slide-and-cluster models for spindle assembly* Current Biology 2007

[15] Ohi R., Burbank K., Liu Q., Mitchison T.J. *Nonredundant functions of Kinesin-13s during meiotic spindle assembly* Current Biology 2007

[16] Severin F., Habermann B., Huffaker T., Hyman T. *Stu2 promotes mitotic spindle elongation in anaphase* J. Cell Biology 2001

[17] Hinow P. *Continuous model for microtubule dynamics with catastrophe, rescue and nucleation processes.* Physical Review E 2009

[18] Sept D., Limbach H.J., Bolterauer H., Tuszynski J.A. *A chemical kinetics model for microtubule oscillations* Journal theoretical biology 1999

[19] Janosi, I.M., Chretien D., Flyvbjerg H. *Structural microtubule cap: Stability, catastrophe, rescue, and third state* Biophysics Journal 2002

[20] Joglekar A.P., Hunt A.J. *A simple, mechanistic model for directional instability during Mitotic chromosome movements* Biophysics Journal 2002

[21] Spurck, T. P., O. G. Stonington, J. A. Snyder, J. D. Pickett-Heaps, A. Bajer, and J. Mole-Bajer. *UV microbeam irradiations of the mitotic spindle. II. Spindle fiber dynamics and force production* Journal of Cell Biology 1990

[22] Arthur Forer, T. Spurck, J.D. Pickett-Heaps. *Ultraviolet microbeam irradiations of spindle fibres in crane-fly spermatocytes and newt epithelial cells: resolution of previously conflicting observations* Protoplasma 1997

[23] A.B. Illagan, Arthur Forer, T. Spurck. *Backward chromosome movement in anaphase, after irradiation of kinetechores or kinetechore fibres* Protoplasma 1997

[24] Botvinick E.L., Venugopalan V., Shah J.V., Liaw L.H., Berns Michael *Controlled ablation of microtubules using a picosecond laser* Biophysics Journal 2004

[25] Wakida N.M., Lee C.S., Botvinick E.L., Shi L.Z., Dvornikov A., Berns Michael *Laser nanosurgery of single microtubules reveals location-dependent depolymerization rates.* J Biomed Opt. 2007

6 Ablation of kinetochore in metaphase spindle

6.1 Introduction

As described previously in Chapter 3 and 5, microtubules form a bipolar based spindle that exerts force on chromosomes for congression on the metaphase plate and segregation of sister chromatids to each new daughter cell. The essential link between chromosomes and the spindle is through kinetochore attachment [1, 2]. Each sister chromatid has one active kinetochore which captures microtubules from one spindle pole and when the opposing sister chromatid captures microtubules from the other spindle pole, tension is established across the chromatid pair with force generation mainly occurring at the kinetochore [1, 3, 4].

Sister chromatids with their kinetochores are initially scattered randomly throughout the cytoplasm and microtubules attach to them through a seek-and-capture method [5]. Monitoring of correct kinetochore-pole attachment is critical for accurate genomic segregation [6] and is monitored through the spindle assembly checkpoint (SAC) [7]. There is a continuing debate over the role of tension [8, 9, 10, 11] and attachment [12] in SAC release [for reviews see 13, 14].

In 1981 [15] it was observed that irradiation of a single sister chromatid resulted not only in the loss of directed chromosome movement, but also in chromosome movement away from the metaphase plate with velocities of 3 to 7 micrometers/min observed [15]. Of the 92 kinetochores irradiated in [15], only 42 kinetochores were considered successfully irradiated and at least 20 of them showed no visible effect from the ablation presumably because the energy delivered was below threshold. New kinetochore mark-

ers [16] and advances in biochemical techniques allow us to target kinetochores with a higher degree of accuracy to elucidate the affect of kinetochore destruction on kinetochore and chromosome movement. Of particular interest is why microtubule ablation, as performed in chapter 5, showed no effect on directed chromosome motion or in loss of tension on the kinetochores.

6.2 Results

6.2.1 Laser ablation of cdc20-YFP PtK2 cells

Ptk2 cells are stably transfected with cdc20-YFP [16] which binds to the kinetochore in metaphase mitotic cells (Figure 1). Cells are chosen where the chromosomes have congressed to the metaphase plate and undergo a few minutes of observed oscillation on the metaphase plate. This implies that the sister kinetochores are both attached and under tension. Cells are also chosen where the kinetochore can be distinctly and clearly ablated without hitting other kinetochores or chromosomes in or out of the plane.

Laser ablation regions are highlighted by a green Region of Interest (ROI, Figure 2). Successful ablation of a single kinetochore results in loss of fluorescence at the kinetochore and movement towards the opposing pole (Figure 2). This movement of the irradiated chromosome is shown in Figure 3 along with control non-ablated kinetochores which show that the unablated kinetochores continue oscillation around the metaphase plate while the ablated kinetochore moves off the metaphase plate. Out of a total of 63 kinetochores targeted and ablated, only 9 undergo a clear cut ”slingshot” effect (movement towards the pole facing the un-irradiated kinetochore; Figure 4).

6.3 Discussion

Laser ablation that clearly irradiates and destroys a single kinetochore of sister chromatids (under tension) results in chromosome movement (hereafter known as ’slingshot’) towards the opposing pole. This result agrees with earlier observations [15], but with cdc20-YFP fluorescence we are able to visualize and ablate the kinetochore with a high degree of accuracy. So why are so few ”slingshot” results (9/63) observed? There

are 3 possible explanations: (1) the targeted sister chromatids were not under tension and ablation of the kinetochore did not result in any net force change on the chromatids, (2) irradiation of the kinetochore did not result in a complete destruction of the kinetochore thus microtubule attachments were still present and maintained a bipolar tension (3) the targeted ablation missed the kinetochore.

The first possibility (oscillating mono-oriented chromosomes positioned near the metaphase plate) is unlikely since this would not be expected to be seen as frequently as 57/63 cases. The second explanation is possible as in some observed cases, the laser ablation photobleaches the cdc20-YFP but the fluorescence is observed to return within a few minutes. In the third explanation, the kinetochore is missed completely whether due to movement of the chromosome while positioning to fire, or irradiating it when it is slightly out of plane due to movement. In the future, multiple z plane cuts and larger box cuts could be used to better ensure a completely irradiated kinetochore and reduction in the likelihood of missing the kinetochore completely. In the experiment described here, it is likely that all three of the above explanations may have played a role in the low number of successful ”slingshot” events.

These results indicate that complete destruction of the kinetochore is necessary for the observed slingshot movement. In addition, in Chapter 5, routine ablation of areas immediately in front of and in between pole and kinetochores was performed and no slingshot movement was ever observed (Chapter 5). In the case of destroying microtubules only and not the kinetochore anchoring point, the leftover microtubule stub (of whatever size) is able to re-polymerize and form lateral attachments (through motor proteins, side-side microtubule polymerization) to nearby microtubules which restores the opposing force and tension so that the cell does not undergo any displacement at all.

Could disruption of a significant number of microtubules not have an affect on chromosome movement in mitosis? In [17], chromosomes movement and individual kinetochore-microtubules are counted and in many cases, the force produced, the number of kinetochore-microtubules present on each sister chromatid and the movement observed do not match with 2 kinetochore-microtubules ’overpowering’ 11 kinetochore microtubules [17]. These results, and ours, are inconsistent with models which predict that force production and chromosome movement depends on kinetochore-microtubule

number. In our case, we could ablate and disrupt a significant number of microtubules, whether by partially disrupting the kinetochore so less can bind to it or direct ablation of nearby kinetochore microtubules. Force is produced at the kinetochore and requires the existence of the kinetochore and 'some' microtubules but this can be a very small number or even 'partial' stubs due to interactions with microtubule motor proteins.

6.4 Conclusion

This work shows that the "slingshot" effect first observed in 1981 [15] can be reproduced with the 532 nm laser in fluorescent fusion-protein PtK2 cells. However, these experiments are only preliminary in elucidating the relationship between number of kinetochore microtubules, the kinetochore, and force production. Future experiments could use drugs that inhibit Aurora B or select plus-end directed motor proteins. Aurora B acts as a tension sensor at the kinetochore and ablation of the microtubules and the kinetochore could be performed in order to see if the slingshot effect still occurs and examining the role of cdc14 and its' presumed inability to be transported to kinetochore due to spindle disruption.

6.5 Acknowledgements

Chapter 6 was done with Tsay Angela and Shi Linda.

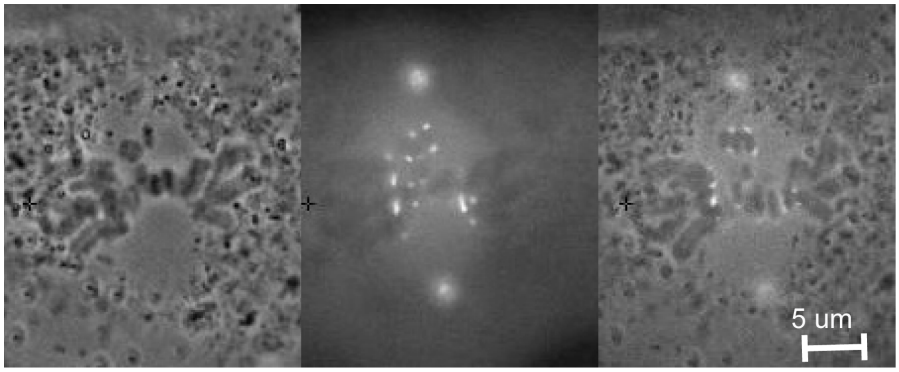

Figure 6.1: phase, fluorescence and overlay of metaphase mitotic spindle with cdc20 on kinetochores.

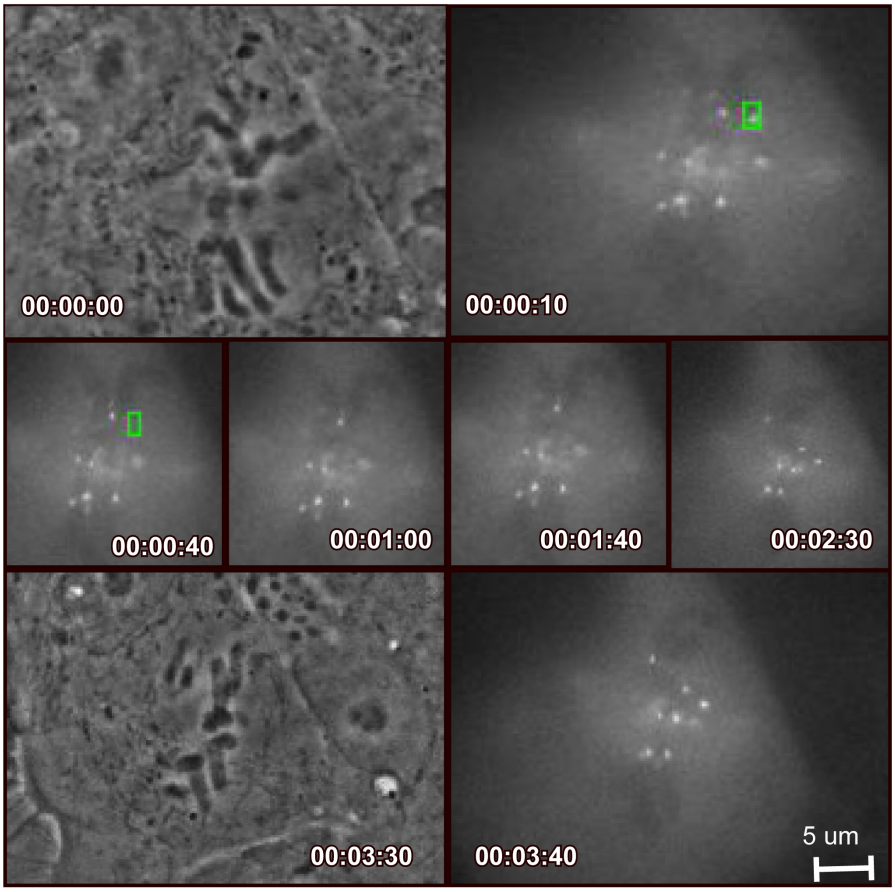

Figure 6.2: Laser ablation hits kinetochore at T = 00:00:40, and the chromosome movement is followed with T = 00:03:30 showing the chromosome clearly off the metaphase plate, and no fluorescence at the hit kinetochore.Time stamps indicated in each figure take 00:00:00 pre ablation and are formatted as hh:mm:ss. Scale bar represents 5 micrometers.

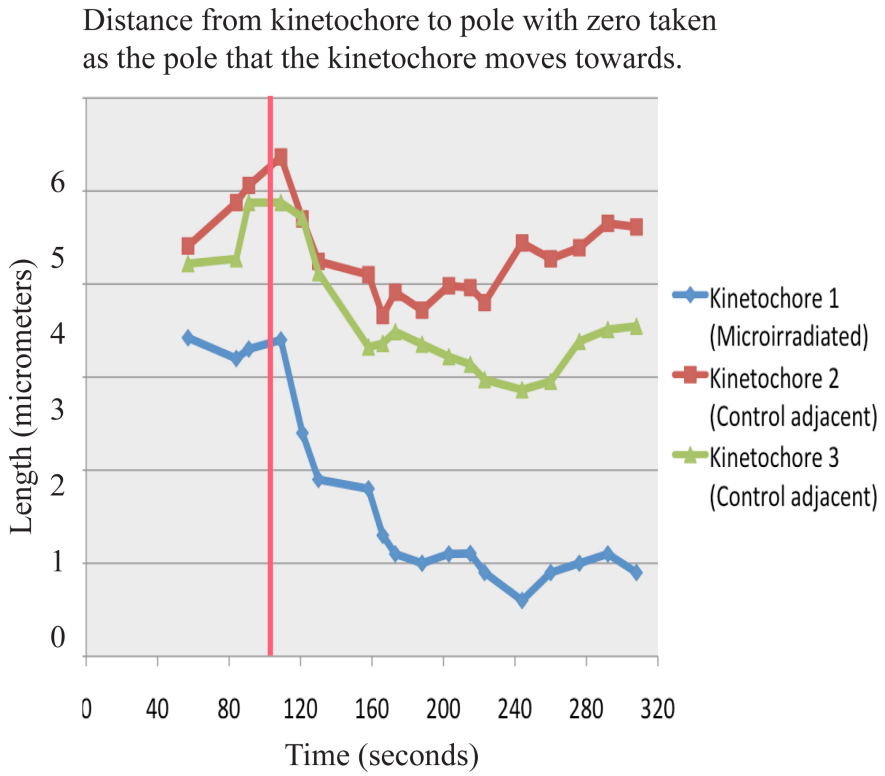

Figure 6.3: Distance from Pole to Kinetochore is taken with zero being the pole that the chromosome slingshots towards. Red vertical line marks time of ablation. Control kinetochores (near ablated kinetochore) are plotted to show unaffected normal oscillation compared to slingshot displacement.

Result of ablation	N	%
Slingshot	9	14
No Slingshot	57	86
Total cells	63	100

Figure 6.4: Ablation is targeted at kinetochores and in clear cut cases of destruction, slingshot is observed with high frequency, but photobleaching and 'partial' ablation result in incomplete destruction or complete missing of the kinetochore.

6.6 Bibliography

[1] Walczak Clare E., Cai Shang, Khodjakov Alexey. *Mechanisms of chromosome behaviour during mitosis* Nat Rev Mol Cell Biology 2010

[2] Rieder Conly L., Cole Richard W., Khodjakov Alexey, Sluder Greenfield. *The checkpoint delaying anaphase in response to chromosome monoorientation is mediated by an inhibitory signal produced by unattached kinetochores* Journal of Cell Biology 1995

[3] Kops Geert J. P. L., Saurin Adrian T., Meraldi Patrick. *Finding the middle ground: how kinetochores power chromosome congression.* Cell. Mol. Life Science 2010

[4] Civelekoglu-Scholey Gul, Scholey Jonathan M. *Mitotic force generators and chromosome segregation* Cell. Mol. Life Science 2010

[5] Rieder C.L., E.D. Salmon *The vertebrate cell kinetochore and its roles during mitosis.* Trends Cell Biology 1998

[6] Yuen K. W., Montpetit B., Hieter P. *The kinetochore and cancer: What's the connection?* Current Opinion Cell Biology 2005

[7] McEwen Bruce F., Dong Yimin. *Releasing the spindle assembly checkpoint without tension* Journal of Cell Biology 2009

[8] Maresca Thomas J., Salmon Edward D. *Intrakinetochore stretch is associated with changes in kinetochore phosphorylation and spindle assembly checkpoint activity.* Journal of Cell Biology 2009

[9] Uchida Kazuhiko S.K., Takagaki Kentaro, Kumada Kazuki, Hirayama Youko, Noda Tetsuo Noda, et al. *Kinetochore stretching inactivates the spindle assembly checkpoint* Journal of Cell Biology 2009

[10] Akiyoshi Bungo, Sarangapani Krishna K., Powers Andrew F., Nelson Christian R., Reichow Steve L., et al. *Tension directly stabilizes reconstituted kinetochore-microtubule attachments* Nature 2010

[11] Nezi Luigi, Musacchio Andrea *Sister chromatid tension and the spindle assembly checkpoint* Current Opinion in Cell Biology 2009

[12] Waters Jennifer C., Chen Rey-Huei, Murray Andrew W., Salmon E.D. *Localization of Mad2 to kinetochores depends on microtubule attachment, not tension.* Journal of Cell Biology 1998

[13] Pinsky B.A., Biggins S. *The spindle checkpoint: tension versus attachment.* Trends Cell Biology 2005

[14] Musacchio A., Salmon E.D. *The spindle-assembly checkpoint in space and time.* Nature Rev. Mol. Cell Biology 2007

[15] McNeil Patricia, Berns M.W. *Chromosome behavior after laser microirradiation of a single kinetochore in mitotic PtK2 cells.* Journal of Cell Biology 1981

[16] Yu Hongtao *Cdc20: A WD40 activator for a cell cycle degradation machine* Molecular Cell Review 2007

[17] McEwen Bruce F., Heagle Amy B., Cassels Grisel O., Buttle Karolyn F., Rieder Conly L. *Kinetochore fiber maturation in Ptk1 cells and its implications for the mechanisms of chromosome congression and anaphase onset.* Journal of Cell Biology 1997

7 Ablation of anaphase mitotic spindle

7.1 Introduction

Mitosis is a complex biomechanical rearrangement of chromosomes and organelles into two daughter cells and precise timing is required to couple anaphase progression (separation of chromosomes to each sister pole) to initiation of the cytokinetic furrow. How the cell determines the cell division plane depends on midzone and astral microtubules [1, 2] and the re-localization of essential midbody proteins [3, 4] to the midzone. These distinct proteins are located on the chromosome during metaphase [5] and are known as chromosome passenger proteins [6, 7] since they share the unique property of being translocated from chromosome to the midzone at anaphase onset.

Prominent passenger proteins are INCENP, Aurora B and Survivin. INCENP is the scaffold for the chromosome passenger complex (CPC) [8] and INCENP binds Aurora B [9] and Survivin [10] forming a INCENP-Aurora B-Survivin structure. Aurora B gradient regulates midzone activity [6, 9, 11, 12, 13] of CPC and other key proteins, and Survivin regulates Aurora B activity [14]. Temporal and spatial integration of chromosomal and cytoskeletal events is achieved by the targeting and re-localization of chromosome passenger proteins from chromosomes immediately after anaphase onset to the spindle midzone and has been shown to require dynamic microtubules [15], MKIp2, Cdc14 and Plk1 [17], INCENP [8,10], Aurora B [11, 12, 13] and Survivin [13, 14] for successful translocation of INCENP-Aurora B-Survivin.

In this study, we use a 532 nm laser to ablate microtubules on both sides of the mitotic spindle immediately after anaphase onset which results in (1) a disorganized mitotic spindle and (2) Aurora B not relocalizing to the spindle midzone and (3) failure of cytokinesis as chromosome passenger proteins stay on the chromosomes. These results

demonstrate that the translocation of chromosome passenger proteins occurs right after anaphase onset and that a bipolar-organized mitotic spindle is required for the chromosome passenger proteins to come off the chromosome.

7.2 Results

7.2.1 Aurora B control

PtK2 cells are stably transfected to carry Aurora B-GFP as shown in Figure 1. Aurora B localizes to centromeres and across the entire chromosome (Figure 1A, 1B) and in metaphase, all Aurora B is localized to chromosomes (Figure 1A) which then re-localizes to the spindle midzone within a few minutes after anaphase onset (Figure 1B).

7.2.2 Laser ablation of PtK2-CFP-Tubulin

PtK2 cells are stably transfected with CFP-Tubulin as described in Chapter 5. A single laser ablation on one side of the mitotic spindle is identical to chapter 5 ablation of metaphase spindle. Loss of fluorescence is followed by recovery and the cell successfully divides (Chapter 5).

Laser ablation performed on both sides of the mitotic spindle immediately after anaphase onset results in no cytokinetic furrow forming and a disorganized spindle as shown in Figure 2. 56 cells undergo a delayed furrow formation and progress through cytokinesis in approximately 1 hour. 27 cells do not form a furrow at all, even several hours after anaphase onset and exhibit a disorganized bent central spindle. 34 ablated cells divide normally (N total = 117, CFP-Tubulin, Figure 4).

7.2.3 Laser ablation of PtK2-Aurora B-GFP

PtK2 cells that are stably transfected with Aurora B-GFP are ablated immediately after anaphase onset in areas that would be presumed to sever the midzone from each pole (N = 147, Aurora B-GFP, Figure 4). Of these, 16 were observed to not form

a cytokinetic furrow at all and still had Aurora B stuck to the chromosomes hours after anaphase onset (Figure 3). Of the cells that do divide, Aurora B re-localizes to the midzone and appears similar to Figure 1B but with less fluorescence.

7.3 Discussion

Ablation of a single side of the mitotic spindle does not affect spindle organization or chromosome passenger protein movement. This agrees with monopolar spindles being able to position the furrow and divide [2]. Ablation of both sides of the mitotic spindle results in (1) disorganized central spindle (Figure 2) and (2) Aurora B not coming off chromosomes (Figure 3).

Current models of chromosome passenger proteins involve INCENP-Aurora B [8, 11] forming at centromeres and the complex being 'stuck' on chromosomes until Cdc14 regulates the release of the INCENP-Aurora B complex from centromeres [17]. The INCENP-Aurora B complex binds to Tubulin [15] and the motor protein MKIp2/plk1 [16, 17] uses the central spindle to transport the complex to the spindle midzone. Of particular importance from this model is that Cdc14 is required to release INCENP-Aurora B from chromosomes and that Cdc14 depends on MKIp2 for transport to the centromere and MKIp2 plays an additional role in transporting the entire complex to the spindle midzone.

This leads to two proposed models. (1) Disruption of the mitotic spindle causes a dysfunctional central spindle and MKIp2 and cdc14 are unable to reach the centromere to unlock INCENP-Aurora B or (2) the disruption of the mitotic spindle is temporary but due to the dual roles of MKIp2 for transporting to the centromere and then to the midzone, the first role is eliminated, and the second role proceeds on schedule which results in Cdc14 never reaching and unlocking the INCENP-Aurora B complex from the chromosomes.

The timing of the ablation (immediately after anaphase onset) and the fact that, despite recovery of spindle connection within 1 minute (chapter 5, Figure 2) the momentary disruption of the mitotic spindle causes a permanent defect in Aurora B being unable to come off centromere-chromosomes (Figure 3, Figure 4). This implies that

Cdc14 and MKIp2 attempt to reach the centromere immediately after anaphase onset and the central spindle is not yet disorganized (Figure 2, early). This would support the second model.

In the cases when the cell divides but with a significant delay (Figure 2, 3, 4) it is most likely due to incomplete 'full' cuts on each side. As a result of a 'partial' cut across the spindle, some MKIp2 and Cdc14 are able to localize to the centromeres. Due to a limited supply of motor proteins, not all Aurora B-INCENP is released from the chromosomes and successfully transported to the spindle midzone. An Aurora B gradient [11, 12, 13] is required for signaling of the cytokinetic furrow and proper cytokinesis. A weak gradient could be unable to reach a critical signaling mass for proper cytokinesis or could take much longer to phosphorylate target substrates resulting in the observed delay in cytokinesis (Figure 4).

7.4 Conclusion

While this work is still preliminary in determining the exact mechanism and nature of the cytokinetic defect, it is clear that disruption of the mitotic spindle on both sides results in the mislocalization of the Aurora B-INCENP complex and that this disruption is based on microtubule-transport and the inability of Aurora B-INCENP to come off centromere-chromosomes. The most likely model is that MKIp2 transports Cdc14 to centromeres via microtubules and that Cdc14 directly interacts with Aurora B-INCENP to release them from the centromere as opposed to the current model where MKIp2 is suggested to interact directly with Aurora B. The MKIp2 attempts to reach the centromere but there is no feedback mechanism for failure to reach the centromere, and the transport protein moves to the central spindle zone resulting in Aurora B-INCENP waiting at the centromere indefinitely.

7.5 Acknowledgements

Chapter 7 was done with Samantha Zeitlin.

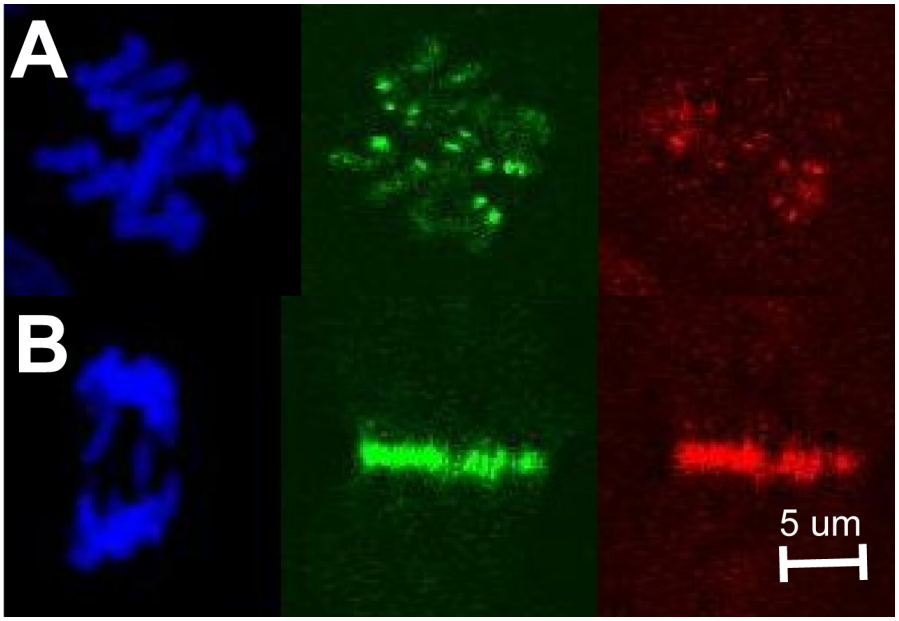

Figure 7.1: Aurora B localization at (A) metaphase and (B) anaphase. Blue is DAPI-chromosomes, Green and Red are Aurora B-GFP and Aurora B-antibody staining respectively, showing proper localization of Aurora B in control cells.

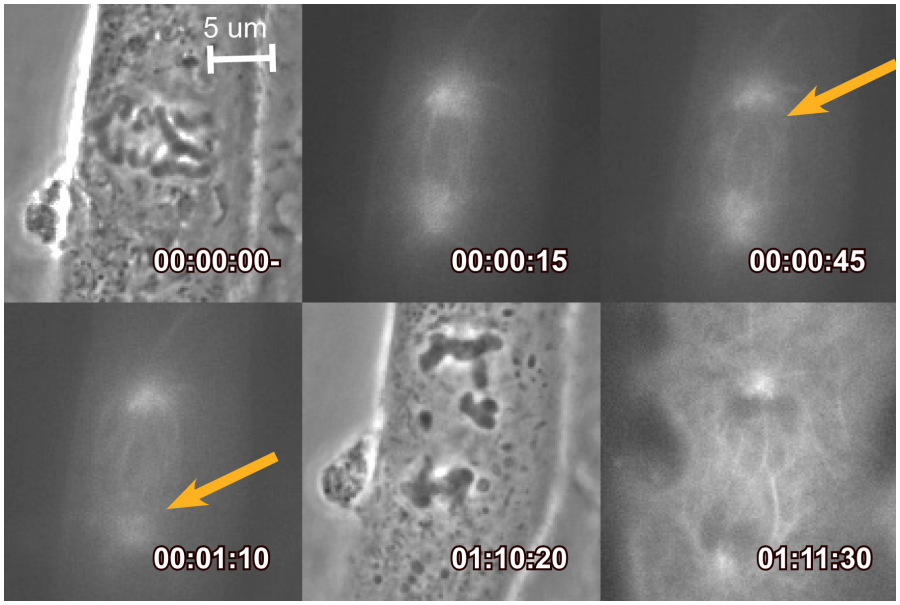

Figure 7.2: Precut phase and fluorescence is shown in T = 00:00:00- and 00:00:15 respectively. At T = 00:00:45, top is ablated, and bottom is ablated at T = 00:01:10. The cell does not form a furrow or divide and at T = 01:10:20 and 01:11:30, a 'normal' phase picture is observed with an abnormal spindle present. Time stamps indicated in each figure take 00:00:00 pre ablation and are formatted as hh:mm:ss. Scale bar represents 5 micrometers.

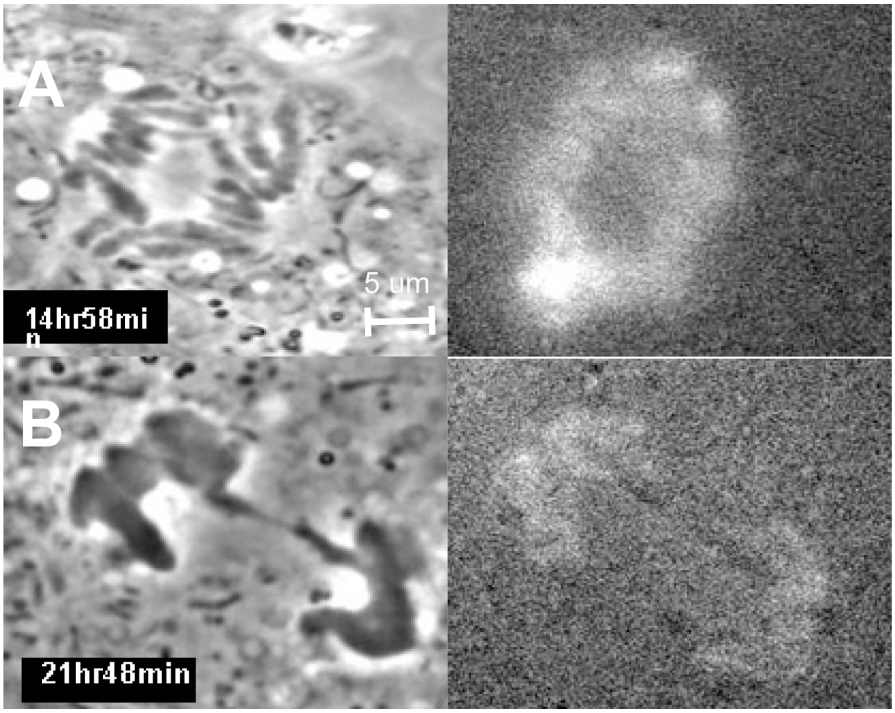

Figure 7.3: (A) shows anaphase spindle with Aurora B still on chromosomes after laser ablation. (B) Shows the same cell approximately 7 hours later that has still not divided and has Aurora B still on the chromosomes. Scale bar represents 5 micrometers.

Results from cutting both sides Tubulin-CFP	N	%	Mean Time (min)
Cell divides anyways	34	29	20
Cell has delayed division	56	48	65
Cell never divides	27	23	NA
Total cells	117	100	
Results from cutting both sides AuroraB-GFP	N	%	Mean Time (min)
Cell divides anyways	119	81	19
Cell has delayed division	12	8	75
Cell never divides	16	11	NA
Total cells	147	100	

Figure 7.4: Table shows results for CFP-Tubulin and GFP-Aurora B respectively. All cells were ablated on both sides of the mitotic spindle completely and immediately after anaphase onset. Due to 3D mitotic spindle structure, timing, and 'blind' cutting of microtubules in Aurora B-GFP, the numbers show much higher occurence of 'division' despite the attempts at laser ablation.

7.6 Bibliography

[1] Murata-Hori Maki, Wang Yu-li. *Both midzone and astral microtubules are involved in the delivery of cytokinesis signals: insights from the mobility of Aurora B.* Journal of Cell Biology 2002

[2] Canman Julie C., Cameron Lisa A., Maddox Paul S., Kapoor Tarun M., Salmon E.D., et al. *Determining the position of the cell division plane.* Nature 2003

[3] Canman Julie C., Sharma Nitin, Straight Aaron, Shannon Katie B., Salmon E.D., et al. *Anaphase onset does not require the microtubule dependent depletion of kinetochore and centromere binding proteins.* Journal of Cell Science 115 2002

[4] Terada Y, Tatsuka M, Suzuki F., Yasuda Y, Fujita S., et al. *A mammalian midbody associated protein required for cytokinesis* Journal of Cell Biology 2009

[5] Earnshaw William C., Cooke Carol A. *Analysis of the distribution of the INCENPs throughout mitosis reveals the existence of a pathway of structural changes in the chromosomes during metaphase and early events in cleavage furrow formation.* Journal of Cell Science 1991

[6] Xu Zhenjie, Ogawa Hiromi, Paola Vagnarelli, Earnshaw William C., Samejima Kumiko et al. *INCENP-Aurora B interactions modulate kinase activity and chromosome passenger complex localization* Journal of Cell Biology 2009

[7] Terada Yasuhiko *Role of Chromosomal passenger complex in chromosome segregation and cytokinesis.* Nature 2003

[8] Cooke C.A., Heck M.M., Earnshaw W.C. *The inner centromere protein (INCENP) antigens: movement from inner centromere to midbody during mitosis* Journal of Cell Biology 1987

[9] Sessa F., Mapelli M., Ciferri C., Stukenberg P.T., Musacchio A., et al. *Mechanism of Aurora B activation by INCENP and inhibition by hesperadin* Molecular Cell. 2005

[10] Wheatley Sally P., Carvalho Ana, Vagnarelli Paola, Earnshaw William C. *INCENP is required for proper targeting of Survivin to the centromeres and the anaphase spindle during mitosis* Current Biology, Elesvier Science 2001

[11] Mistry Hitesh B., MacCallum David E., Jackson Robert C., Chaplain Mark A.J., Davidson Fordyce A. *Modeling the temporal evolution of the spindle assembly checkpoint and the role of Aurora B kinase.* PNAS 2008

[12] Fuller Brian G., Lampson Michael A., Foley Emily A, Stukenberg P. Todd, Kapoor Tarun M, et al. *Midzone activation of Aurora B in anaphase produces an intracellular phosphorylation gradient.* Nature 2008

[13] Delacour-Larose Marlene, Molla Annie, Skoufias Dimitrios A., Margolis Robert L., Dimitrov Stefan. *Distinct dynamics of Aurora B and Survivin during mitosis.* Cell Cycle 2004

[14] Bolton M.A., Lan W., Powers S.E., Stukenberg P.T., et al. *Aurora B kinase exists in a complex with survivin and INCENP and its kinase activity is stimulated by survivin binding and phosphorylation.* Molecular Biology Cell. 2002

[15] Wheatley Sally P, Kandels-Lewis Stefanie E., Adams Richard R., Ainsztein Alexandra M., Earnshaw William C. *INCENP binds directly to tubulin and requires dynamic microtubules to target to the cleavage furrow.* Experimental Cell Research 2001

[16] Gruneberg Ulrike, Neef Rudiger, Honda Reiko, Nigg Erich A., Barr Francis A. *Relocalization of Aurora B from centromeres to the central spindle at the metaphase to anaphase transition requires MKIp2* Journal of Cell Biology 2004

[17] Neef R., Preisinger C., Sutcliffe J., Mayer T.U., Barr F.A. *Phosphorylation of mitotic kinesis-like protein 2 by polo-like kinase 1 is required for cytokinesis* Journal of Cell Biology 2003

8 Optical Studies on CENP-A

8.1 Importance in biology

DNA repair in chromatin is thought to occur in a stepwise manner. Cells must recognize a damage event, and recruit repair machinery to the site of damage. Damage signaling includes phosphorylation of *ataxia telangiectasia mutated* (ATM), which phosphorylates Chk2, H2AX, Nbs1, and many other proteins involved in the repair of DNA damage. [reviewed in 1]. Chromatin remodeling provides access to the damaged DNA (reviewed in [2, 3]) and, according to current models, chromatin is restored some time after DNA repair is completed [4].

The kinetics of chromatin remodeling at sites of DNA damage span minutes to hours. Histone H2AX phosphorylation is absent from up to 6 kb on either side of a double-strand break, but spreads outward at least 40 kb on both sides [5, 6]. After UV damage, new histone H3.1 appears approximately 30 min after damage [4], presumably due to reassembly after DNA repair. In contrast, bound H2B was detected surrounding double-strand breaks for up to 4 h, then replaced 10 h later [7]. Finally, despite triggering DNA damage signaling, unprotected telomere free DNA ends do not induce detectable chromatin turnover at all [8]. Thus, the extent and kinetics of histone turnover and replacement to sites of DNA damage are currently unclear.

Centromere protein A (CENP-A), a component of centromeric chromatin, is an essential histone H3 variant in all eukaryotic species examined to date. CENP-A is known to be required for [9, 10], and may be sufficient to promote [11, 12], centromere identity and assembly of the associated kinetochore protein complex, which mediates chromosome segregation during cell division. Since centromeric DNA sequences are not conserved in metazoans (reviewed in [13]), CENP-A presumably exerts its role in

centromere specification via a sequence-independent mechanism. Previously, it was observed that widespread DNA damage induced assembly of Xenopus CENP-A onto sperm DNA in cell-free egg extracts [14]. In this study, using the Robolase system, we tested the hypothesis that that localized laser-induced DNA damage is sufficient to recruit human and mouse CENP-A in vivo.

8.2 Results

8.2.1 Endogenous CENP-A recruited to DNA damage sites

To generate double-strand breaks in DNA in living human cells, we used the laser system described previously in Chapter 3 of this thesis and (Materials and Methods)[12]. Laser targeting along a 0.4 um-wide line (Figure1A) and phosphorylation of H2AX[reviewed in [15], was routinely detected. ATM and Rad51, both thought to be bound primarily at double-strand breaks, were also detected (Supplementary Appendix A) as were phosphorylated Nbs1 and 53BP1 (Figure 1B). CENP-A signals in laser targeted lines of interphase cells were observed in almost all cells (87% of 143b and 85% of HeLa, n = 30 and 20, respectively). In all cases, endogenous CENP-A was still detectable at centromeres (smaller foci; grayscale or green in Figure 1), demonstrating that CENP-A is not removed from centromeres in response to DNA damage.

8.2.2 Rapid accumulation of GFP-CENP-A at sites of DNA damage

To examine the kinetics of CENP-A targeting to sites of DNA damage, laser targeting was performed on two clonal human Hek293 cell lines expressing a GFP-CENP-A fusion protein [10] after FRT-mediated integration at a defined locus. Similar results were obtained with both lines. CENP-A mRNA increased approximately 7-fold within 24 h of induction (AppendixA-S2) and the 44 kDa GFP-CENP-A protein accumulated to approximately the initial level of endogenous CENP-A which was in turn reduced to about one third of its earlier level (AppendixA-S2). The decrease in endogenous CENP-A may be due to competition between transfected and endogenous CENP-A for stabilization by CENP-A binding factors. [3, 17, 18, 19, 20] Within 4 hours of

induction, GFP-CENP-A (AppendixA Figure 2C and D, green) co-localized with endogenous centromeres (detected using human anti-centromere auto-antisera (Appendix Figure 2C, red) and was distributed throughout nuclei (Appendix). After longer induction times (>24h), all cells exhibited centromeric foci surrounded by a generalized nuclear signal. The GFP signal was not removed by extraction with non-ionic detergents before fixation (AppendixA-S2). Timing of CENP-A recruitment to sites of DNA damage was determined after induction of GFP-CENP-A expression in the two clonal cell lines. Cells were visualized with phase-contrast and fluorescence microscopy, and specific areas were chosen for laser targeting (boxes in Figure 2 A-C). Laser exposure produced an initial 1.5 um^2 photobleached area (Fig 2 C and E). However, the GFP-CENP-A accumulated in a smaller (= 0.6 um^2) spot in the center of the photobleached region, consistent with H2AX phosphorylation (see figure 4). This was expected since the multiphoton effect that creates double-strand breaks is limited to a smaller volume: comparable photobleaching was observed at 6-fold lower laser doses, but this was insufficient to induce DNA damage. Fluorescence recovery within the photobleached zone required at least 1 h(e.g., cell 8 in figure 2 E and F), much longer than the <1 s that would be expected for a soluble approximately 45-kDa protein, confirming that most nuclear GFP-CENP-A was not freely diffusible. Damage consistently induced CENP-A foci in 71% of targeted cells (+- 10%, n = 176 interphase cells; for example, eight of 10 cells shown in Fig. 2), within an average of 5 min (+- 2 min, n = 82 interphase cells), including >30 experiments on separate days (n $\approx$ 100 cells per experiment). Once formed, each CENP-A focus remained stationary, and increased in fluorescent intensity for about 1 hour (Figure 2F). Foci formed with identical frequency and kinetics at both room temperature (25 C) and 37 C. However, at 37 C, GFP-CENP-A accumulations at targeted sites appeared and became brighter, and then were abruptly lost (e.g., between 63 min and 68 min in Fig 2G). Foci were not lost at 25 C, as some were still visible 18 h later. Cells with foci were never observed to enter mitosis.

The high frequency with which CENP-A accumulated at sites of laser exposure in asynchronous samples suggested that this can occur throughout the majority of interphase, as seen for endogenous CENP-A. Comparing the nuclear areas of cells that formed foci after laser exposure (n = 31, AppendixS3), with the areas of the randomly

cycling cells surrounding them (n = 450; AppendixS3) confirmed that CENP-A focus formation was not restricted to a subset of interphase cell cycle stages. Conversely, no cell cycle stage (aside from mitosis) was refractory to CENP-A focus formation. Finally, DNA damage-induced focus formation was not a phenomenon limited to immortalized cells. GFP-tagged human CENP-A was transiently transfected into primary human fibroblasts, and laser induced damage produced CENP-A foci with rapid kinetics (AppendixS4).

8.2.3 Rapid accumulation of GFP-CENP-A at sites of I-Scel Cleavage

To further test whether a double-strand break is sufficient to recruit CENP-A to DNA, we used the site-specific endonuclease I-SceI in a mouse NIH2/4 cell line (TM815 cells) which carries a single I-SceI target site flanked by LacI repeats. A GFP-tagged version of mouse CENP-A (GFP-mCENP-A) was constructed and expressed by transfection in these cells. As expected, GFP-mCENP-A was recruited to sites of laser-induced DNA damage with kinetics similar to GFP-tagged human CENP-A (GFP-hCENP-A) in human cells (Fig. Appendix). After transient expression of I-SceI, a single double strand break, marked by the presence of phosphorylated histone H2AX, was generated at the lacI array [visualized using mCherry-lacR (red)] (Fig. 3A). In 47% of cells, GFP-mCENP-A (green) was recruited along with phosphorylated histone H2AX (blue) (Fig. 3A). (The less than 100% efficiency is expected in this triple transfection experiment.) Additionally, TM815 cells were co-transfected with GFP-mCENP-A and an RFP-tagged fusion of I-SceI with the glucocorticoid receptor. Before addition of the synthetic glucocoricoid triamcinolone acetonide (TA), RFP-I-SceI-GR was cytoplasmic, and GFP-mCENP-A was detected throughout nuclei (Fig. 3B). Within 1 h after TA addition, RFP-I-SceI-GR translocated into nuclei, and in 57% of the cells (n = 100) phosphorylated histoneH2AXappeared at the I-SceI cleavage site (marked with CFP-LacR) along with a large GFP-mCENP-A focus (Fig. 3B). GFP-hCENP-A was also recruited to double stranded DNA breaks in a diploid human cell line carrying I-SceI sites at two loci. Transient co-transfection (Fig. 3C) was used to express GFP-hCENP-A and RFP-I-SceI-GR (30). Before addition of TA, RFP-I-SceI-GR was detected in the

cytoplasm, and GFP-hCENP-A was detected throughout the nucleus, with visible foci at centromeres (Fig. 3C). After addition of TA, RFP-I-SceI-GR became nuclear within 1 h and GFP-hCENP-A formed one or two new foci in 75% of the cells (n = 100 per experiment, repeated three times). Cells with two foci displayed one larger focus and one smaller focus (Fig. 3D), as expected for this cell line with multiple target sites for cleavage on chromosome 6 and a single site on chromosome 10. Remarkably, GFP-hCENP-A formed a focus as rapidly as 1 min after addition of TA (Fig. 3E). Taken together, these results demonstrate that CENP-A is rapidly recruited to defined DNA double-strand breaks.

8.2.4 Histones H3.1 and H2B do not accumulate at double-strand breaks

Next, we tested whether other histones accumulated at sites of DNA damage. Despite CENP-A accumulation and H2AX phosphorylation at sites of laser targeting (Fig. 1), neither YFP-H2B (n = 72 cells per experiment, repeated 3 times) (Fig. 4) nor YFP-H3.1 (n=75 cells per experiment; see Appendix) accumulated in targeted areas in live or fixed cells. Instead, both YFP-H2B (Fig. 4 and AppendixS6) and YFP-H3.1 (AppendixS5) expressing cells gradually recovered fluorescence in the laser targeted areas with similar kinetics (34h, n=10 cells each), consistent with a previous study of chromatin reassembly of fluorescently tagged core histones. Neither YFP-H2B nor YFP-H3.1 focal accumulations were observed, even after fixation and staining with anti-GFP antibodies to detect photobleached YFP-tagged histones. Moreover, even using transient transfection to produce a majority of histone H3.1 as a GFP-tagged protein, no GFP-H3.1 foci were ever observed after laser targeting (n = 63 cells; Appendix).

8.2.5 The Centromere-Targeting Domain of CENP-A (the CATD) Can Drive Histone H3 to Sites of DNA Damage.

It was reported previously that substitution into histone H3.1 of the CENP-A centromere targeting domain, or CATD, the central 31 amino acid portion of CENP-A (the last 6 residues of alpha helix1, all of loop 1, and all of alpha helix 2) is sufficient

to promote assembly of chimeric histone H3.1 to centromeres. Since CENP-A accumulated at sites of DNA damage in a majority of cells, but histone H3.1 never did, we tested whether this centromere targeting domain would cause accumulation of chimeric H3.1 at sites of DNA damage. Genes encoding a panel of CENP-A:H3.1 chimeric proteins were tagged with GFP and expressed in HeLa and HCT116 cells using transient transfection. The CATD was able to drive recruitment of histone H3.1 to sites of DNA damage, albeit at lower frequency than wild-type CENP-A (Fig. 5 A and B). The complementary mutations in CENP-A, replacing parts of the CATD with the analogous sequences of histone H3.1, reduced or abolished targeting to sites of laser exposure (Fig. 5A, HSA, HH2, H2.1, and H2.3), collectively identifying the $\alpha 2$ helix (mutant HH2) as the most critical region. Thus, recruitment to sites of DNA damage and assembly at centromeres utilizes a common targeting motif within CENP-A.

8.2.6 Other centromeric proteins are also recruited to sites of DNA damage.

Since CENP-A recruitment to sites of DNA damage and centromeres requires the same domains, we examined whether other centromeric proteins were also recruited to sites of DNA damage. GFP-tagged expression constructs for CENP-N, CENP-U, CENP-T, and CENP-M [20, 22, 23] were each transiently transfected into HCT116 cells, and these cells were subjected to laser exposure. In most (80%) targeted cells, CENP-N-GFP accumulated very rapidly (within 2 min) at sites of DNA damage (Fig. 5C). CENP-U-GFP was recruited to these sites of DNA damage with comparable kinetics (2 min) and as frequently (75%), although the foci were consistently smaller than those formed by CENP-N-GFP (Fig. 5D). CENP-T-GFP accumulated less often (44%) at sites of DNA damage, and only became visible later (30 min on average; Fig. 5E). In contrast, CENP-M-GFP did not accumulate at sites of DNA damage, and its recovery within the bleached areas was very rapid (Fig. S7B)., consistent with freely diffusing protein [21]. Taken together, these results demonstrate that, in addition to CENP-A, components of the CENP-ANAC, including CENP-N and CENP-U, are rapidly recruited to sites of DNA damage, while others (e.g., CENP-T) assemble after CENP-A, consistent with the order of assembly at centromeres [22, 23, 24].

8.2.7 CENP-A Recruitment to Double-Strand Breaks Is Enhanced by NHEJ but Independent of H2AX.

In mammalian cells, non-homologous end joining (NHEJ) is thought to be the predominant pathway for double-strand break repair. Early steps in NHEJ involve binding of the Ku86/Ku70 heterodimer to free DNA ends, followed by the DNA-dependent protein kinase catalytic subunit (DNA-PKcs), and eventual ligation by DNA ligase IV. To measure CENP-A accumulation after laser-induced damage, GFP-CENP-A was transiently transfected into HCT116 cell lines lacking various components of the NHEJ pathway. Laser exposure induced GFP-CENP-A foci at high frequency in parental (WT) HCT116 cells (57+- 10%; Fig. 6A), whereas foci occurred approximately 5-fold less frequently in HCT116 derivatives deficient in Ligase IV-/- or DNA-PKcs-/- (10%; Fig. 6A). In HCT116 cells heterozygous for Ku86 (Ku86+/-), CENP-A accumulation was detected at an intermediate frequency (19%; Fig. 6A). Together, these data suggested that the highest frequency of CENP-A accumulation at sites of damage correlates with activity of the NHEJ DNA repair pathway. To further test this hypothesis, GFP-tagged Ligase IV was transiently transfected into WT or Ligase IV-/- HCT116 cells (Appendix). In the absence of DNA damage, GFP-Ligase IV localized throughout the nucleus, with weak GFP signal in the cytoplasm, consistent with a previous report of Ligase IV localization by immunofluorescence. After laser targeting, the majority of GFP-Ligase IV was bleached, indicating that it is highly dynamic. GFP-Ligase IV rapidly formed a bright focus at the site of laser exposure in almost all WT (Appendix; 96%, n = 55) and Ligase IV-/- cells (Appendix, 88%, n = 57). Similar foci were detected with a GFP-tagged mutant, R278H, reported to have reduced (5 to 10% of WT) catalytic activity, in both WT (Fig. S8C, 94Next, constructs encoding wild-type or mutant Ligase IV fused to mCherry (instead of GFP) were transiently co-transfected along with GFP-CENP-A into HCT116 WT and Ligase IV-/- cells, and double-positive cells were laser targeted (Fig. 6B). As expected, expressing mCherry-Ligase IV did not increase the frequency of GFP-CENP-A foci in WT cells after laser exposure (57%; n = 20), but did increase the frequency in Ligase IV-/- cells (28%; n = 29), while mCherry-Ligase IVR278H produced an intermediate effect (17%; n=12) (Fig. 6B). The observation that CENP-A is recruited to sites of damage so rapidly, and apparently even in the absence of Ligase

IV activity, raised the possibility that CENP-A recruitment might participate in DNA repair. Since CENP-A depleted cells or cells unable to load CENP-A are non-viable, to test whether CENP-A could promote cell survival after DNA damage, inducible GFP-hCENP-A cells were exposed in triplicate to three doses of ionizing radiation (0 Gy, 2 Gy, and 10 Gy), with or without induction of GFP-hCENP-A. Parental 293 cells (Fig. 6C, open boxes) displayed 26% hypercondensed nuclei, indicative of cell death, within 24 h of 2 Gy, whereas cells induced to express GFP-hCENP-A (triangles) were protected (only 2%hypercondensed nuclei). Non-induced cells exhibited intermediate sensitivity at 2 Gy (5% hypercondensed nuclei), probably due to basal GFP-hCENP-A expression (see below). Both the parental and non-induced GFP-hCENP-A cells exhibited extensive cell death after 10 Gy (Fig. 6C, boxes). To test whether cells could continue dividing after radiation in a CENP-A-dependent manner, clonogenic survival assays were performed. After 8 Gy, parental 293 cells were uniformly killed, but induction of GFP-hCENP-A promoted cell survival and sustained colony growth (Fig. 6D). Intermediate numbers of surviving colonies were observed with the two independent clonal lines in the absence of tetracycline-mediated induction of GFP-hCENP-A. Survival was accompanied by increased levels of CENP-A (detected as increased GFP fluorescence), (Appendix) presumably from transient stabilization of GFP-hCENP-A. Finally, to test whether CENP-A recruitment requires histone H2AX, GFP-mCENP-A was transiently transfected into mouse embryonic fibroblasts (MEFs) from H2AX null mice and cells were laser targeted after 48 h (Fig. 6E and F). Absence of H2AX did not affect GFP-mCENP-A focus formation, with similar frequencies of rapid recruitment in laser targeted WT (43 +- 3%; n = 65) and H2AX null (32 +- 4%; n = 72) MEFs.

8.3 Discussion

Our observations using laser-induced DNA damage and I-SceI cleavage now establish that CENP-A accumulates at double strand DNA breaks in normal and immortalized human and mouse cells. Recruitment of CENP-A, CENP-N and CENP-U occurs within 12 min, a timescale as fast as that seen for phosphorylation of H2AX or other components of DNA repair (e.g., frequencies at which each is recruited to DNA damage

foci.) (BE) Human HCT116 cells were transiently transfected. DNAdamage was induced by laser targeting, and frequencies of focal accumulation at site of DNA damage were measured. (B)GFP-H3CATD. (C) GFP-CENP-N. (D) GFP-CENP-U. (E) GFP-CENP-T. ATM, Nbs1; sam44]. CENP-A recruitment is transient, disappearing again within approximately 1 h, and it is independent of H2AX. A comparison with CENP-A spot size and intensity at centromeres, estimated to contain approximately 5,000 to 15,000 CENP-A nucleosomes, suggests that CENP-A spreads outward surrounding a double-strand DNA break.

Mammalian CENP-A assembles into nucleosomes in vitro and has been found in nucleosomes of asynchronous cells. It has also been proposed that CENP-N interacts with CENP-A in nucleosomal form. We would caution, however, that it has not been established whether DNA damage dependent CENP-A loading represents assembly into nucleosomes. At least three models for CENP-A binding are plausible (Fig. 6G). First, CENP-A could be assembled into nucleosomes (Fig. 6G, left). If so, the failure of H2B-GFP to re-accumulate at these damage foci would require that CENP-A must be assembled along with H2B, H2A, and H4 from the original (photobleached) nucleosomes or an adjacent (photobleached) pool. A specific possibility is the selective removal of H3 (with or without H4) from individual nucleosomes and their replacement with CENP-A or CENP-A/H4. Second, CENP-A (and CENP-N and CENP-U) could bind on top of existing chromatin (Fig. 6G,middle). Third, a final alternative (Fig.6G, right) is that DNA repair occurs in a nucleosome-free zone, as proposed previously [6]. This would require removing histone H3-containing nucleosomes and recruiting CENP-A bound in a non-nucleosomal form that lacks H2A and H2B, as has been proposed for budding yeast centromeres. While it is clear that CENP-A recruitment to double-strand breaks occurs in both human and mouse cells, including primary cells, the function of CENP-A at double-strand breaks has not been defined. Our demonstration that CENP-A is recruited to double-strand breaks independent of H2AX suggests that it is not part of the damage checkpoint. In contrast, the cell-cycle independence of CENP-A recruitment, rapid kinetics, and correlation with LigaseIV catalytic activity, suggest that CENP-A may be recruited to double-strand breaks along with components of the NHEJ pathway, and raises the possibility that CENP-A participates in DNA repair. Finally, when

added to our earlier demonstration that CENP-A assembly at centromeres of Xenopus sperm requires DNA repair activities stockpiled in egg cytosol, CENP-A recruitment with some of its centromeric partners to double strand DNA breaks suggests a mechanism for the formation of new centromeres (neo-centromeres), which are only rarely detected as stable events. Since the timing of CENP-A disappearance from double-strand breaks correlates with the timing of DNA repair, our evidence provides the initial support for a model in which CENP-A is recruited along with repair machinery, and removed as repair is completed. CENP-A retention at these sites along with CENP-N and CENP-U would provide the nucleus for a new centromere, but only after an extremely rare convergence of permissive conditions. These conditions could include (1) failure to complete DNA repair and remove CENP-A, (2) coincidental timing of DNA damage and centromeric chromatin replication, the latter of which has been argued to occur only during G1, or (3) defective DNA damage checkpoint signaling, allowing cells to enter mitosis prematurely.

8.4 Materials and Methods

GFP-CENP-A stable inducible cell lines were generated based on a published plasmid [10] and commercial Flp-in Hek293 cells (Invitrogen). Transient transfections were performed in various cell lines using Lipofectamine2000 (Invitrogen). A series of control experiments were performed to determine the average laser power to consistently create detectable DNA damage. Low power (5.5 mW before objective) created DNA damage detected by immunofluoresence for H2AX and other damage markers in fixed cells. 11.2 mW was used as the maximum dose for cells expressing GFP-tagged proteins. In every experiment with GFP-tagged proteins, stable inducible GFP-CENP-A expressing cells were used to verify consistent frequency of focus formation at this dose. The average power measured before the objective was 5.5, 11, and 16.5 mW. Thus, the average power after the objective was 3.75, 7.5, and 11.2 mW in the focused spot. Since the 63x (1.4 NA) microscope objective focuses the beam to a diffraction limited spot diameter of 464 nm, peak irradiances of 2.5 x 10^9, 4.9 x 10^9, and 7.35 x 10^9 W/cm^2 were achieved in the focused spot. For one line scan of 5 microns (with 10 spots/line),

2,234.4 μJ of total energy (energy/pulse x no. of pulses per spot x no. of spots in the line) was delivered to each cell. We estimate that this amount of energy will create on average 110 breaks per targeted box.

Laser Sample Preparation.

For laser microirradiation experiments, cells were cultured in 35-mm glass-bottom dishes (Mattek catalog# P35G-1.514-C), coated by incubation with 10 microg/mL fibronectin in PBS (30 to 60 minutes at 37 C). After coating, fibronectin was aspirated, and cells were plated in the presence of tetracycline 18 to 24 h before laser microirradiation.

8.5 Summary

We demonstrated that CENP-A is rapidly recruited to double-strand breaks in DNA, along with three components (CENP-N, CENP-T, and CENP-U) associated with CENP-A at centromeres. CENP-A accumulation at DNA breaks is enchanced by active non-homologous end-joining but does not require DNA-PKcs or Ligase IV, and is independent of H2AX. Thus, induction of double-strand break is sufficient to recruit CENP-A in human and mouse cells and may also have a function in DNA repair.

8.6 Acknowledgements

Chapter 8, in part, is published in Zeitlin, G. Samantha, Baker M. Norman, Chapados R. Brian, Soutoglou Evi, Wang Y.J. Jean, Berns W. Michael, Cleveland W. Don. ”Double-strand DNA breaks recruit the centromeric histone CENP-A”, *Proceedings of the National Academy of Sciences of the United States of America*, 106(37):15762-7, 2009. The dissertation author was co-first-author of the paper.

8.7 Figures

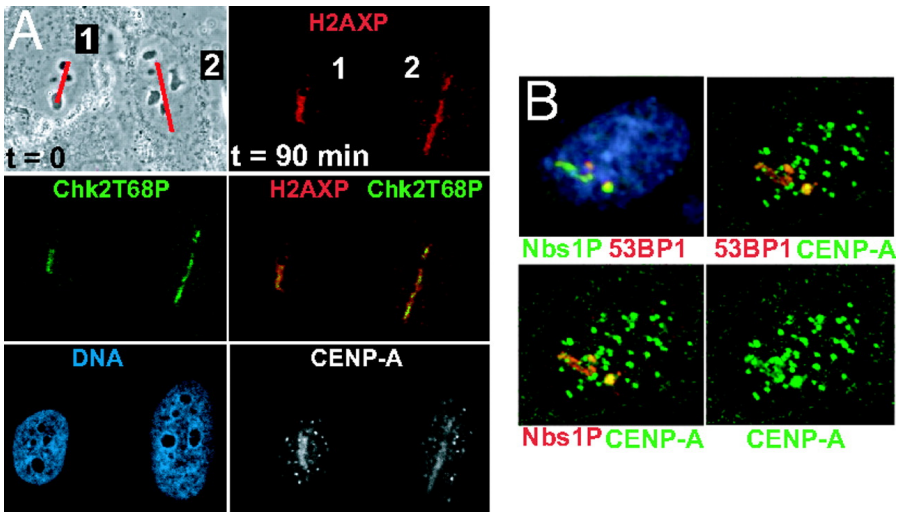

Figure 8.1: Endogenous CENP-A localizes to sites of laser-induced damage, along with DNA repair markers phosphorylated H2AX, Chk2, Nbs1, and 53BP1: (A) (top left) phase contrast image of human osteosarcoma (143b) cells just before laser targeting along a line (red); (Other panels) matched confocal immunofluorescent imaging 90 min (at 25 Celsius) after laser targeting; (Red) phospho-histone H2AX; (green) Thr-68 phospho-Chk2; (blue) DNA detected with DAPI;(grayscale endogenous CENP-A signal. Note the small foci in the CENP-A images are centromeres. Note that the cells are motile: the orientation of cell number 2 changed in the 90 min after targeting. (B) HeLa cell 90 min. (at 25 Celsius) after laser targeting along a single line. (Blue) DNA, (red) 54BP1 or Nbs1 phospho-Ser-343, and (green) Cenp-A. Other foci in the CENP-A image are centromeres.

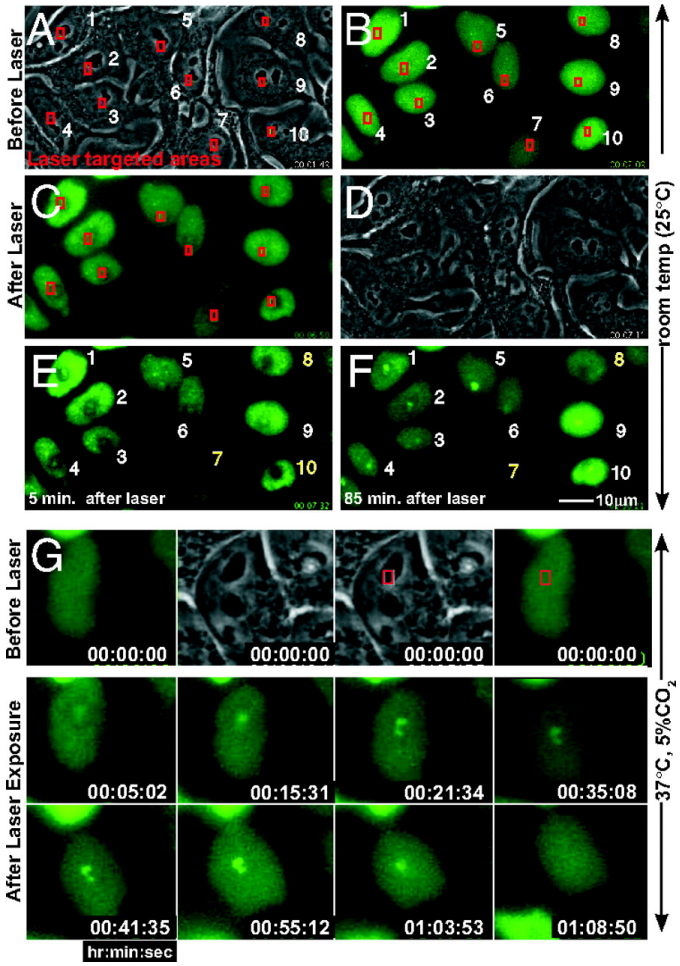

Figure 8.2: Rapid GFP-CENP-A accumulation at sites of DNA damage. (AF) GFP-CENP-A cells before and after laser targeting at 25 C. Phase contrast (A) before and (D) 5 min. after targeting the areas boxed in red. Epifluorescence images of GFP-CENP-A, immediately (B) before and (C) 4 or (E) 5 min. after initiating laser exposure. In most cells (numbered in white), GFP-CENP-A accumulated at the sites of targeting. [Cells numbered 7, 8 and 10 (in yellow) were bleached during laser targeting,] (F) Within 85 min, GFP-CENP-A formed foci within targeted regions. (G) Laser targeting as in (AF), maintained at 37 C after targeting: a CENP-A focus appears within 5 min after laser exposure, reaches its peak intensity 1 h after laser exposure, and then disappears approximately 15 min later. Timestamp represents hours:minutes:seconds.

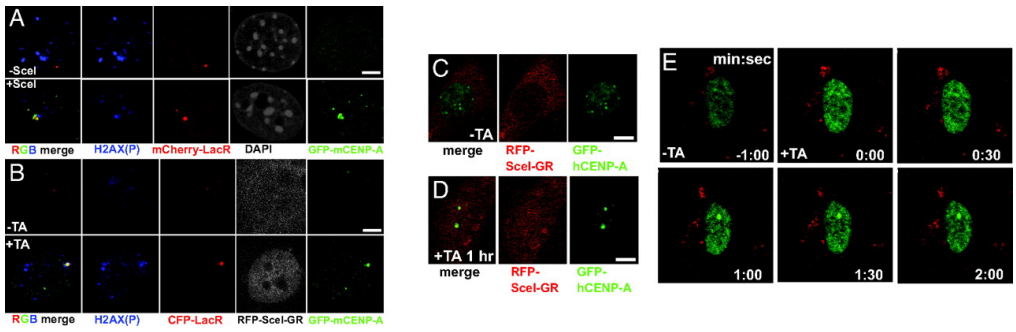

Figure 8.3: Rapid GFP-CENP-A accumulation at double-strand breaks induced by I-SceI cleavage in human and mouse cells. (A) Mouse cells carrying an I-SceI target site co-integrated with lacO repeats (30) after transient transfection to express (green) GFP-mCENP-A and (red) mCherry-lacR and (top) without or (bottom) with HA-tagged I-SceI. (Blue) -H2AX; (grayscale) DNA detected with DAPI. (B) The same mouse cell line as in (A), transiently co-transfected to express (green) GFP-mCENP-A, (red) CFP-lacR and (grayscale) RFP-I-SceI-GR and (top) without TA or (bottom) after TA addition for 1 h. (Blue) -H2AX. (CE) Human cells carrying a single SceI target site on chromosome 10 and multiple SceI target sites on chromosome 6 were transiently co-transfected to express GFP-CENP-A and RFP-I-SceI-GR. (C and D) Cells imaged for (red) RFP-SceI-GR or (green) GFP-hCENP-A and (C) without or (D) 1 h. after addition of TA, which induces nuclear accumulation of RFP-I-SceI-GR to cleave the DNA. (E) Timelapse images of a single cell transfected as in (C and D) immediately before and after addition of TA. Timestamp is minutes:seconds.

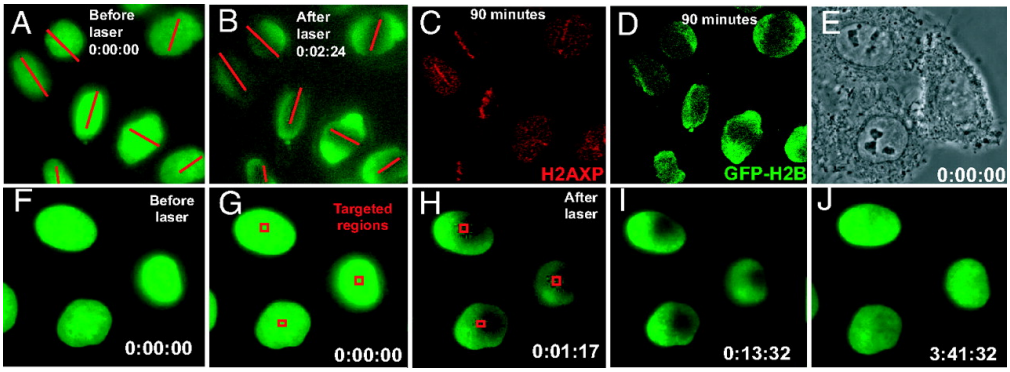

Figure 8.4: Histone H2B never accumulates in areas of laser-induced DNA damage. (AD) Epifluorescence images of HeLa cells stably expressing YFP-H2B (A) before and (BD) after laser exposure (red lines). (C) -H2AX and (D) YFP-H2B 90 min. after laser exposure. (E) Phase contrast image of HeLa cells stably expressing YFP-H2B before laser targeting. (FJ) YFP-H2B epifluorescence of the cells in (E) and (F and G) before or (HJ) after laser targeting. Red squares in (G and H) denote laser targeted areas. Timestamp is hours:minutes:seconds.

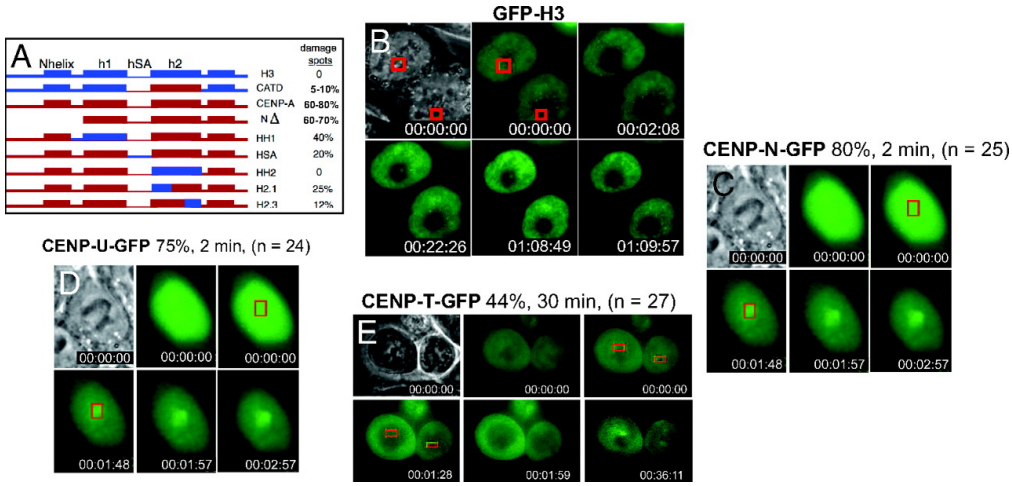

Figure 8.5: CENP-A recruitment to sites of DNA damage requires its centromere-targeting domain (CATD) and recruits centromeric nucleosome-associated factors CENP-N and CENP-U. (A) Schematic of CENP-A/H3 chimeric proteins and frequencies at which each is recruited to DNA damage foci. (BE) Human HCT116 cells were transiently transfected. DNA damage was induced by laser targeting, and frequencies of focal accumulation at site of DNA damage were measured. (B) GFP-H3CATD. (C) GFP-CENP-N. (D) GFP-CENP-U. (E) GFP-CENP-T.

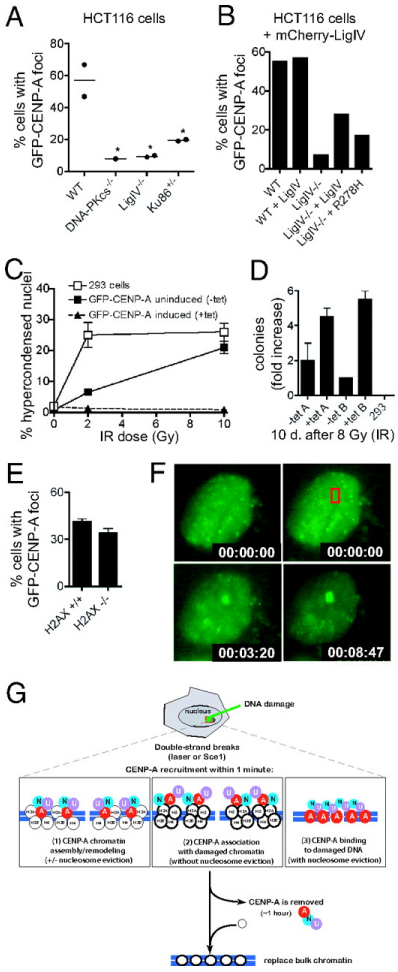

Figure 8.6: CENP-A in function in DNA repair independent of H2AX, and possible models for CENP-A assembly at sites of DNA repair. (A) HCT116 cells generated by targeted disruption of NHEJ genes were transiently transfected to express GFP-CENP-A; (B) Frequencies of GFP-CENP-A recruitment to sites of laser-induced DNA damage in Ligase IV/ cells transfected to express mCherry-LigaseIV or mCherry-LigaseIV-R278H. (C) Percentages of cell death following 0 Gy, 2 Gy, and 10 Gy irradiation (done in triplicate) in cells with a stably integrated, GFP-CENP-A gene, either with or without tetracyline-mediated gene induction. (D) Cell survival in a colony formation assay after 8 Gy irradiation of parental 293 cells or inducible GFP-CENP-A cells. (E) Frequency of (transiently transfected) GFP-mCENP-A recruitment to sites of laser-induced DNA damage in wild-type and H2AX null MEFs. (F) GFP-mCENP-A recruitment to focal DNA damage (red box) in an H2AX null cell. (G) Model for CENP-A recruitment to sites of DNA damage.

8.8 Bibliography

[1] Shrivastav M, De Haro LP, Nickoloff JA *Regulation of DNA double-strand break pathway choice* Cell Res 18:134-137. 2008

[2] Bao Y, Shen X *SnapShot: Chromatin remodeling complexes*. Cell 129:632 2007

[3] Osley MA, Tsukuda T, Nickoloff JA *ATP-dependent chromatin remodeling factors and DNA damage repair*. Mutat Res 618:6580 2007

[4] Polo SE, Roche D, Almouzni G *New histone incorporation marks sites of UV repair in human cells*. Cell 127:481493. 2006

[5] Berkovich E, Monnat RJ, Jr, KastanMB *Assessment of protein dynamics andDNA repair following generation of DNA double-strand breaks at defined genomic sites.*. Nat Protoc 3:915922 2008

[6] Tsukuda T, Fleming AB, Nickoloff JA, OsleyMA *Chromatin remodeling at a DNA double-strand break site in Saccharomyces cerevisiae.*. Nature 438:379383 2005

[7] Berkovich E, Monnat RJ, Jr, Kastan MB *Roles of ATM and NBS1 in chromatin structure modulation and DNA double-strand break repair*. Nat Cell Biol 9:683690 2007

[8] Wu P, de Lange T *No overt nucleosome eviction at deprotected telomeres*. Cell Biol 28:57245735 2008

[9] Howman EV, et al. *Early disruption of centromeric chromatin organization in centromere protein A (Cenpa) null mice*. Proc Natl Acad Sci USA 97:11481153 2000

[10] Sugimoto K, Fukuda R, Himeno M *Centromere/kinetochore localization of human centromere protein A (CENP-A) exogenously expressed as a fusion to green fluorescent protein.*. Cell Struct Funct 25:253261 2000

[11] Heun P, et al. *Mislocalization of the Drosophila centromere-specific histone CID promotes formation of functional ectopic kinetochores.*. Dev Cell 10:303315 2006

[12] Van Hooser AA, et al. *Specification of kinetochore-forming chromatin by the histone H3 variant CENP-A.*. J Cell Sci 114:35293542 2001

[13] Murphy TD, Karpen GH *Centromeres take flight: Alpha satellite and the quest for the human centromere*. Cell 93:317320. 1998

[14] Zeitlin SG, Patel S, Kavli B, Slupphaug G *Xenopus CENP-A assembly into chromatin requires base excision repair proteins*. DNA Repair (Amst) 4:760772. 2005

[15] Fillingham J, Keogh M-C, Krogan NJ *GammaH2AX and its role in DNA doublestrand break repair.*. Biochem Cell Biol 84:568577. 2006

[16] Tsvetkov L, Xu X, Li J, Stern DF *Polo-like kinase 1 and Chk2 interact and colocalize to centrosomes and the midbody.*. J Biol Chem 278:8468-8475 2003

[17] Collins KA, Furuyama S, Biggins S *Proteolysis contributes to the exclusive centromere localization of the yeast Cse4/CENP-A histone H3 variant.*. Curr Biol 14:19681972. 2004

[18] Foltz DR, et al. *ThehumanCENP-A centromeric nucleosome-associated complex.*. Nat Cell Biol 8:458469. 2006

[19] Moreno-Moreno O, Torras-Llort M, Azorin F *Proteolysis restricts localization of CID, the centromere-specific histone H3 variant of Drosophila, to centromeres.*. Nucleic Acids Res 34:62476255. 2006

[20] Black BE, et al. *Centromere identity maintained by nucleosomes assembled with histone H3 containing the CENP-A targeting domain*. Mol Cell 25:309322. 2007

[21] Dundr M, Misteli T *Measuring dynamics of nuclear proteins by photobleaching.*. Curr Protoc Cell Biol 13:13.15. 2003

[22] Hellwig D, et al *Live-cell imaging reveals sustained centromere binding of CENP-T via CENP-A and CENP-B.*. J Biophotonics 1:245254 2008

[23] Hori T ,et al. *CCAN makes multiple contacts with centromeric DNA to provide distinct pathways to the outer kinetochore*. Cell 135:10391052 2008

[24] Carroll CW, Silva MC, Godek KM, Jansen LE, Straight AF *Centromere assembly requires the direct recognition of CENP-A nucleosomes by CENP-N.*. Nat Cell Biol 11:896902 2009

9 Summary and conclusions

9.1 Summary

The purpose of this dissertation was to (1) develop and fine-tune the laser microscope system (Robolase), (2) use this system to investigate specific biological problems related to mitosis and related processes, and (3) show that lasers have a valuable niche role due to their spatial and temporal specificity. Chapter 2 discusses the theory and mechanisms of optical ablation and the multiphoton micro-plasma type of damage and its application in perturbing DNA and microtubules. Chapter 3 discusses the hardware, software and the Robolase setup.

Chapter 4 discusses the laser ablation and the affect of targeting and damaging chromosome tips, the presumed telomere regions in anaphase. Studies with telomeres reveal several roles for the telomere, from serving as a check against cancer, a buffer against aging, and harboring of key DNA damage repair and recognition proteins. In this study it was shown that telomere disruption, most likely via DNA damage, is able to communicate to the cytokinetic machinery and cause perturbations in cytokinesis, the final stage of cell division.

Chapter 5 describes and discusses the effect of laser ablation of specific regions of microtubules in the metaphase mitotic spindle. Microtubules are perturbed by the laser and the effect of the laser ablation on the highly dynamic mitotic spindle is observed. The spindle re-shapes itself and controls its rate equations and steady-state to insure that the spindle is balanced and both half-spindles are of equal length. By doing a 'prolonged' perturbation via repeated ablation of the mitotic spindle, which prevents microtubule re-polymerization, it was shown that bipolar spindle attachment is required for this dynamic equilibrium process.

Chapter 6 discusses laser ablation of kinetochores during metaphase. Each sister chromatid has a single kinetochore and ablation of the kinetochore results in loss of microtubule attachment and force. A chromatid pair with both sisters having microtubule attachments is ablated at one kinetochore and the chromatid pair springs back towards the pole that still has a kinetochore-to-pole microtubule attachment. Ablation of the microtubule region directly in front of kinetochore but not destruction of the anchoring kinetochore itself does not result in movement of the chromosomes. This demonstrates that in some cell lines, like PtK2, microtubules re-polymerize side-to-side and have motor proteins linking them and providing force so that even a small kinetochore-microtubule stub is enough to anchor chromosomes in place at the metaphase plate.

Chapter 7 discusses the laser ablation of microtubules in anaphase and the failure of cytokinesis due to the disruption of the anaphase mitotic spindle. Microtubule ablation during metaphase allows full recovery of bipolar spindle but ablation of both sides of the mitotic spindle simultaneously un-anchor the pole-to-pole microtubules and allow for misaligned microtubule re-polymerization and a disordered central spindle while still maintaining bipolar structure outwardly. This disarray of microtubules prevents the proper signaling and localization of chromosome passenger proteins and the cleavage furrow presumably through the inability of cdc14 to localize and unlock Aurora B at the centromere.

Chapter 8 discusses the laser ablation of DNA in interphase and the recruitment of DNA damage repair and recognition proteins. The ATM repair pathway and several key DNA markers are well characterized and known but the role of CENP-A in this process was not well understood. In this study, it was shown that CENP-A also localizes to DNA damage and that it plays an important role in the recruitment and repair of DNA damage.

In summary, this dissertation has described the laser microscope and its use in studying 5 separate biological problems. Using this system, it was revealed that (1) there is a telomere-mediated checkpoint that can cause dysfunctional cytokinesis, (2) there is a requirement of bipolar spindle attachment (tension) for balancing of the spindle and its' rate equations, (3) CENP-A localizes to DNA damage and plays a role in recruitment and repair of DNA damage, (4) spindle disruption in anaphase results in a disordered

spindle and causes the delocalization of Aurora B, and (5) ablation of a kinetochore in metaphase results in the individual chromatid 'springing' back towards the pole that still has a kinetochore-to-pole microtubule attachment, while ablation of microtubule region directly in front of the kinetochore does not result in chromosome displacement. The results of all 5 series of experiments described in this thesis demonstrate that the laser has a valuable niche role in biological studies that could not be easily accomplished by biochemical techniques that are global, catastrophic, or permanent in their disruption.

9.2 Future work

For this dissertation, studies were focused predominately on laser ablation as the tool for perturbing a biological system. In the future, the studies can be extended to include several key biochemistry techniques and to perform perturbations with biochemistry in addition to the laser in order to elucidate key roles of specific structures in mitosis.

For the telomere study, a defective cytokinesis is observed and the exact pathway and method is not known. Aurora B and other chromosome passenger proteins play a key role in successful cytokinesis and transfection and further studies of those would be helpful in determining how the telomeres control the progression of cytokinesis. The method of disruption of a telomere and how it realizes there is disruption is most likely due to DNA damage and thus further studies into ATM and other DNA damage proteins can resolve how the telomere signals that it is disrupted. The telomeres were also targeted and disrupted via tip ablation which gave a statistical probability of actual creation of a disrupted telomere event. Transfection of telomere markers into cells would improve accuracy and the number of disruption events and could even allow this to be done in a different cell line.

For the spindle study, force-balancing in the mitotic spindle is observed and shown to be dependent on bipolar spindle attachment. The laser has a niche role but it can also be combined with suitable biochemistry techniques to observe the effects of laser perturbation on spindles that lack key motor proteins, altered physiological conditions or alter microtubule dynamics. In addition, there are several mathematical and

computational models that describe mitotic spindle mechanics and laser perturbation could provide an additional subset of data that result in more accurate models.

9.3 Conclusions

In summary, the system described here provides an optically-based laser microscope to study biological problems. This system has been used to demonstrate (1) telomere-specific disruption links to cytokinesis, (2) bipolar spindle attachment is necessary for spindle dynamics, (3) CENP-A localizes to DNA damage and plays a role in the repair, (4) Aurora B de-localizes with anaphase spindle disruption, and (5) kinetochore destruction results in ”slingshot” effect. In conclusion, laser ablation is a powerful tool for furthering our understanding of key biological structures by selective perturbation. The laser approach allows a specific spatial and temporal disruption that advances our understanding of these structures in ways that normal biochemistry can not achieve alone.

A Supplemental Cenp-A

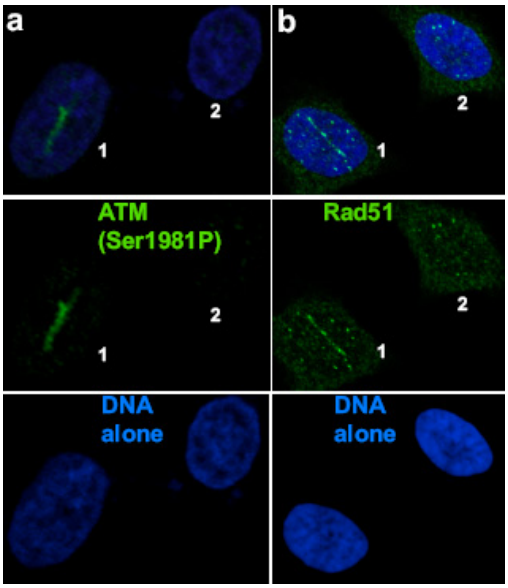

Figure A.1: Laser targeting activates ATM and recruits Rad51. Immunofluorescence detection of markers for double-strand breaks. HeLa cells were exposed (cell #1) or not exposed (cell #2) to laser targeting, fixed and incubated with antibodies to detect activated (phosphorylated at Ser-1981) ATM kinase (a) or for Rad51 (b), shown in green. DNA (detected with DAPI) is shown in blue).

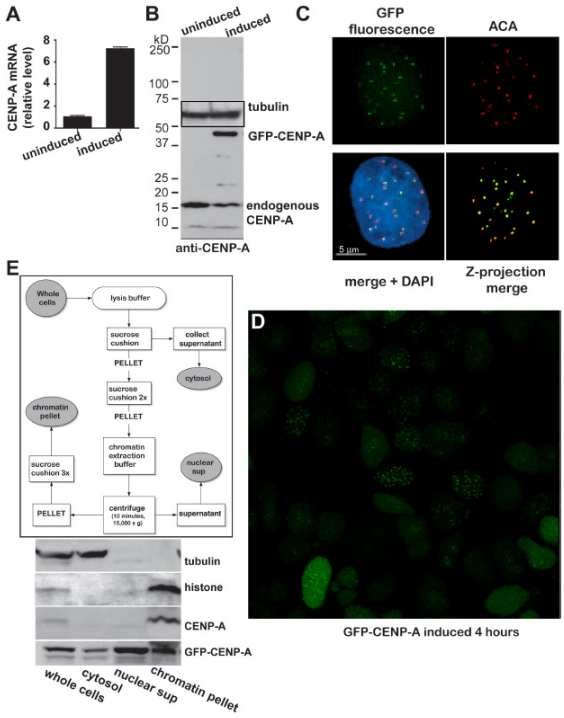

Figure A.2: Characterization of inducible GFP-CENP-A cell lines. (A) Relative levels of CENP-AmRNA before (non-induced) and after addition of tetracycline (induced) were measured using quantitative RT-PCR. (B) Relative levels of tagged and endogenous CENP-A protein were measured by western analysis with an antibody that detects both proteins with and without tetracycline induction. Tubulin was detected as a loading control. (C) Co-localization of GFP-CENP-A fluorescence [previously characterized (1)] with endogenous centromeres (detected with human autoimmune anti-centromere antisera, hACA, in red) was assessed using single confocal slices. DNA is detected with DAPI and shown in blue. Since GFP-CENP-A and hACA levels are not always equal, a Z-projection is shown (far right) where levels were equalized to emphasize overlap (yellow). (D) Variable pattern of GFP-CENP-A localization at early time-points after induction is shown in an example confocal image. Similar results were obtained with multiple clonal cell lines. (E) The majority of endogenous CENP-A (anti-CENP-A) and core histone fraction (anti-H3 antibody) are tightly bound to DNA, since these remain in the chromatin subfraction (chr) after washing with high salt and detergent. Approximately equal quantities of GFP-CENP-A (anti-GFP) are detected in both a nuclear fraction extracted by high salt and detergent (nuclear sup) and an insoluble fraction (chromatin pellet).

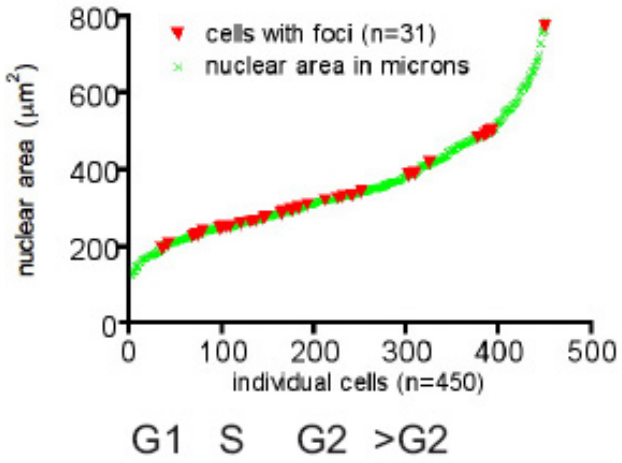

Figure A.3: Nuclear size analysis of cell cycle stage distribution of cells displaying CENP-A focus formation. A dish of cells exposed to laser targeting was fixed with formaldehyde, and DNA was detected with DAPI. Images were collected on a population of cells, and nuclear areas were calculated for this population (green x's). The nuclear areas of cells with GFP-CENP-A foci were mapped onto this distribution (red triangles).

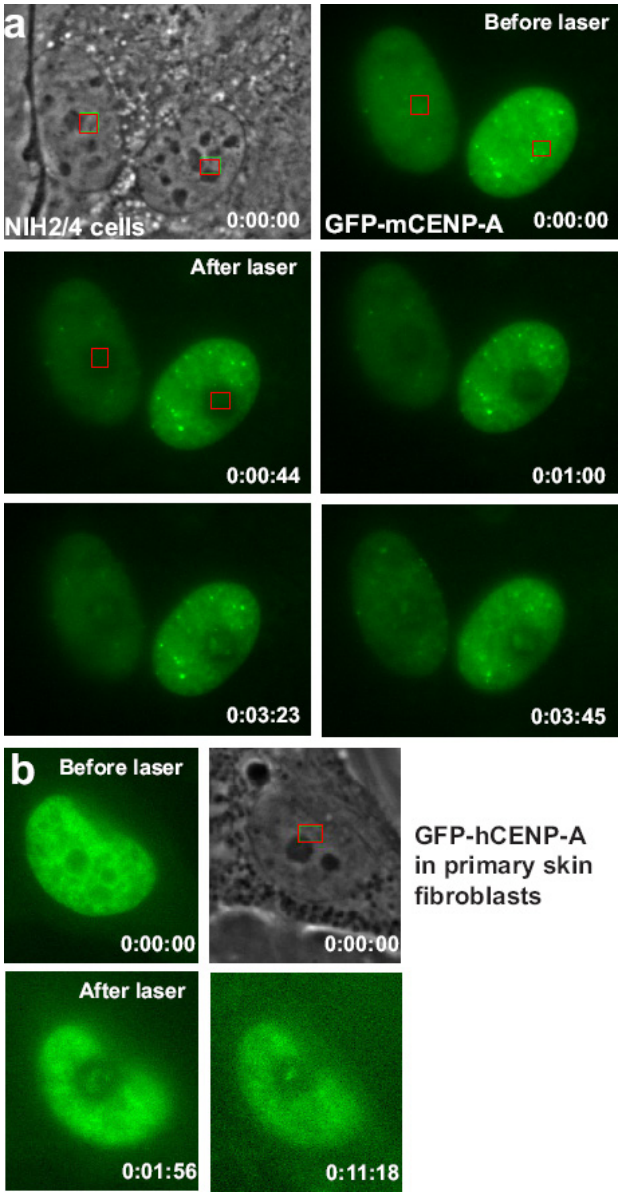

Figure A.4: GFP-tagged mouse CENP-A accumulates in areas of laser-induced DNA damage in mouse cells, and GFP-tagged human CENP-A behaves similarly in primary human cells. (a) GFP-tagged mouse CENP-A was transiently transfected into NIH 2/4 cells, and these cells were subjected to laser exposure. (b) GFP-tagged human CENP-A was transiently transfected into primary human GM3491 cells, and these cells were subjected to laser exposure. Timestamp represents hours:minutes:seconds.

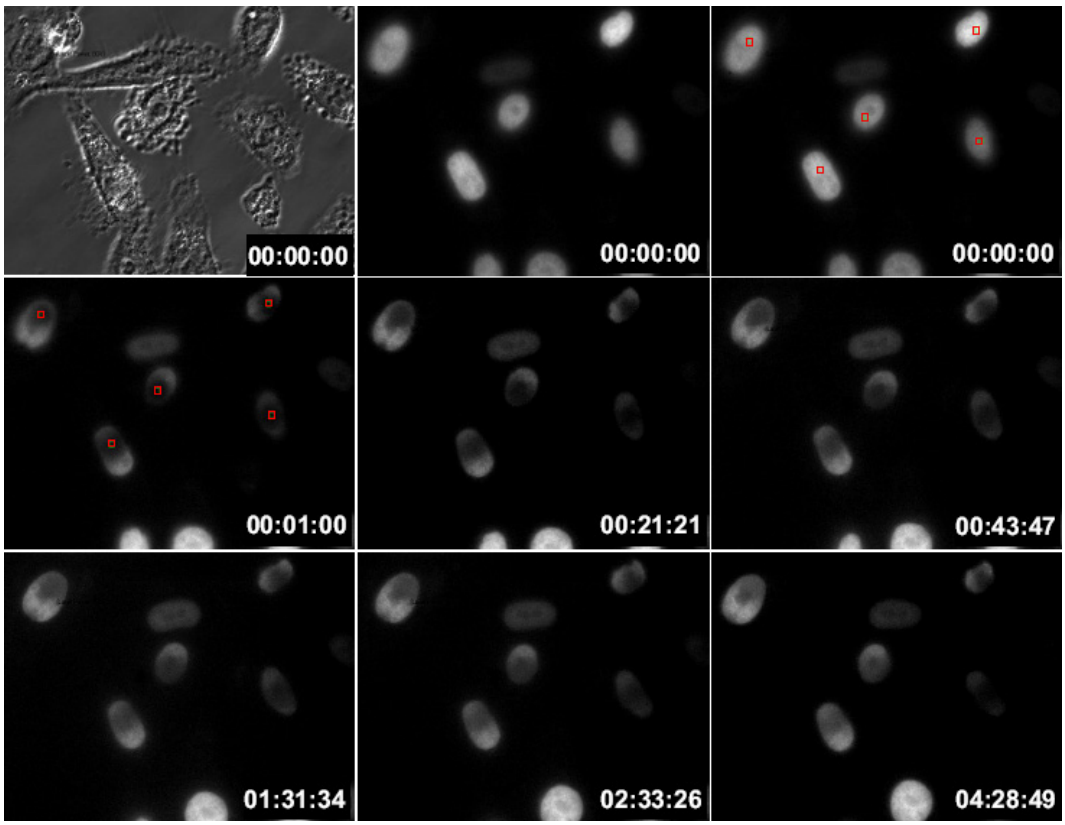

Figure A.5: Example extended timelapse of YFP-H3.1 recovery after laser targeting. Targeted areas are shown in red. Timestamp is shown in hours:minutes:seconds. YFP is shown in grayscale.

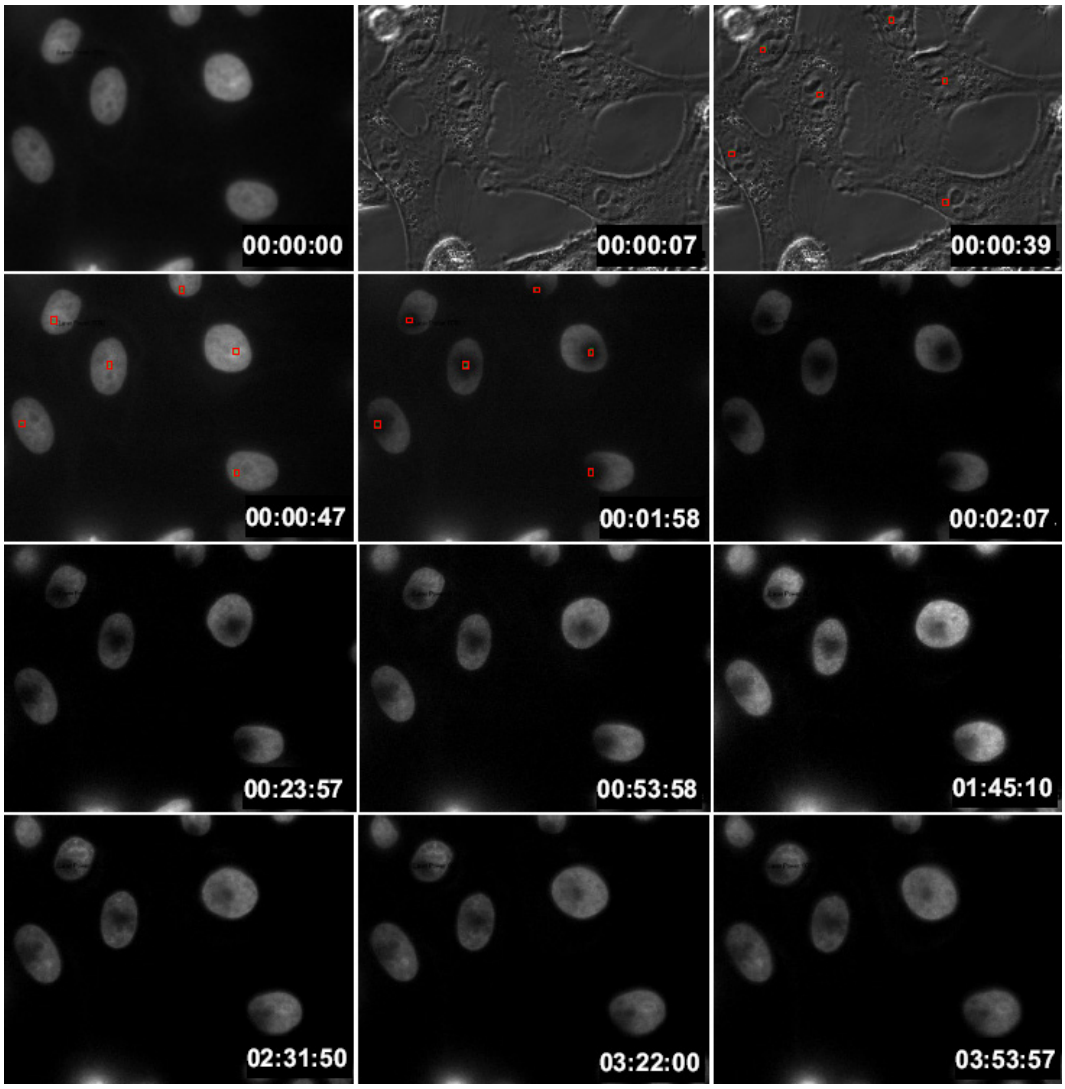

Figure A.6: Example extended timelapse of YFP-H2B recovery after laser targeting. Targeted areas are shown in red. Timestamp is shown in hours:minutes:seconds. YFP is shown in grayscale.

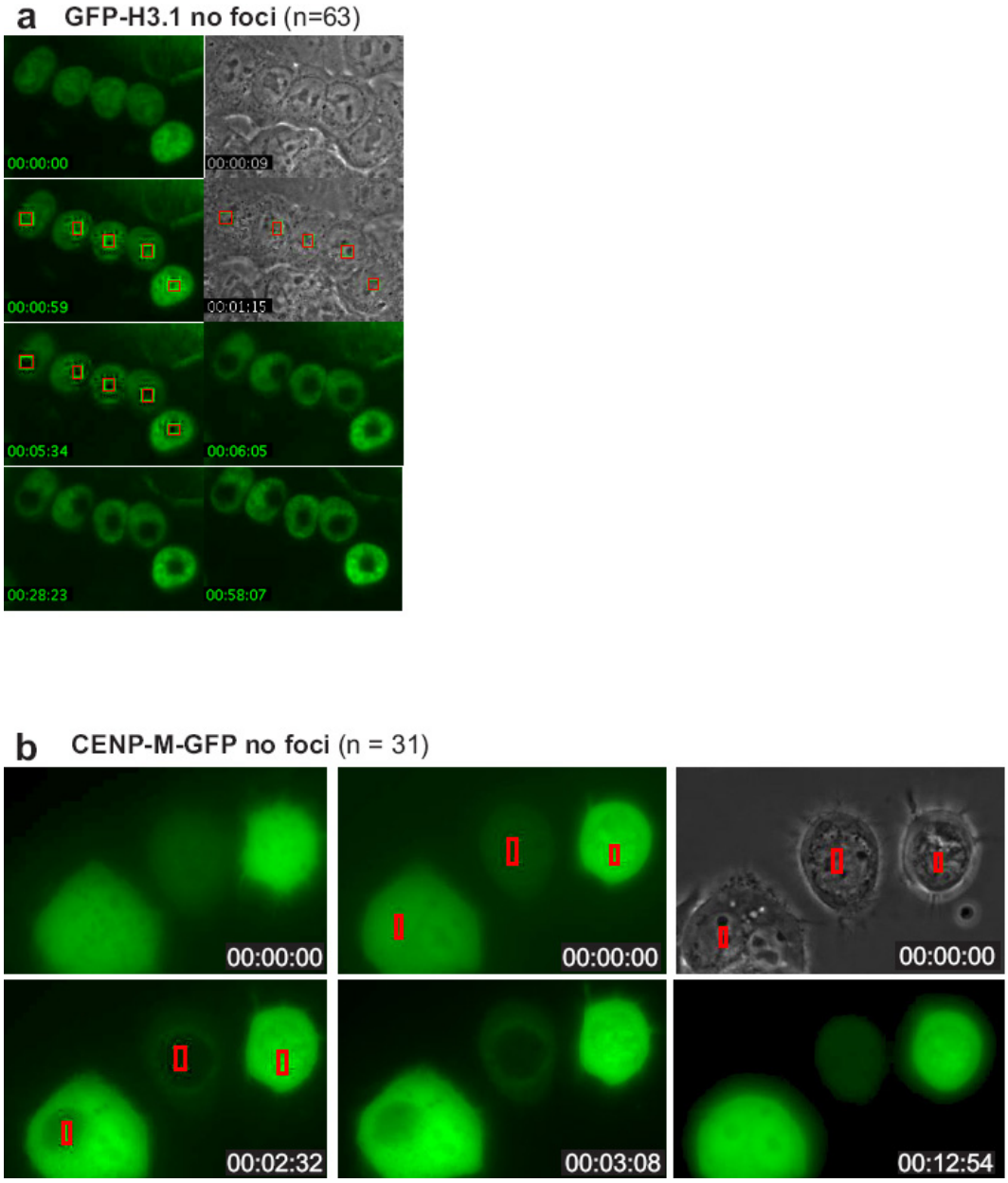

Figure A.7: No focal accumulations in cells transiently transfected to overexpress GFP-H3.1 or GFP-CENP-M. (a) Example images from transient transfections of GFP-H3.1 expression plasmid in HCT116 cells. No accumulations were observed in areas of laser targeting (red boxes). (b) GFP-CENP-M nuclear fluorescence bleached extensively but recovered rapidly, although accumulation at the site of laser targeting was not observed (n = 31 cells). Timestamp represents hours:minutes:seconds.

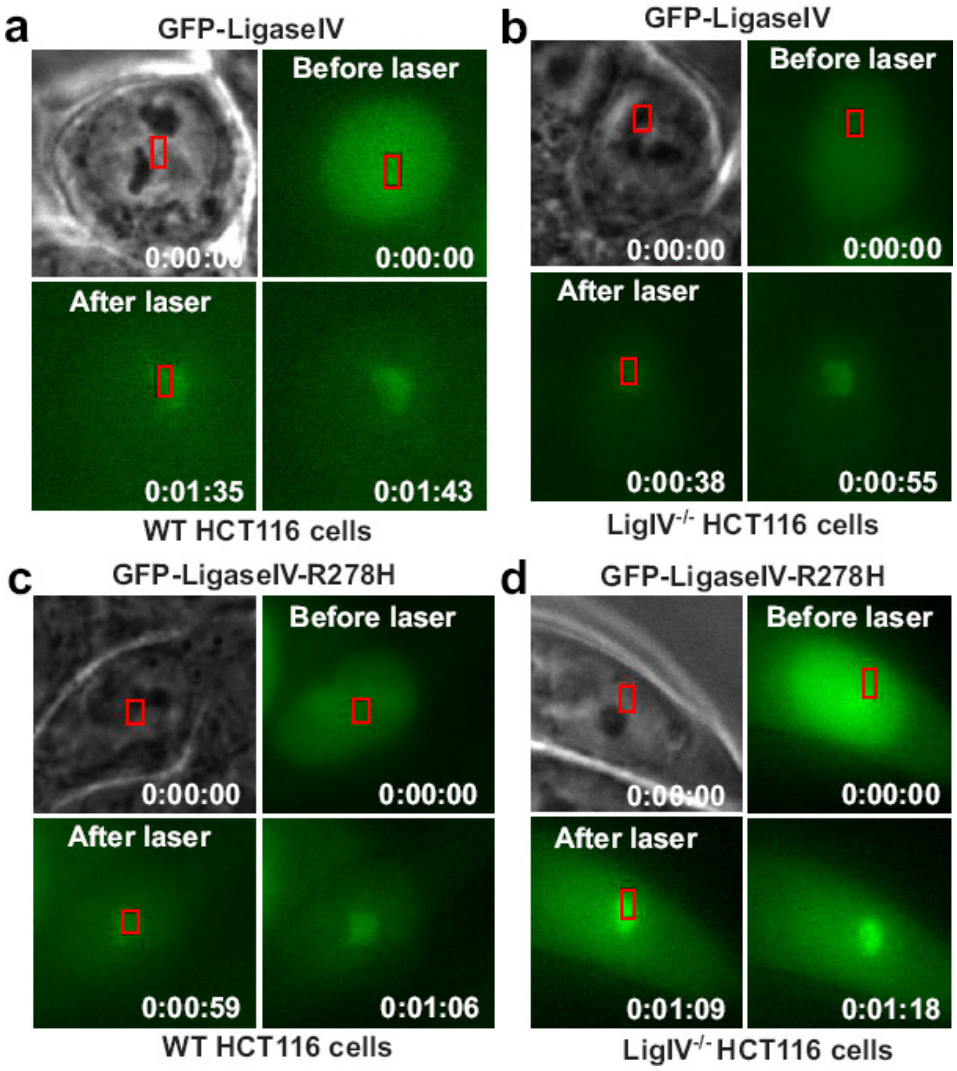

Figure A.8: Ligase IV recruitment to sites of laser-induced DNA damage. GFP-LigaseIV focus formation after laser exposure inWT(a) or LigaseIV-/- (b) HCT116 cells. GFP-LigaseIV-R278H focus formation after laser exposure in WT (c) or LigaseIV-/- (d) HCT116 cells. Timestamp represents hours:minutes:seconds.

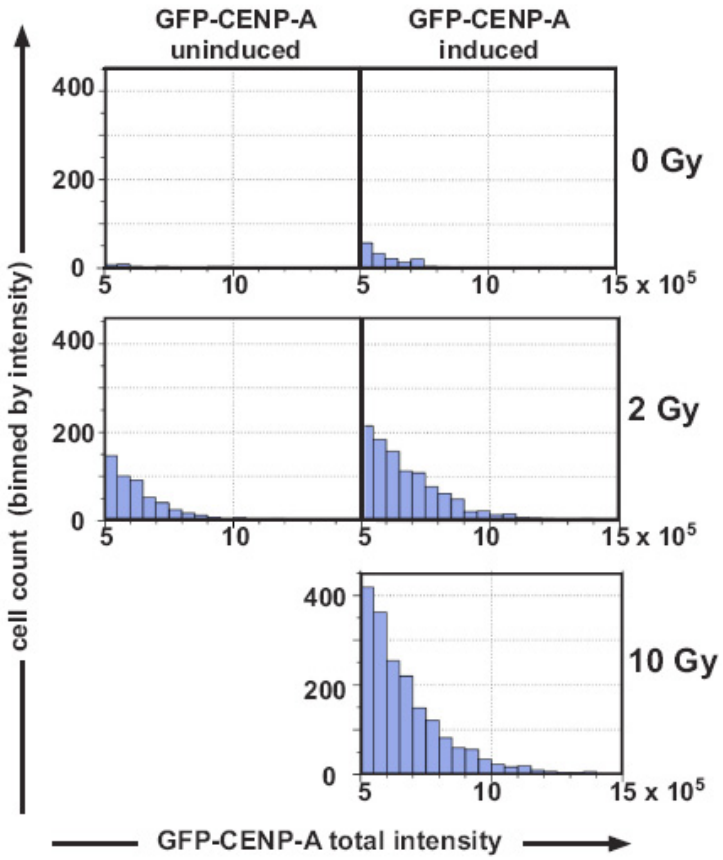

Figure A.9: GFP-CENP-A-positive cells accumulate, and GFP fluorescence levels increase, transiently after radiation-induced DNA damage. Population analysis demonstrated that GFP-CENP-A signals increased transiently after irradiation in a dose-dependent manner, suggesting post-translational stabilization of GFP-CENP-A protein in response to DNA damage.

B Robolase user manual

B.0.1 Preface

Robolase II is a labview program designed and operated by the Biophotonics lab at UCSD. The Biophotonics lab is led by Dr. Michael Berns and operated by Dr. Zhixia(Linda) Shi. Robolase II is an innovative research program that allows the user to use laser scissors to cut cells. These cells can be followed in real-time and have pictures taken to record the progress of the cells.

B.0.2 Safety Notes:

Because Robolase II uses a 532 nm picosecond laser, it is necessary to always wear goggles when operating the laser. These goggles have a shade of red tint which blocks out the green laser beam from contact with your eyes. Using the green tinted goggles will not provide safety from the laser.

When handling all types of cells, it is advised that you wear gloves. Although the lab generally does not use any cells that are known to cause cancer or any other illnesses, taking the precaution to wear gloves when handling cells is always a good idea.

B.0.3 Hardware Specifications:

Axiovert microscope; Hamamatsu camera; Spectra Physics 532 nm laser; Alienware Computer: Intel Core 2 Duo 2.67 GHz, 2 GB Ram, Windows XP

B.0.4 System Overview

The Robolase II system is comprised of 5 panels, each with up to 5 different tabs.

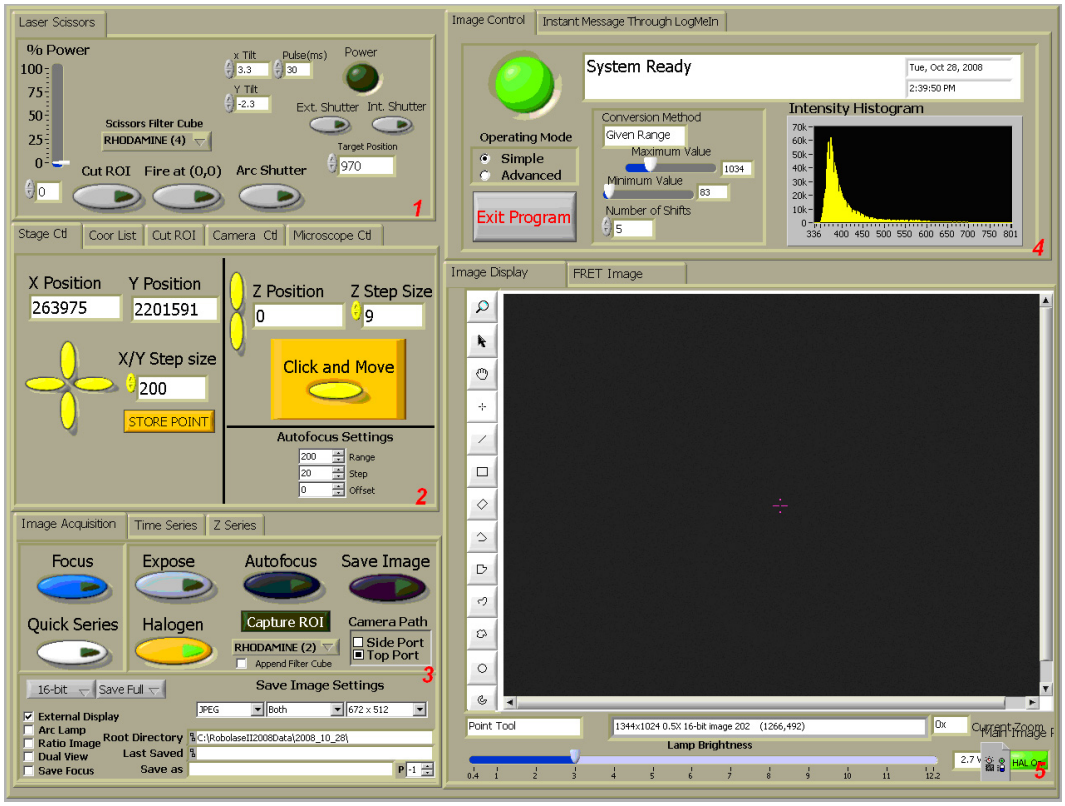

Figure B.1: System with individual panels 1,2,3,4, and 5 numbered in red.

B.1 Use of RobolaseII

B.1.1 How to turn on the system

Labview Program:

To turn on Labview, open the project explorer window for labview, and find the file labeled Robolase II.vi. Open this and it will bring you to the Front Diagram. Now to turn on Robolase, you must click the start arrow button located in the top left panel of labview, or click on the big green button in Robolase labeled Start System (Panel 4).

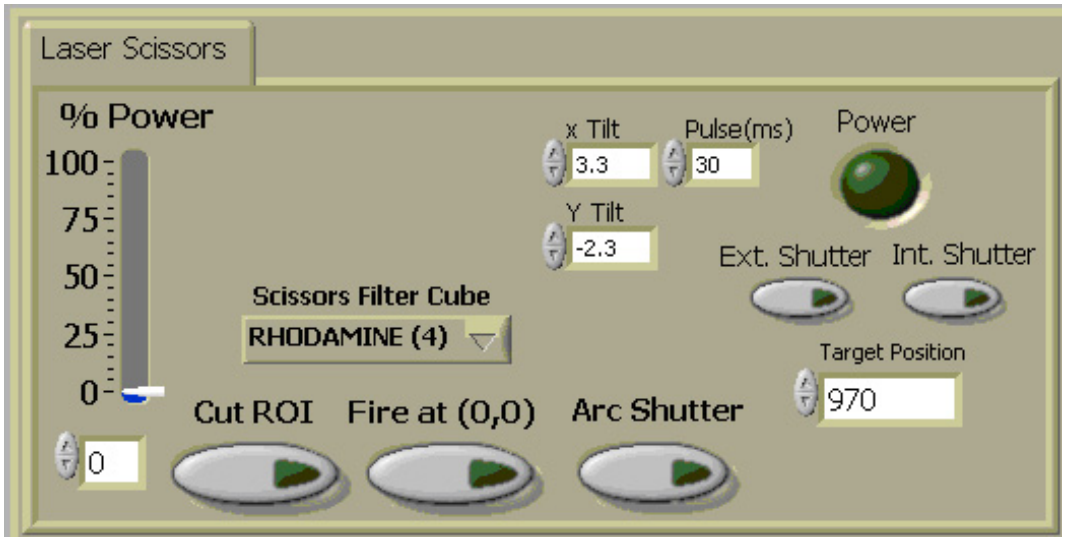

Figure B.2: Panel1 has only 1 tab labeled Laser Scissors.

Once the green button is on, the system is running.

Microscope:

To turn on the Axiovert microscope, press the green switch located on the right side of the microscope. When the green light is on, the microscope is on.

Laser:

To turn on the laser, turn the key on the laser power unit located on the floor beneath the Robolase system. The key should be in the on position, which is when the key is horizontal. To turn on the laser in Robolase, you must hit the smaller green button labeled, power (Panel 1). This will initiate a countdown of 15 seconds which allows the laser to turn on.

Arclamp:

To turn on the Arc Lamp, turn on the switch on the Arc lamp housing unit located on the Robolase II table. The machine takes a few minutes to warm up, so turn this on a few minutes before any experiment has begun. The Arc lamp allows the user to use fluorescence lighting in their experiment.

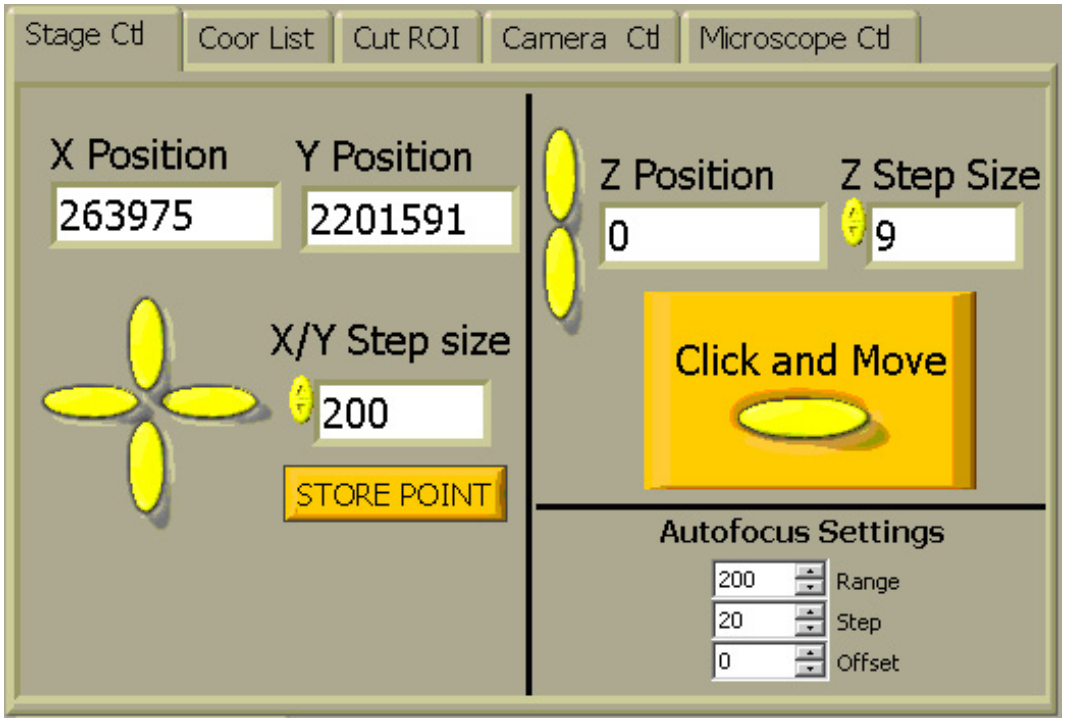

Figure B.3: Panel2 has 5 different tabs. Above is the first tab: Stage Control tab.

B.1.2 Cells that can be used

Petri dishes:

Most cells can be placed in a Petri dish and is the most common type of dish used if the cells need to be fixed or stained after or during and experiment. Petri dishes can be mounted on the stage that has a circle in the middle.

Rose Chambers:

A rose chamber is an alternative to using Petri dishes. Rose chambers are mainly used for anaerobic cells and can be mounted on a rose chamber stage.

Multi-well plates:

For experiments using more than one well, we provide the ability to use multiple wells. We have plates that can hold up to 4 Petri dishes or have 96 different wells for 96 different cells.

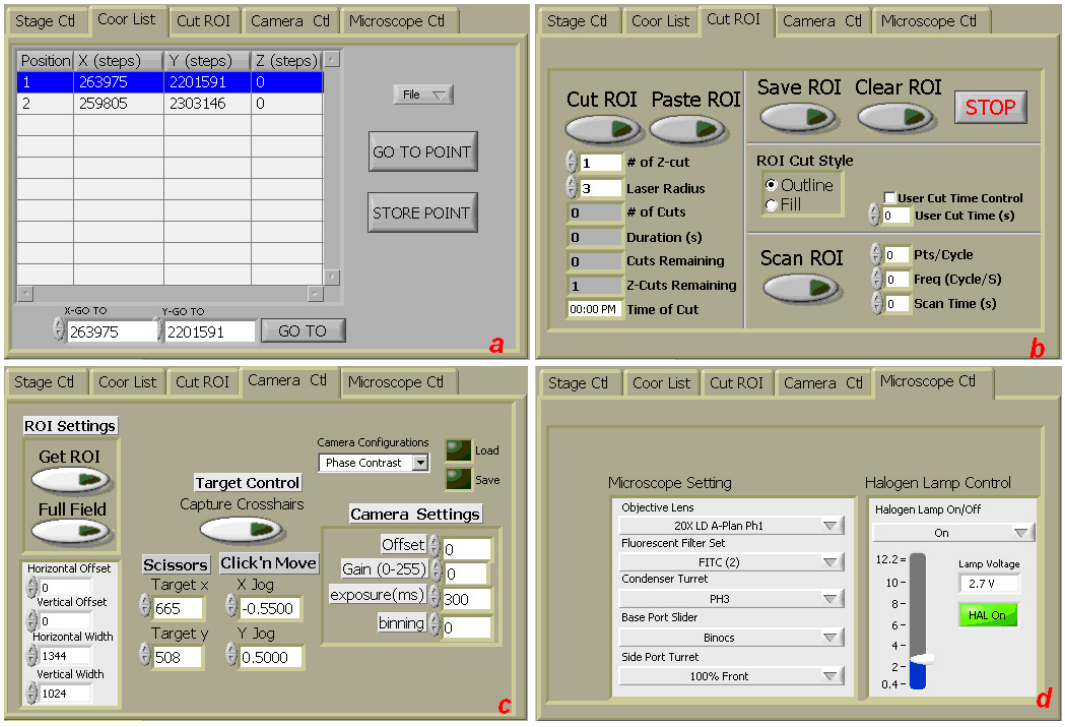

Figure B.4: Collage of the 4 other tabs in order from left to right: Coordinate List(a), Cut ROI(b), Camera control(c), and Microscope Control (d).

Incubated stage (OKOLAB)

The incubated stage allows the user to simulate an in-vivo environment on the cells. The OKOLAB incubated stage is located next to the Robolase table, and requires both CO2 and air. Depending on how much CO2 you need (5% or 10%), the OKOLAB manual will tell you exactly how much CO2 and air you need to reach the desired CO2 level.

B.1.3 Protocol: How to mount and find cells on the stage

Objective cleanliness

A clean objective is very important when imaging cells. To make sure the objective is clean before each use, take a strip of lens paper and wipe the objective with one clean swipe in one direction. Before you place the cells on the microscope, place a drop of oil on the objective using the Zeiss brown bottle. One dab or drop of oil is

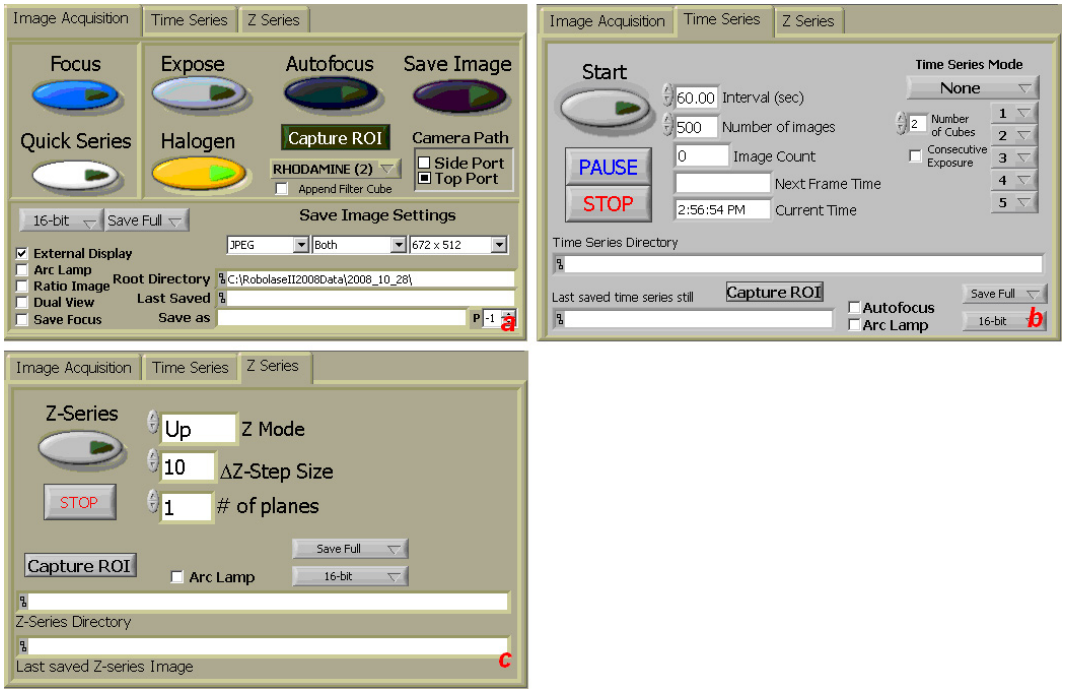

Figure B.5: Panel 3 is comprised of 3 tabs. Left to right: Image acquisition (a), Time Series(b), Z series (c).

often enough. If too much is placed, the image will not show up clearly. After you are done with an experiment, make sure to wipe off the oil on the objective with a new piece of lens paper. Then, place a drop of the lens cleaner on the lens paper and wipe the objective with it. Then wipe it off with a clean lens paper to completely clean the objective.

Finding the right stage:

Depending on which type of cells you are going to use, find the corresponding stage that will fit the cells. The various stages are found in the top drawer directly to the left of the Robolase II computer. In order to put the stage on the microscope correctly, place the top corners of the stage in first, and then press down on the bottom two corners to correctly place the stage on the microscope.

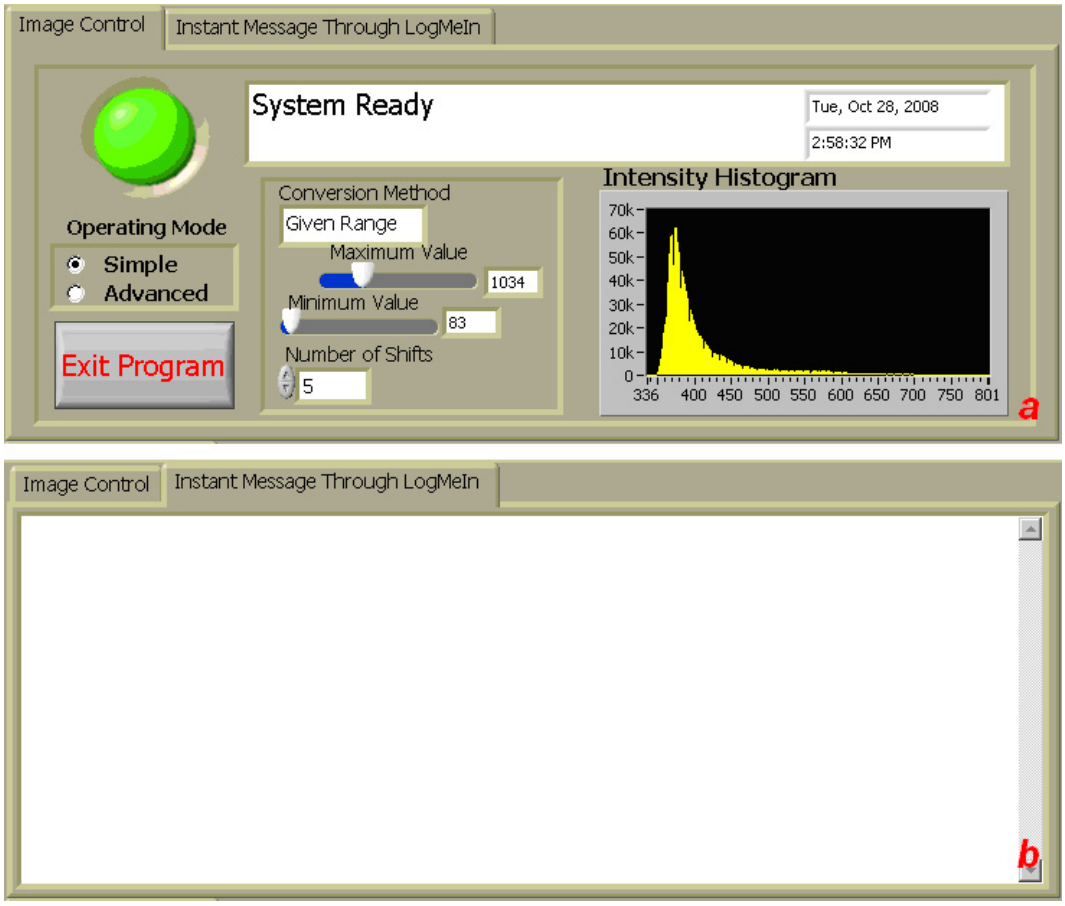

Figure B.6: Panel 4 is comprised of 2 tabs. Image control (a), Time instant message through Logmein (b).

B.1.4 How to find cells properly

Kohler Illumination

Kohler illumination allows the user to find the proper field of view with the proper focal plane. This is the first stage in focusing the cells. To use kohler illumination, the two knobs slightly below the halogen lamp will be used, as well as the knob that moves the condenser up and down. First, move the silver filter all the way to the back so that little light can come through the condenser. You will know it is all the way at the back when you can see a tiny hexagon through the eyepiece. Then, move the condenser up and down until the sharpest image is available. Move the hexagon that is seen to the middle by moving the two knobs below the halogen lamp. Once it is in the middle, pull

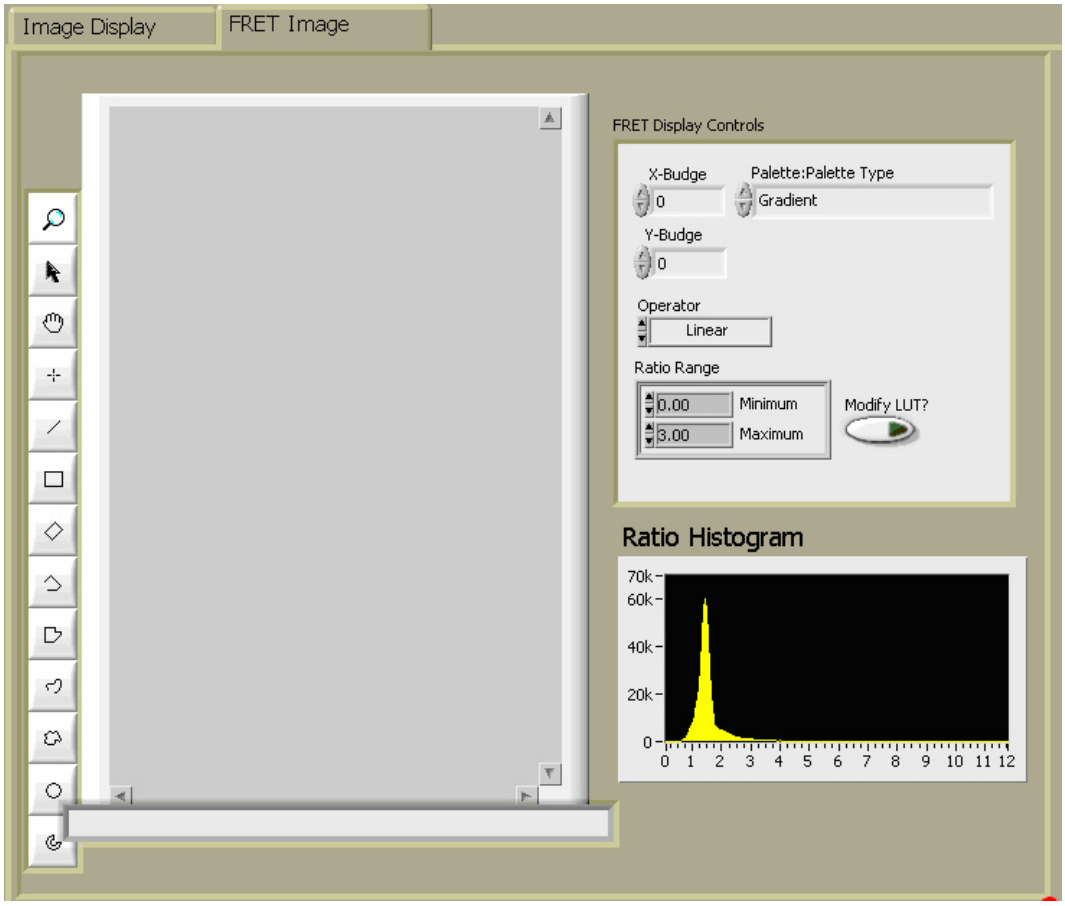

Figure B.7: Panel 5 comprises 2 panels. FRET Image (a), Image Display (b).

the silver filter back towards you until all sides of the hexagon have hit the field of view and the hexagon is no longer visible. Note that the hexagon gets larger as you pull it towards you.

Focusing

To focus the cells, Kohler illumination must be done first. After Kohler, move the focus knob up and down to find the right focal plane for the cells. If you want to see the cells live in Robolase, the focus button must be pressed.

B.1.5 Image Acquisition

In order to take images, make sure the cells are loaded and are in focus through the eyepiece of the microscope. Move the switch located on the front of the microscope from the eyepiece to the camera port so that image can be seen in Robolase.

This section will mainly utilize the features on the Image Acquisition tab on Panel 3.

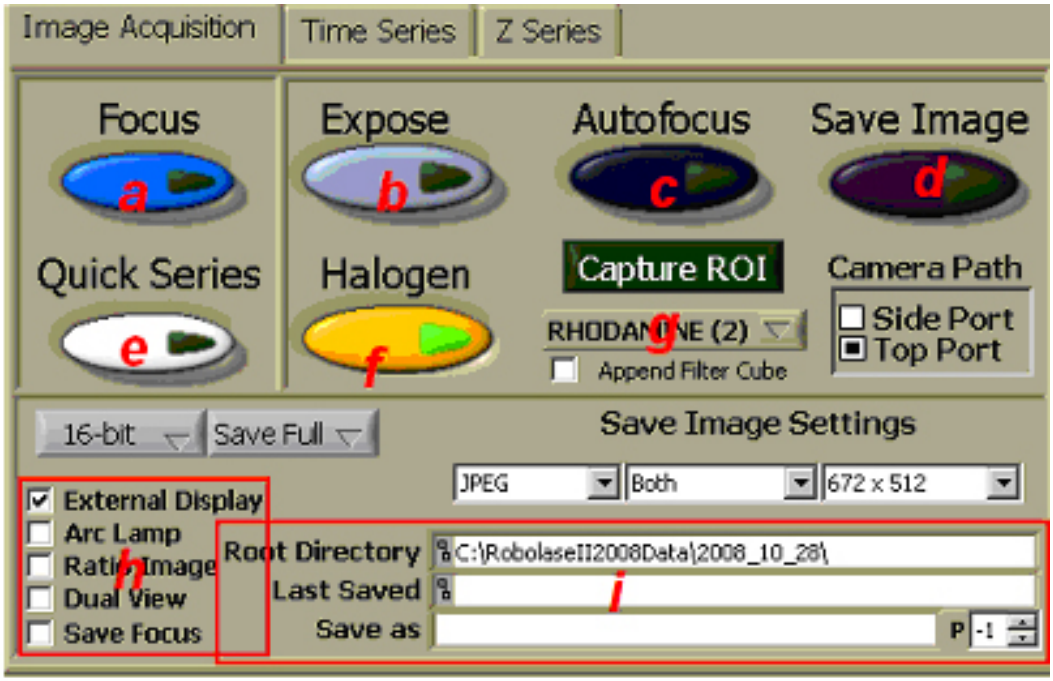

Figure B.8: Panel 3 Time Acquisition Tab features labeled a, b, c, d, e, f, g, h, i.

Use the Focus (panel3.a) button to utilize the focus knob on the microscope to put cells in focus. Note that without pressing focus, the image on Robolase will not change in real time. Use the Expose (panel3.b) button to snap the image so that it can be seen on Robolase. Use the Autofocus (panel3.c) button to let the computer use an algorithm to focus in on the best image possible. It is always better to manually focus, as the auto focus may not focus on the proper cells. Use the Save Image (panel3.d) button to save the image seen on Robolase. This button will save the image into a folder specified in panel3i. Use the Quick Series (panel3.e) button to take a quick set of images. Use the Halogen (panel3.f) button to enable/disable the halogen light. This will allow you to see the phase image of the cells. Use the filter cube (panel3.g) button to

change to different filter cubes on the turret in the microscope. Labels on this drop down tab do not necessarily relate to the correct filter cubes. Always make sure the correct filter cube is in the turret and that it corresponds to the number on Robolase. The boxes in (panel3.h) allow you to change some of the image settings. Check marks in the boxes denote that the function is currently being used. Click on the box to create or delete a check mark. The most commonly used buttons are External Display and Arc lamp. External display shows the image that will be saved onto another monitor (if available and working.) Arc lamp turns on the arc lamp for fluorescent imaging. The text boxes in (panel3i) tell you where and how an image will be saved. The top box labeled, Root directory, tells you where the image will be saved. Last saved tells you where the last image was saved. Save as allows you to label the image appropriately. P allows you to add a prefix to the label so you can use multiple fields of view.

B.1.6 Snap/Focus image

Phase Image:

To take a phase image, turn off the arclamp panel3.h (uncheck the box) and look at the cells by pressing expose. The Halogen button panel3.f should be on so that the phase image can be seen.

Fluorescence Image:

To take a fluorescence image, just load the appropriate cells, (stained with a fluorescent protein) either on a Petri dish or Rose chamber, and click the arclamp button in panel3.h. (make sure the box is checked) Arc shutter is off by default. To turn on the arclamp, make sure the hardware of the arclamp is on and that the light is on.

Note that an image containing both fluorescent and phase is possible, but the halogen light is often much stronger than the arc lamp.

B.1.7 Autofocus

Autofocus is an algorithm created by Stevie Harsono in the Robolase systems that calculates the best possible image, and automatically places you in the correct focal

plane. The settings and range for the autofocus section can be found in the Autofocus Settings section in panel 2. A higher range means that the autofocus will go through more focal planes. Because autofocus calculates the best possible image, the focal plane it brings you to may not be the best focal plane. Always make sure that the image seen is the correct and proper image.

B.1.8 Save image

To save an image, press the button labeled Save Image. The image will be saved in a folder specified by the Root Directory. Note that if the focus button is pressed, The Save Image button will need to be held longer so that it can take an image.

File name and location

Robolase automatically saves files in a folder designated by default. The images are currently saved in the folder ”C:RobolaseII2010Data”, and then are sorted by date. In order to change the location of the save location, change the root directory box in panel 3 (.i) to the desired location. To save the image under a certain file name, enter in the desired name in the box labeled Save as. Each image will save under that name, and will have a different image number, which is automatically labeled by Robolase. To see the recently saved image, the box labeled Last Saved will tell you the directory and file name of the last saved image.

B.1.9 Type of image and resolution (size)

Type:

Images in Robolase can be saved in two formats, .tiff, and .jpg. Tiff files are usually higher in resolution and therefore take up more hard drive space. To save the images in either tiff or jpeg, use the drop down boxes in the save image settings section of panel 3 and select which format you want to save.

Resolution:

The final drop down box on the right side determines the resolution of the image that will be saved. A larger resolution will result in a much clearer picture and is the size that should be saved if the images will be used for publications. The smaller size resolution is ideal for initial experiments where quality of the images is un-important.

Overlay or no overlay:

To save the image with the laser cut line, use the drop down box under Save Image Settings and use Overlay ROI to save the image with the overlay (laser cut lines). There is also the option to have no overlay, which has no laser cut lines. The best option is to save under both which does both overlay and no overlay. Note that .tiff files cannot be saved with an overlay.

B.1.10 Multiple fields of view

Store location and "Go to"

To store the location of the field of view after finding the one you want, go to the Coor List tab and click the Store Point panel2.d button. This will save the x,y coordinates for the field of view in panel2.a. and can be seen in panel2.b. To go to the saved coordinate, click the Go To Point button panel2.c. This function will bring you to the saved coordinate that you want.

Saving Locations:

The saved locations can be done for multiple fields of view and can be saved as a text file for later use. The text file can be uploaded and the coordinate list will show up in Robolase. To save the location as a text file, click the File button, panel2.e and click save. You can now save the file under any name.

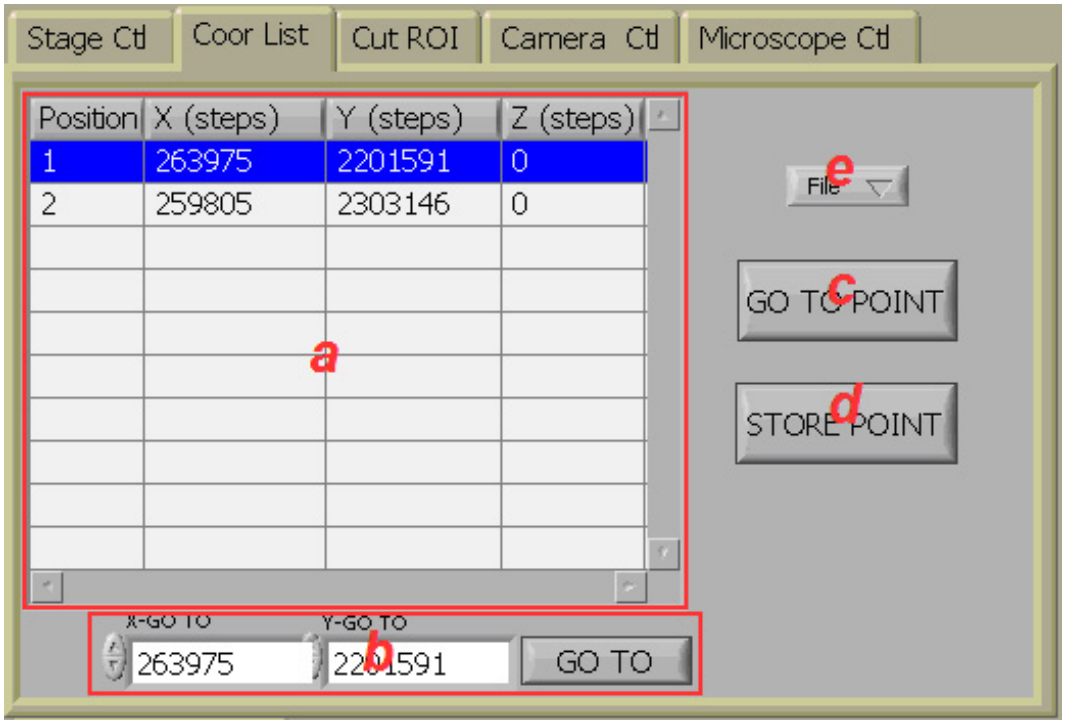

Figure B.9: Panel 2 coordinate list tab features labeled a, b, c, d, e.

B.1.11 Time series

Robolase allows you to create a time series when watching cells. A Time Series is a series of images taken in a certain time where each image is taken at a specified interval.

Use the Start (10.a) button to begin the time series. The user also has the ability to Pause (10.b) or STOP (10.c) the time series. The images will be saved in an individual time series folder found in the folder containing the days images, shown in 10.d. Box 10.g, shows the 3 indicator boxes that will display the image count, the time in which the next image will be taken, and the current time. To change the interval in which images are taken, change the interval box in 10.f as well as the amount of images you want to take. The images are taken in intervals of seconds, so 60 denotes 1 minute, not 60 images in 1 minute. You can also set the time series to stop at a certain time by putting how many images will be taken. By default, the time series will stop after 500 images have been taken.

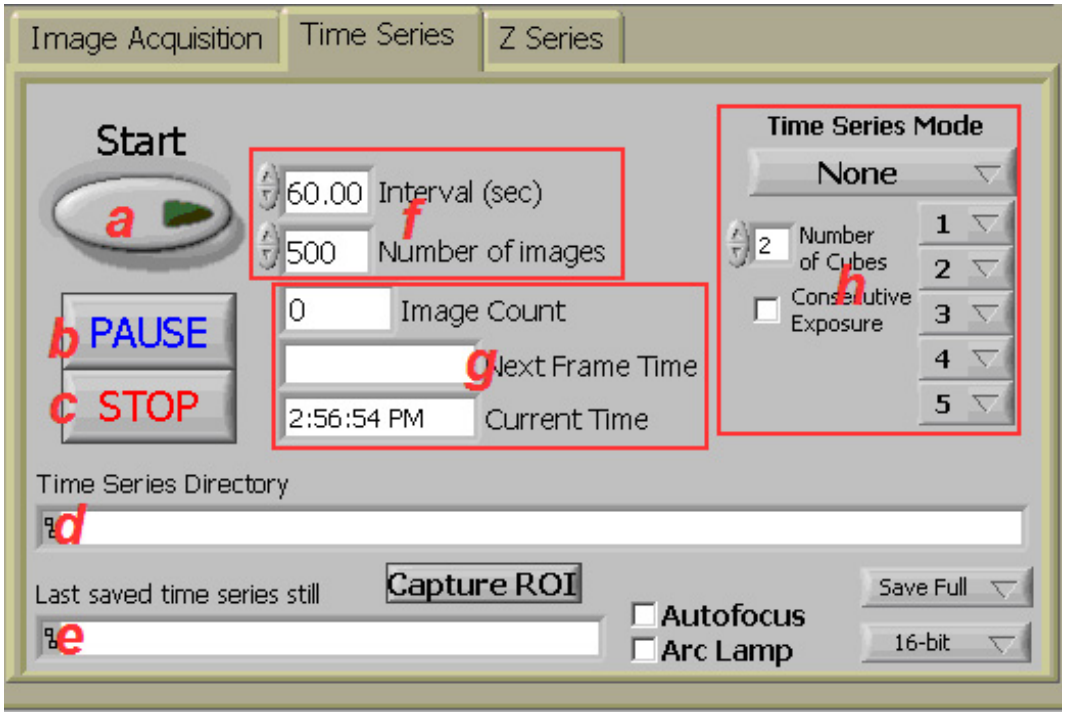

Figure B.10: Panel 3 Time series tab features labeled a, b, c, d, e, f, g, h.

Time series with different filter cubes:

To take a time series with different filter cubes, use the drop down box in 10.h, and select Auto Filter. The numbers on the right are the given turrets for each filter cube. There are a total of 5 possible filter cubes. In order to run the time series, you need to check the box that says Consecutive exposure as well as indicate the number of cubes that will be used. The images will be saved starting from turret 1 and going to the corresponding amount of cubes being used.

Time Series with autofocus:

To take a time series with autofocus, click the autofocus button under the time series tab. This will allow Robolase to use the algorithm used for autofocus before each image is taken in the series.

External display:

The external display button located in panel 3 allows the user to see the microscope image on an external secondary monitor. This image is seen in full screen, is fully processed, and will be a replica of the saved image.

B.1.12 Stage Control

X,Y Stage: up/down/left/right

To move the stage in different directions, move the joystick located next to the microscope. Moving the joystick can be tricky at first, the best way to understand how the joystick works would be to test it out. The focus button needs to be pressed if you want to move the joystick and see the cells in real time on Robolase. Sometimes the stage may begin to move after you have found a field of view. This occurs if the joystick isn't perfectly zeroed. Simply move the joystick a little bit until it is zeroed or recalibrate the joystick.

The x,y coordinates can also be moved in Robolase. Panel3 shows the functions that allow the user to move the stage via Robolase.

The x and y coordinates can be changed in panel3.a, but the stage can be moved up and down via panel3.b. The buttons denote the movements of a joystick. When using these buttons instead of a joystick, the movement increment size can be changed in panel3.c. The positions can also be stored by clicking panel3.d. The button panel3.f, allows you to move the image to wherever you click on the display. Clicking panel3.f will move the center of the stage to wherever you click.

Z stage: Focus

To change the Z plane, simply turn the focus knob. The Z plane in Robolase is known as the focal plane, and can be manually controlled, or controlled by Robolase.

To change the Z stage in Robolase, change the numbers in panel3.e to denote whether u want to move up or down. A higher number indicates going up in the Z plane, where a smaller number denotes going down.

B.1.13 Camera settings

The Hamamatsu camera and Robolase have several features that allow the user to see images better. There are two ways of doing this, by changing the exposure time to the light, and to change the contrast of the image, known as the gain.

Exposure:

The exposure time is measured in milliseconds, and can be changed under the camera control tab (Panel B4.c). To change the exposure time, just put in the desired time. A larger time will allow for more light to reach the cell, but can also induce photo bleaching.

Gain:

The gain is located above the exposure box. A higher gain will increase the contrast ratio of the picture, making the background darker.

B.1.14 Laser Control

Measuring laser power:

To measure the laser power, the power meter is needed. Turn on the power meter first and set the wavelength to 532 nm and press the attenuation button, labeled ATTN. Now, turn open the shutter which is a hardware switch located on the UNIBLITZ box above the microscope. It is the switch on the left side, this will open the shutter allowing you to measure the power. Now on the microscope, switch the objective so that an open filter cube slot is available. Place the measuring device from the power meter on the objective hole to measure the power. Turn on the laser, and click Int. Shutter and press 'Fire at (0,0).' To change power, change the %Power section in Panel 1 of Robolase. Record all the measured powers starting from 0% and working your way up to around 60%. The optimally measured power should be around 11.2 mw for Red blood cell (RBC) ablation. This generally falls in the area of 37-42%, but can vary depending on the laser and person's RBC.

Cutting:

To cut in Robolase, simply draw the desired lines over the image display. Drawing these lines on the cells will send a signal to the laser to draw the lines on the cells. TO initiate the cut sequence, press the button labeled Int. Shutter

After the internal shutter is on, press Cut ROI button to cut the lines you drew. Fire at (0,0) will cut a dot in the middle of the field of view. The scissors filter cube should always be set to Rhodamine.

After cutting cells, always press the expose button to switch the filter cube back to the imaging cube.

Cutting Lines:

The different shapes on the left side of the image display allow the user to cut different types of lines. To cut a straight line, use the straight line button. To cut multiple cells, hold down the control (CTRL) button on the keyboard and being drawing on different cells. However, releasing the ctrl button and drawing a new line will erase all previous lines.

Cutting shapes:

To cut certain shapes in Robolase, use the desired shape buttons located on the left side of the Image display tab. Under the Cut ROI tab, Figure 4.b, the ROI Cut style box will determine how to cut the shape. Outline will create an outline of the shape, while Fill will fill in the shape with laser cuts.

Change laser power or pulse:

To change the laser power, just change the power percentage to the desired percentage. These percentages should correspond to the recorded power of the laser when you measured the laser power. To change the pulse of the laser (how many times it pulses in a minute) change the Pulse amount higher or lower to increase or decrease the pulse. The pulse by default, is set at 30ms.

B.1.15 Logmein control

Robolase was created to allow for remote user use. The biophotonics lab currently uses the program LogMeIn to remotely access Robolase. All of the functions in Robolase can be accessed via LogMeIn and is very helpful when conducting experiments overnight.

The tab in panel 4 is a messaging device designed to allow for messages to be sent from a remote user to a local user.